CR 86287

Kaman AviDyne

BURLINGTON, MASSACHUSETTS

DIVISION OF KAMAN SCIENCES CORPORATION

KAMAN AVIDYNE
a Division of Kaman Sciences Corporation
Burlington, Massachusetts

KAMAN AVIDYNE TR-64

INTERIM SCIENTIFIC REPORT:
AUTOMATIC LONGITUDINAL GUIDANCE FOR VTOL AIRCRAFT

NAS 12-2097

Prepared by
William C. Hoffman

Approved by
John Zvara

Technical Consultants

Professor Arthur E. Bryson, Jr.
Stanford University

Professor Norman D. Ham
Massachusetts Institute of Technology

October 1969

Prepared under Contract No. NAS 12-2097
for the Electronics Research Center
NATIONAL AERONAUTICS AND SPACE ADMINISTRATION

TABLE OF CONTENTS

INTRODUCTION

This report provides interim documentation of a study being performed by Kaman AviDyne for the NASA Electronics Research Center under Contract No. NAS 12-2097. The study objective is to develop and evaluate automatic guidance modes and associated software for Phase II of the NASA/ERC V/STOL Avionics Program. The initial part of the effort, which is described in this report, has been restricted to the longitudinal axis of the guidance system, i.e. the vertical plane.

The purpose of the guidance system is to control the position and velocity of the vehicle to satisfy specified flight objectives, e.g. to transport passengers from one airport to another under zero visibility conditions. In performing this task, the guidance system accepts position and velocity information from the navigation system, and generates velocity commands for the flight control system which provides the direct control of the vehicle maneuvers by control displacements (Figure 1).

The remainder of this report discusses the analytical development of the guidance concept, the simulation employed to evaluate its performance, and the results obtained.

ANALYTICAL DEVELOPMENT

Simplified Model of Controlled Vehicle

As mentioned above, the guidance system is to generate velocity commands to the flight control system. Ideally, these

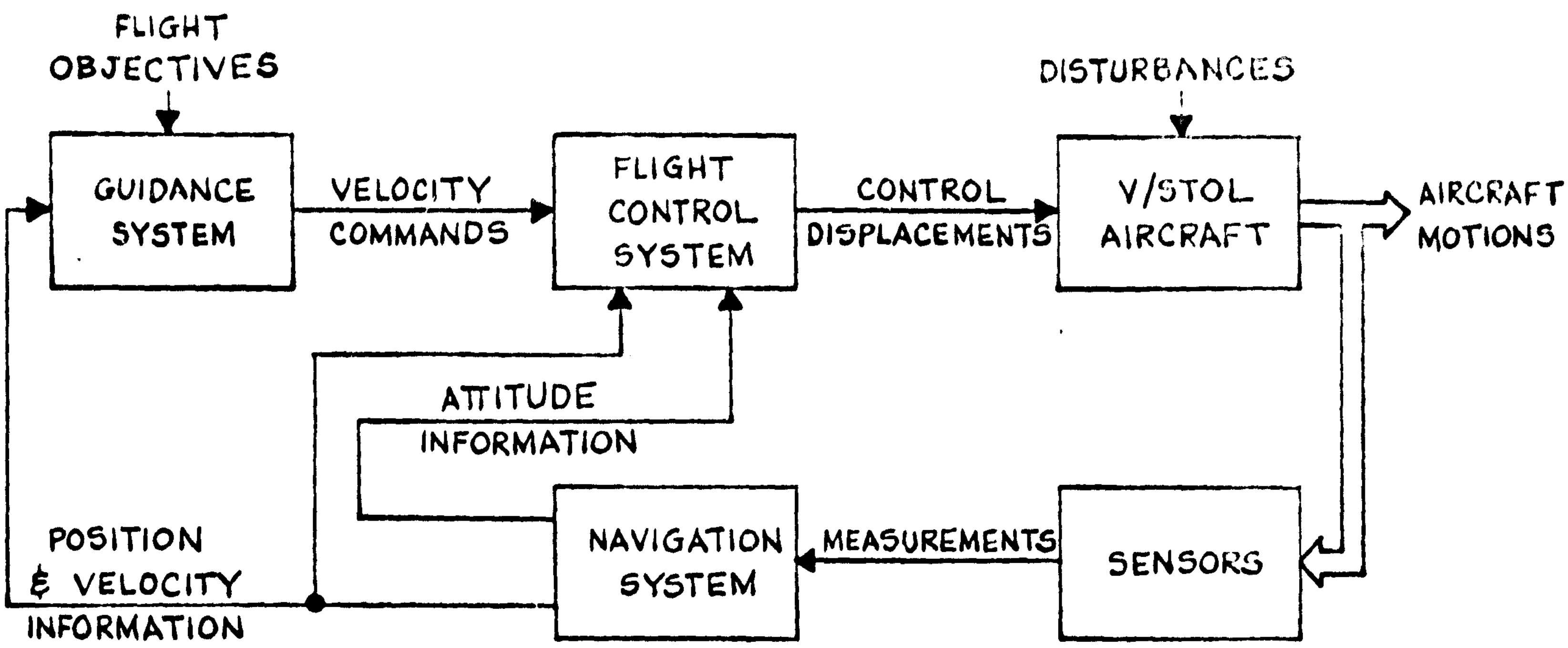

Figure 1. Block Diagram of V/STOL Avionics Systems

commands would be instantaneously achieved by a perfect autopilot. In reality, the combined dynamics of the flight control system and aircraft introduce delays in the response to a command. Fortunately, however, the response time of the controlled vehicle (on the order of a second), is generally short in comparison to the characteristic time of the guidance function (on the order of ten seconds). Thus, as seen from the guidance system, velocity commands are very nearly instantly achieved.

The guidance analysis commenced with the simplest possible representation of the controlled vehicle – a perfect autopilot. That is, actual velocity is equal to commanded velocity:

$$\dot{x} = V_x = V_{x_c} \tag{1}$$

$$\dot{z} = V_z = V_{z_c} \tag{2}$$

where x and z are the position coordinates of the vehicle in the vertical plane; V_x and V_z are, respectively, the horizontal and vertical components of inertial velocity in the vertical plane; V_{x_c} and V_{z_c} are the corresponding velocity commands. (See Figure 2 for a definition of the coordinate system and nomenclature.) Since final time is not of great importance, it is more convenient to use range, x, instead as the independent variable. Dividing (2) by (1) yields a simple, first-order

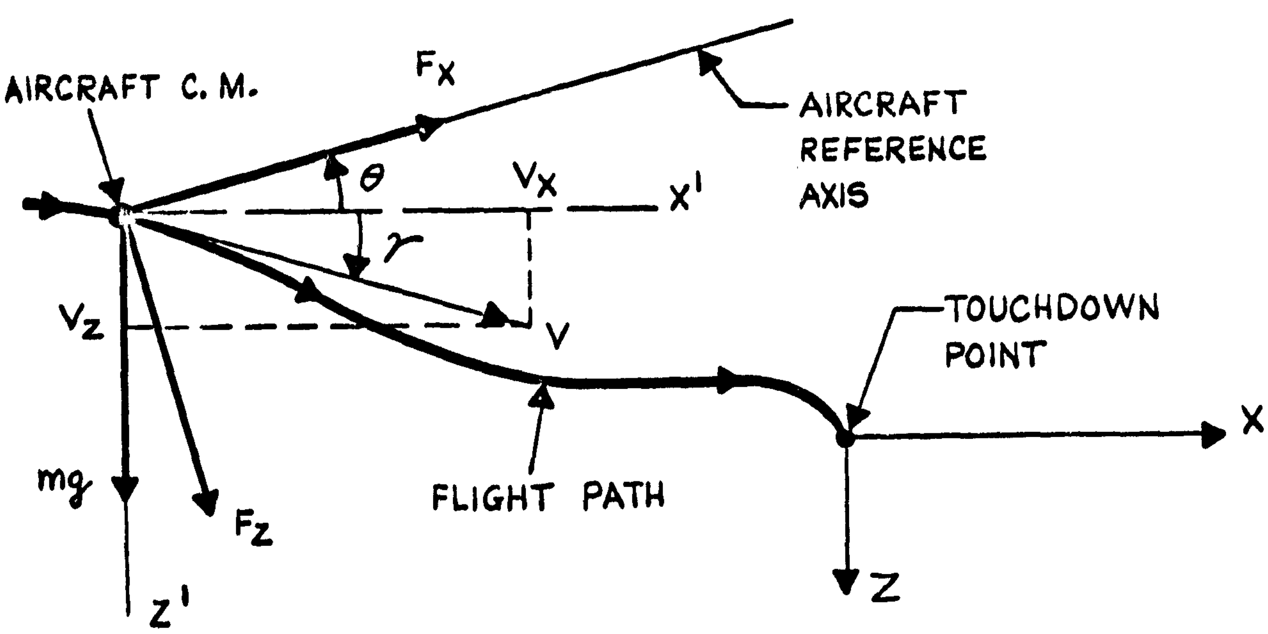

Figure 2. Coordinate System and Nomenclature for Longitudinal Analysis

approximate model of the controlled vehicle dynamics:

$$\frac{dz}{dx} = \frac{V_{z_c}}{V_{x_c}} \tag{3}$$

where z is the single state variable; x is the independent variable; V_{x_c} and V_{z_c} are the control variables.

Linearized Model

The simplified equation of motion, Eq. (3), may be linearized by considering first-order perturbations about a nominal trajectory. The perturbation form of Eq. (3) is

$$d(\delta z)/dx = G\ \delta u \tag{4}$$

where G is a 1×2 matrix

$$G = \left(-V_{z_{c_n}},\ V_{x_{c_n}}\right)\Big/ V_{x_{c_n}}^{\ 2} \tag{5}$$

and the control vector δu is defined as

$$\delta u = \begin{pmatrix} \delta V_{x_c} \\ \delta V_{z_c} \end{pmatrix} \tag{6}$$

The perturbation quantities are defined as

$$\delta(\ ) = (\ ) - (\ )_n \tag{7}$$

where the subscript n denotes the nominal value of the indicated quantity.

Quadratic Synthesis

Having described the approximate motion of the vehicle in the vicinity of the nominal trajectory, we may now apply the quadratic synthesis technique (Ref. 1) to find a linear feedback guidance law. A convenient performance index to choose for this purpose is one which is a quadratic function of the control and state variable perturbations:

$$J = \frac{1}{2} S_f (\delta z)^2_{x=x_f} + \frac{1}{2} \int_{x_i}^{x_f} \left[A \, \delta z^2 + \delta u^T \, B \, \delta u \right] dx \tag{8}$$

where x_i and x_f are, respectively, the initial and final range. The quantities S_f and A weight the penalties associated with terminal and enroute altitude errors, and the matrix B penalizes control deviations during the flight:

$$S_f = \delta z_f^{-2} \tag{9}$$

$$A = \left[(x_f - x_i) \delta z_o^2 \right]^{-1} \tag{10}$$

$$B = \frac{1}{x_f - x_i} \begin{bmatrix} \left(\delta V_{x_{c_o}}\right)^{-2} & 0 \\ 0 & \left(\delta V_{z_{c_o}}\right)^{-2} \end{bmatrix} \tag{11}$$

The parameters δz_f, δz_o, $\delta V_{x_{c_o}}$ and $\delta V_{z_{c_o}}$ must be chosen to provide satisfactory altitude control within allowable limitations on δV_{x_c} and δV_{z_c}.

The minimization of the performance criterion, Eq. (8), subject to the perturbation equation of motion, Eq. (4), yields the linear feedback guidance law

$$\delta u = -C(x)\delta z \qquad (12)$$

where the feedback gain matrix $C(x)$ is defined by

$$C = B^{-1} G^T S \qquad (13)$$

and B^{-1} is the inverse of B [Eq. (11)], G^T is the transpose of G [Eq. (5)] and S is the solution of the matrix Riccati equation

$$\frac{dS}{dx} = GB^{-1} G^T S^2 - A \qquad (14)$$

with the boundary condition

$$S(x_f) = S_f \qquad (15)$$

In expanded form, the guidance law, Eq. (12), is

$$V_{x_c} = V_{x_{c_n}} - C_{V_x}(z-z_n) \qquad (16)$$

$$V_{z_c} = V_{z_{c_n}} - C_{V_z}(z-z_n) \qquad (17)$$

where

$$C_{V_x}(x) = -\frac{(x_f-x_i)V_{z_{c_n}} \delta V_{x_{c_o}}{}^2}{V_{x_{c_n}}{}^2} S(x) \qquad (18)$$

$$C_{V_z}(x) = -\frac{(x_f-x_i)\delta V_{z_{c_o}}{}^2}{V_{x_{c_n}}} S(x) \qquad (19)$$

Figure 3 is a block diagram showing the configuration of the velocity-command guidance system with the simple model of the controlled V/STOL used in the analysis. In the simulation described below, and in actual implementation, the contents of the dashed block "Controlled Aircraft" are replaced by the flight control system and the actual ("bare") helicopter dynamics.

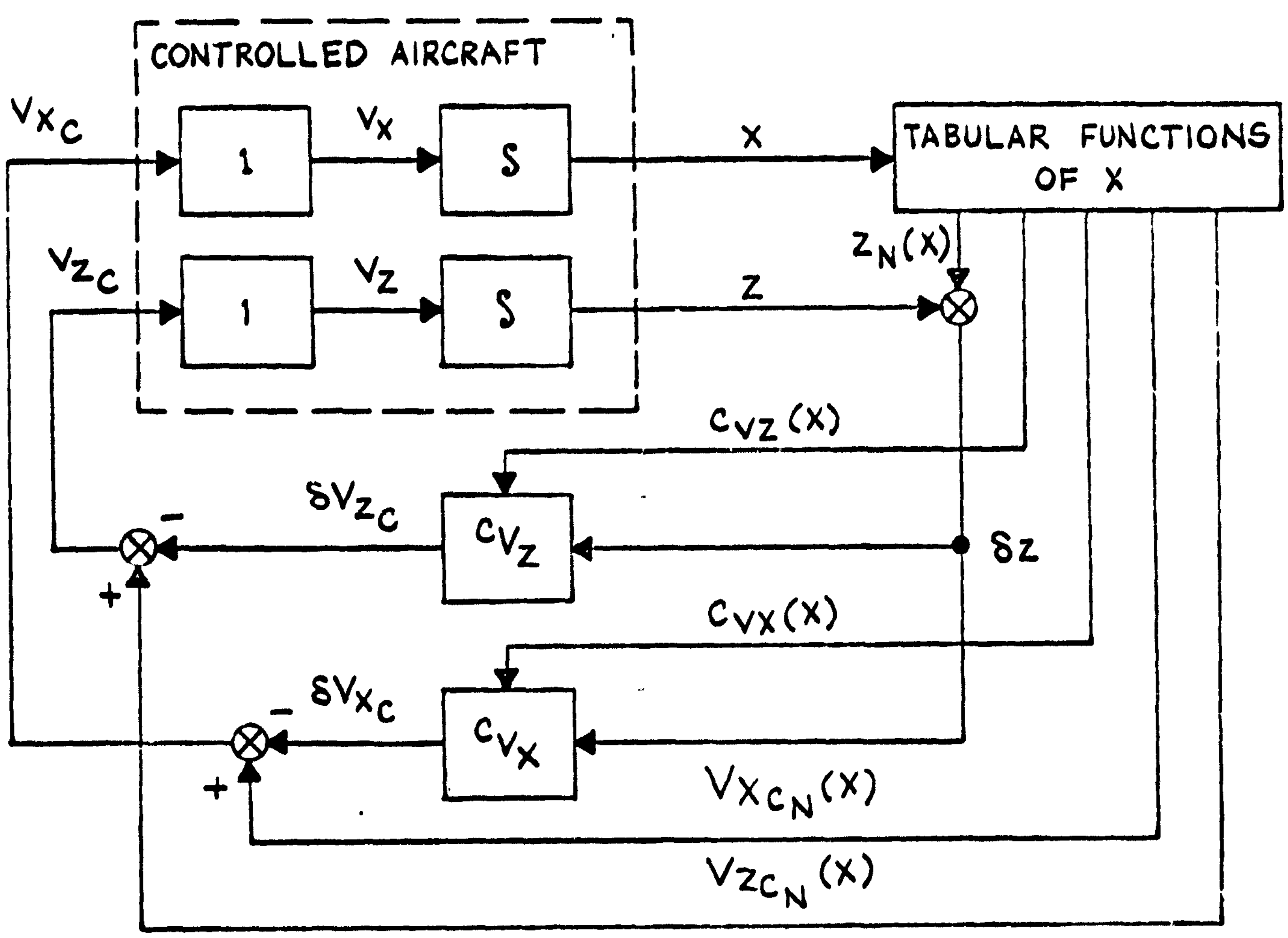

Figure 3. Longitudinal Velocity-Command Guidance System with Simple Model of Controlled V/STOL Aircraft

SIMULATION

To evaluate the performance of the guidance law described above, a digital computer simulation of the longitudinal dynamics of the tandem-rotor YHC-1A helicopter was developed by modifying Program LIFT (Ref. 2). The important changes made in LIFT are discussed below.

Vehicle Model

The first and most significant modification of LIFT was the development of a model which adequately describes the aerodynamics of the helicopter. Two possibilities were investigated:

(1) An Analytical Model – This approach would utilize an approximate analytical model which describes the aerodynamic forces acting on the vehicle as functions of altitude, velocity, pitch attitude and collective stick displacement, where the last two variables are the control inputs to the model. An analytical model which was developed for this purpose is described in Appendix A.

(2) A Near-Trim Model – The alternative approach would utilize the trim and stability derivative data contained in Reference 3 to calculate the aerodynamic forces and moments as functions of altitude, velocity, pitch attitude, pitch rate, and both collective and longitudinal stick displacements.

The advantages of the analytical model for guidance studies are (1) it is simpler, in that it does not include the pitching dynamics of the vehicle, and (2) it is not a linearized model which relies on a near-trim assumption for validity. On the other hand, the near-trim model has the advantage of allowing a more complete simulation of the vehicle dynamics, both translational and rotational, and including the flight control system as well.

The near-trim model was eventually selected for the simulation since it was anticipated that the aircraft would be flown in the vicinity of trim to maintain reasonably comfortable flights. Consequently, the aerodynamic forces and pitching moment acting on the vehicle are represented in LIFT in the following manner:

$$F_x = m g \sin \theta_o + X_u \Delta U + X_w \Delta W + X_q q + X_{\delta_e} \Delta\delta_e + X_{\delta_c} \Delta\delta_c \tag{20}$$

$$F_z = -m g \cos \theta_o + Z_u \Delta U + Z_w \Delta W + Z_q q + Z_{\delta_e} \Delta\delta_e + Z_{\delta_c} \Delta\delta_c \tag{21}$$

$$F_m = M_u \Delta U + M_w \Delta W + M_q q + M_{\delta_e} \Delta\delta_e + M_{\delta_c} \Delta\delta_c \tag{22}$$

where

$$\Delta(\ ) = (\ ) - (\ )_o \tag{23}$$

and the subscript o denotes the trim value of the indicated quantity. The trim values θ_o, δ_{e_o}, δ_{c_o} and the stability derivatives X_u, X_w, etc. are linearly interpolated from data tables as functions of V_x and V_z. The trim values of the velocity components along body axes, U_o and W_o, are

$$U_o = V_x \cos \theta_o + V_z \sin \theta_o \tag{24}$$

$$W_o = -V_x \sin \theta_o + V_z \cos \theta_o \tag{25}$$

The stored data tables for the YHC-1A helicopter were obtained from Reference 3 for the operating conditions shown in Table 1.

Table 1. Operating Conditions for YHC-1A Trim and Stability Derivative Data in Program LIFT

Gross Weight	13,400 lbs
c.m. Position	normal
I_{yy}	75,914 slug-ft^2
Rate of Descent	-1500, 0, +1500 ft/min
Altitude	sea level
Forward Velocity	0,20,40,60,80,100*,120*,140* kts

*Extrapolated values used for non-zero rate of descent cases.

The tables themselves and other vehicle data are contained in Appendix B. Only sea level data were used since (1) complete data for other altitudes were not available, and (2) all flight tests will be restricted to low attitudes (~ 1000 ft) where the data are just slightly different from sea level values. For the non-zero rate of descent cases, data was unavailable for forward speeds greater than 80 kts. Therefore, to complete the tables for the interpolation routine in LIFT, values for the higher speeds were extropolated, as indicated in Appendix B.

Another modification to Program LIFT was the addition of a variable mass capability to account for fuel consumption. This requires the integration of another differential equation:

$$\frac{dm}{dt} = -f(V_x, V_z) \tag{26}$$

The rate of fuel flow f is interpolated from a stored table of trim values obtained from Reference 4 (see Appendix B).

Flight Control System

The second major change made in LIFT involved the inclusion of the velocity-command control system which has been developed by NASA/ERC. This is shown in Figure 4. The addition of three state variables to the program was required to implement the flight control system, as defined below.

$$\frac{dV_{x_{E_I}}}{dt} = V_{x_c} - V_x \tag{27}$$

$$\frac{d\theta_{E_I}}{dt} = \theta_E \tag{28}$$

$$\frac{dV_{z_{c_I}}}{dt} = V_{z_c} \tag{29}$$

where

$$\theta_E = K_{V_x}\left(V_{x_c} - V_x + K_{I_{V_x}} V_{x_{E_I}}\right) - \theta - T_Q q \tag{30}$$

With these definitions, the control deflections are given by

$$\delta_e = K_\theta\left(\theta_E + K_{I_\theta}\,\theta_{E_I}\right) \tag{31}$$

$$\delta_c = K_{V_z}\left[V_{z_c} - V_z + K_z\left(V_{z_{c_I}} - z\right)\right] \tag{32}$$

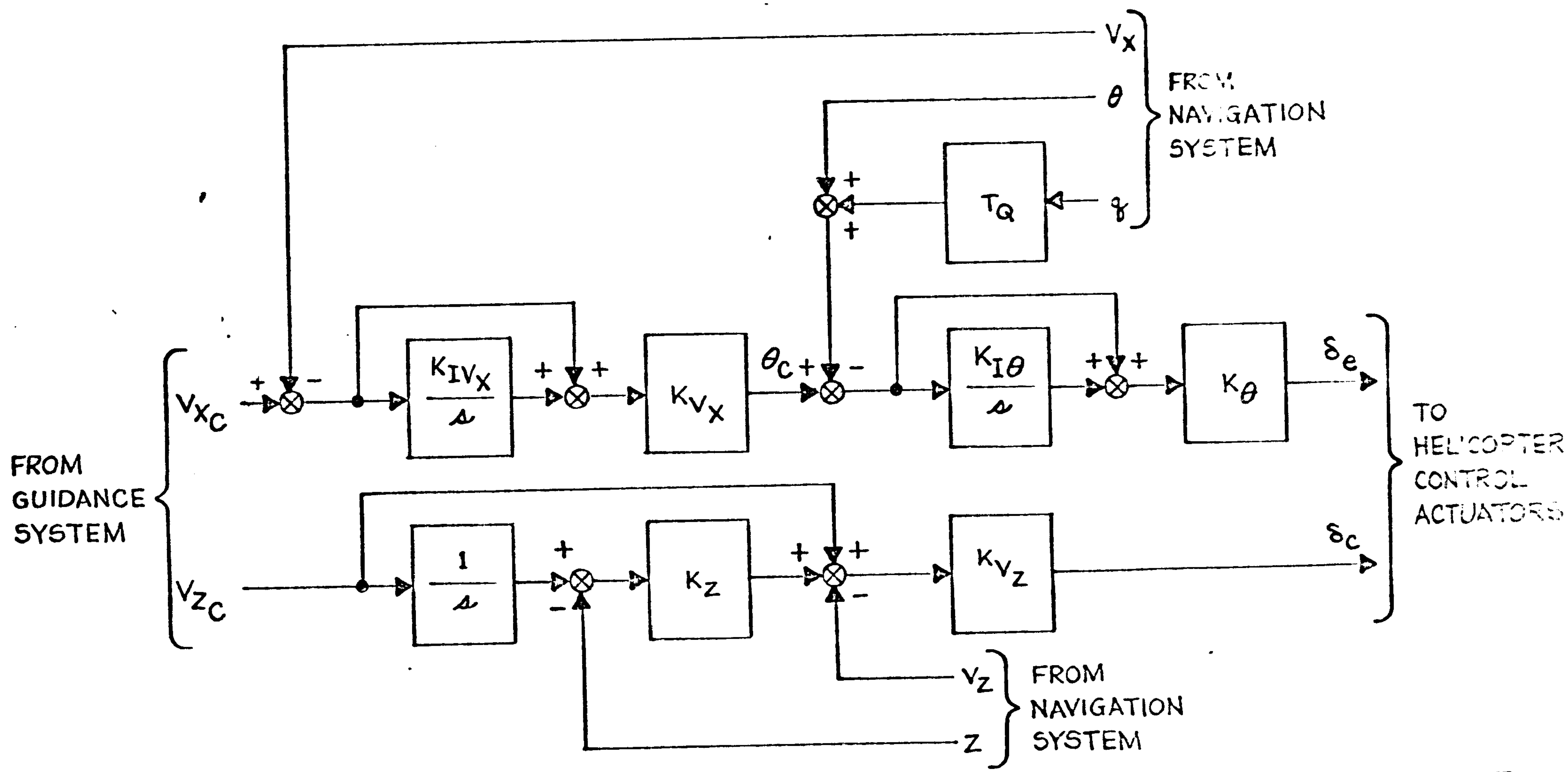

$K_{IV_X} = 0.1\ SEC^{-1}$	$T_Q = 0.5\ SEC$	$K_Z = 1.6\ SEC^{-1}$
$K_{V_X} = -0.03281$ RAD-SEC/M	$K_{I\theta} = 0.2\ SEC^{-1}$	$K_{V_Z} = -3.3335$ CM-SEC/M
	$K_\theta = 50.8$ CM/RAD	

Figure 4. Velocity-Command Flight Control System

One source of difficulty arises in the selection of the initial conditions for $V_{x_{E_I}}$, θ_{E_I} and $V_{z_{c_I}}$. The solution adopted was to assume the helicopter is initially in trim flight at the selected initial V_x, V_z and z. The initial conditions then become

$$V_{x_{E_I}}(t_i) = \frac{\theta_o(V_{x_i}, V_{z_i})}{K_{V_x} K_{V_{x_I}}} \tag{33}$$

$$\theta_{E_I}(t_i) = \frac{\delta_{e_o}(V_{x_i}, V_{z_i})}{K_\theta K_{I_\theta}} \tag{34}$$

$$V_{z_{c_I}}(t_i) = \frac{\delta_{c_o}(V_{x_i}, V_{z_i})}{K_{V_z} K_z} + z_i \tag{35}$$

Guidance System

The last important modification of LIFT was the implementation of the guidance scheme developed in the first section of this report. This requires storing five pre-calculated quantities as functions of the independent variable range, x. The stored histories are the nominal vertical postion, $z_n(x)$; the nominal velocity commands, $V_{x_{c_n}}(x)$ and $V_{z_{c_n}}(x)$; and the feedback gains, $C_{V_x}(x)$ and $C_{V_z}(x)$. At each integration step, the current range is used to interpolate the appropriate values of these quantities, and the velocity commands are generated via Eqs. (16) and (17).

SYSTEM PERFORMANCE

This section presents the results of applying the guidance scheme described above to the approach phase of a VTOL aircraft flight.

Nominal Approach Trajectory

Figure 5 illustrates the nominal approach trajectory, which was based on the one used at NASA/ERC in the flight control system analysis. As shown, the approach phase begins at a range of 3500 m (~ 11,500 ft) from touchdown at an altitude of 250 m (~ 800 ft), with the VTOL initially flying level at 25 m/sec (~ 50 kts). At 3000 m (~ 10,000 ft) from touchdown a constant vertical acceleration transition is initiated. This phase is completed at x = -2600 m (~ -8500 ft), when a flight path angle of -0.1 rad has been achieved. The constant rate of descent of 2.5 m/sec (~ 500 ft/min) is maintained until an altitude of 30 m (~ 100 ft) is reached, at which point the flare maneuver is commenced. The flare itself consists of constant vertical and horizontal accelerations such that the aircraft levels off at an altitude of 10 m (~ 30 ft). The horizontal deceleration is maintained until the velocity has been reduced to 5 m/sec (~ 10 kts). This condition is held for 20 seconds to provide the pilot an opportunity to verify system performance. The remainder of the trajectory consists of a final deceleration to hover above the runway followed by a vertical descent to touchdown.

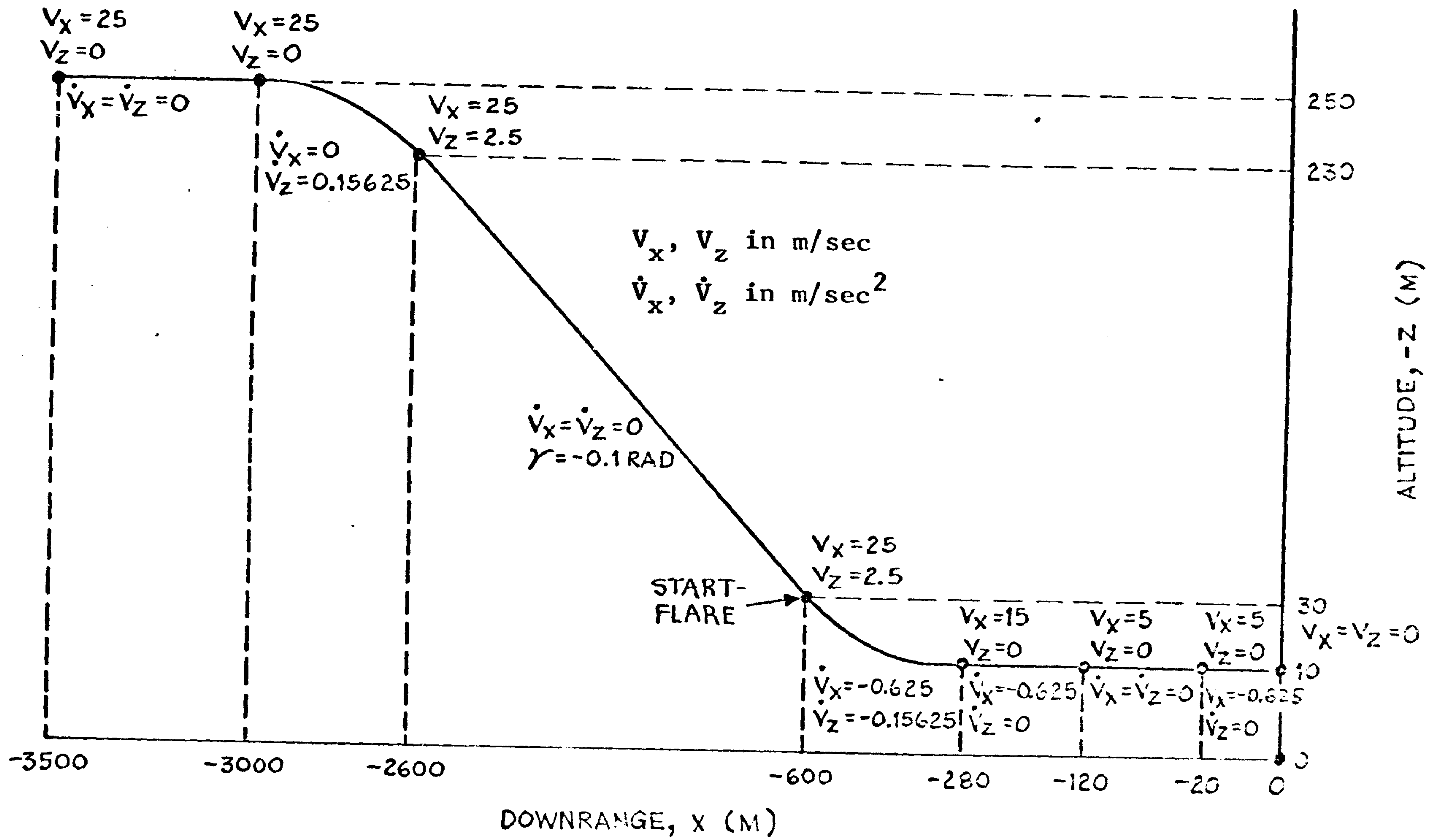

Figure 5. Nominal Approach Trajectory

Figure 6 shows the nominal approach path on a speed vs altitude plot. The shaded areas indicate the "dead man" curves which have been assumed for the YHC-1A. These are the areas from which a safe recovery could not be effected in the event of a single engine failure. Since actual data for the YHC-1A vehicle were unavailable, the "avoid" areas in Figure 6 were approximated from corresponding curves for the Vertol CH-46D vehicle (Reference 5).

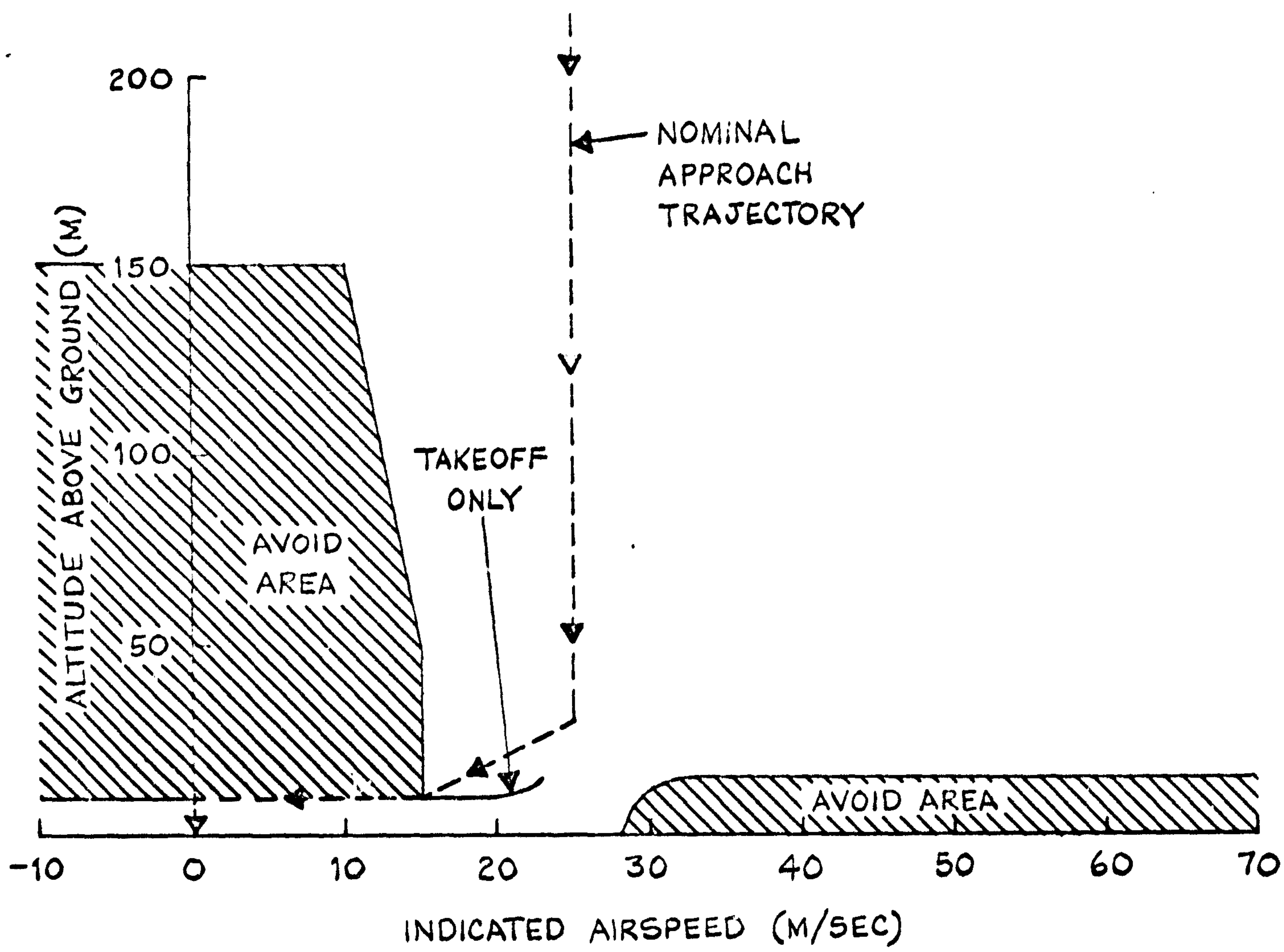

Figure 6. YHC-1A Height for Safe Landing After Single Engine Failure (Assumed) and Nominal Approach Path

Guidance Feedback Gains

Using the nominal trajectory described above, approach guidance feedback gains were calculated by integrating Eq.(14) backwards, i.e. away from the touchdown point. Figures 7 and 8 show the gains for the approach to the start of flare. The weighting parameters which were used to obtain these gains are given in Table 2. The value of δz_o ($\sim\infty$) was selected such that enroute altitude deviations are not penalized. Hence the resulting gains do not attempt to return the vehicle to the nominal path from an off-nominal altitude, but rather try to funnel it into the desired terminal (start-flare) altitude at the final range. It is typical of terminal controllers for the gain magnitudes to increase rapidly as the final range is approached. Note that C_{V_x} is zero during level flight ($x < -3000$ m), i.e. the down-range velocity command is entirely independent of altitude errors.

Table 2. Weighting Parameters for Approach Guidance Gains.

δz_f	1.0 m
δz_o	10^{10} m
$\delta V_{x_{c_o}}$	0.1 m/sec
$\delta V_{z_{c_o}}$	0.1 m/sec

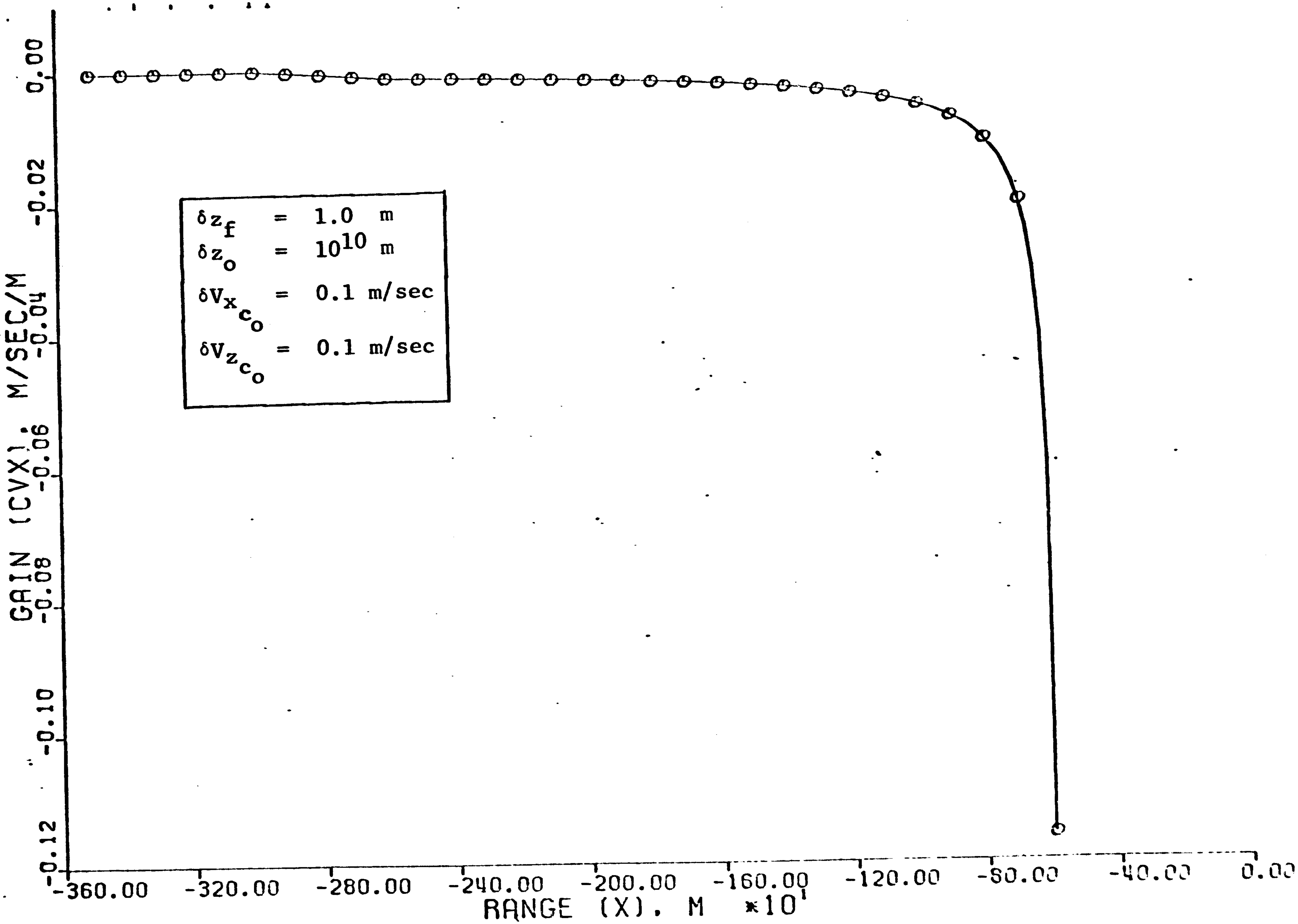

Figure 7. Downrange Velocity Gain for Approach to Start-Flare

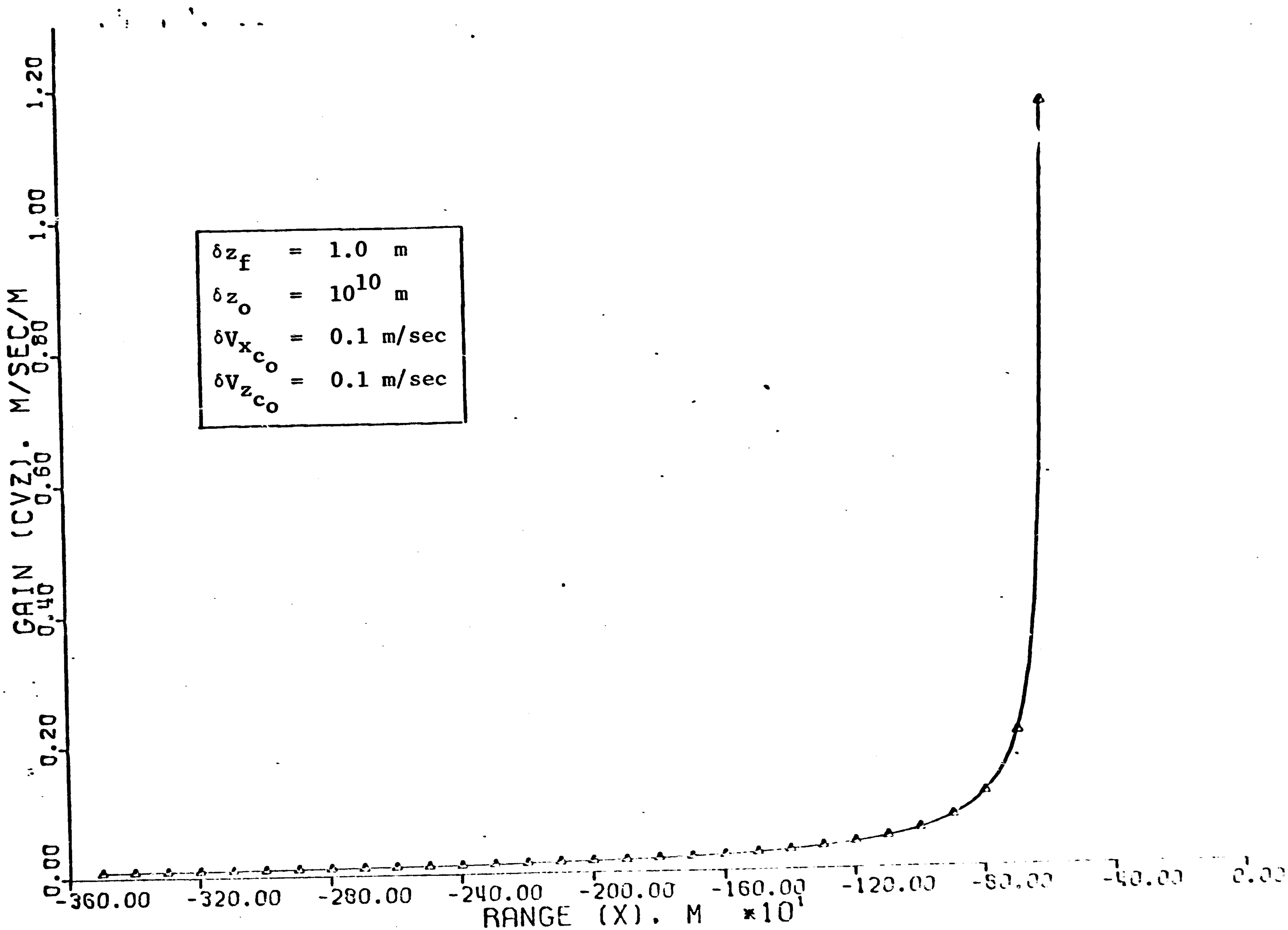

Figure 8. Vertical Velocity Gain for Approach to Start-Flare

As mentioned in the simulation discussion, the six guidance quantities must be stored as functions of range from touchdown. Table 3 gives the stored values which were used for the simulation results that are presented below. Only seven sets of data were stored. The values of the gains given in Table 3 were chosen to give a good piecewise linear fit to the continuous curves shown in Figures 7 and 8.

Simulation Results

A number of approaches were simulated with various off-nominal initial conditions and winds. These are summarized in Table 4, which shows the errors in the altitude and velocities at the start-flare range. The table also indicates for each case the number of the figure which plots the altitude, down-

Table 3. Stored Guidance Quantities for Approach to Start-Flare

x (m)	z_n (m)	$V_{x_{c_n}}$ (m/sec)	$V_{z_{c_n}}$ (m/sec)	C_{V_x} (sec^{-1})	C_{V_z} (sec^{-1})
-3500	-250	25.0	0	0	0.0085
-3000	-250	25.0	0	0	0.0103
-2600	-230	25.0	2.5	-0.00123	0.0123
-1400	-110	25.0	2.5	-0.0027	0.027
- 900	- 60	25.0	2.5	-0.006	0.06
- 700	- 40	25.0	2.5	-0.018	0.18
- 600	- 30	25.0	2.5	-0.06	0.6

range velocity and vertical velocity histories versus the range from touchdown. For comparison, the nominal profiles given in Table 4 are also shown in Figures 9 through 23.

Table 4. Summary of Approaches Simulated and Resulting Terminal Errors

Run No.	Figure No.	Initial Conditions	Winds (m/sec)	δh_f (m)	δV_{x_f} (m/sec)	δV_{z_f} (m/sec)
10	9	Nominal	None	0	0	0
11	10	δh_i = +50 m	None	+ 0.40	-0.05	0.26
12	11	δh_i = -50 m	None	- 0.41	0.05	-0.27
13	12	δV_{x_i} = -10 m/sec	None	0	0	0
14	13	δV_{x_i} = +10 m/sec	None	0	0	0
15	14	δV_{z_i} = - 5 m/sec	None	+ 0.01	0	0
16	15	δV_{z_i} = + 5 m/sec	None	- 0.01	0	-0.01
19	16	Nominal	W_x = 10 m/sec	- 0.01	0	0
20	17	Nominal	W_x = 10 m/sec	0	0	0
21	18	Nominal	W_x = (5 +.02h)m/sec	- 0.01	-0.06	-0.01
22	19	Nominal	W_x = (-5 -.02h)m/sec	+ 0.06	0.12	0.04
23	20	Nominal	W_z = +5 m/sec	- 0.01	0	-0.01
24	21	Nominal	W_z = -5 m/sec	+187.93	-7.72	-2.58
25	22	Nominal	M_i = + 10%	0	0	0
26	23	Nominal	M_i = - 10%	0	0	0

Figure 9 illustrates the system performance for nominal initial conditions and no winds. Except for the transition from level flight to the glide slope, the position and velocities are practically identical to the stored nominal values. In fact, the actual position during the transition is very close to the true nominal, since the stored nominal indicated on the figure is a piecewise linear approximation of the true nominal.

Figures 10 and 11 show the effects of initial altitude errors of ± 50 m. Notice that the guidance system smoothly funnels the helicopter into the nominal start-flare point. Approaches with initial downrange velocity errors of ± 10 m/sec and vertical velocity errors of ± 5 m/sec are shown in Figures 12-15. In all cases the velocity errors are quickly nulled with only very minor altitude errors resulting during the first few seconds of the approach.

The effects of a constant tailwind and headwind of 10 m/sec are shown to be practically negligible in Figures 16 and 17, respectively. Figures 18 and 19 present the results with constant wind shears, i.e. linear variation of wind speed with altitude; these produce a very small steady-state error in downrange velocity. Constant vertical winds of ± 5 m/sec are examined in Figures 20 and 21. A vertical wind toward the ground has very little effect; however, the helicopter cannot penetrate a constant updraft since the collective stick displacement command reaches its lower limit (0 cm).* Finally, Figures 22 and 23 reveal that initial mass errors of ± 10% have practically no effect on the system's performance.

*Allowable control travel limits are included in Appendix B.

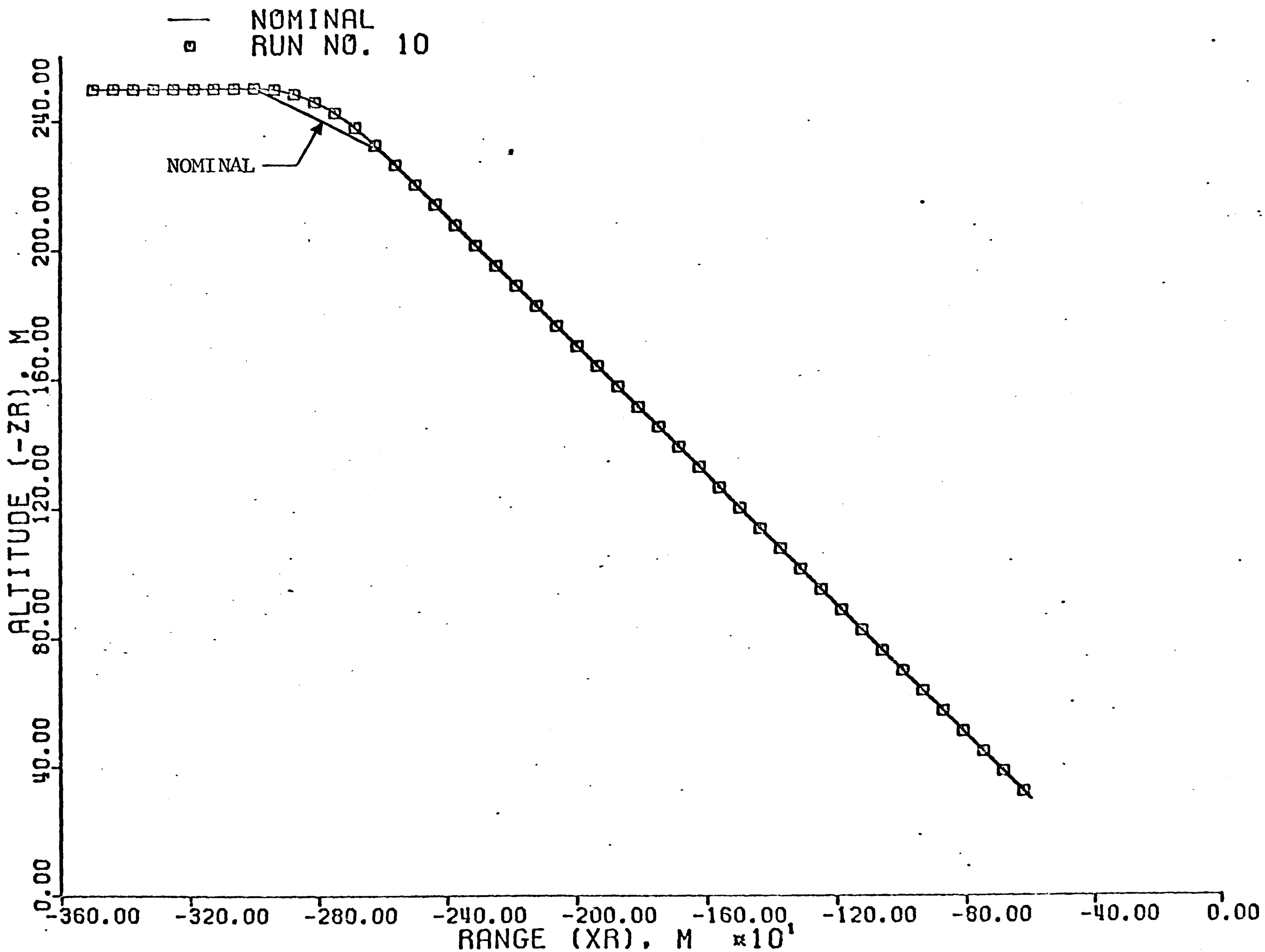

Figure 9a. Altitude vs Range with Nominal Initial Conditions

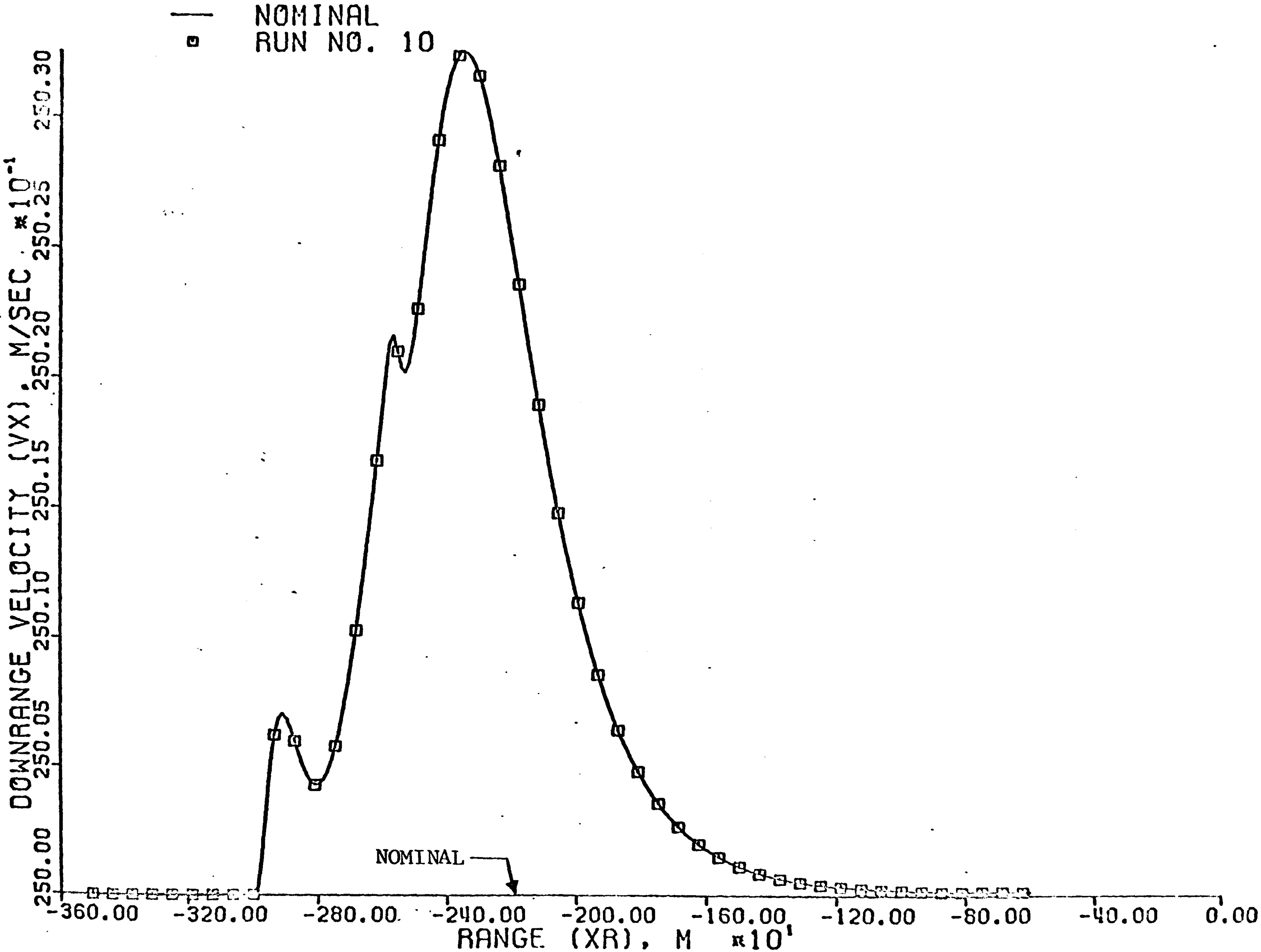

Figure 9b. Downrange Velocity vs Range with Nominal Initial Conditions

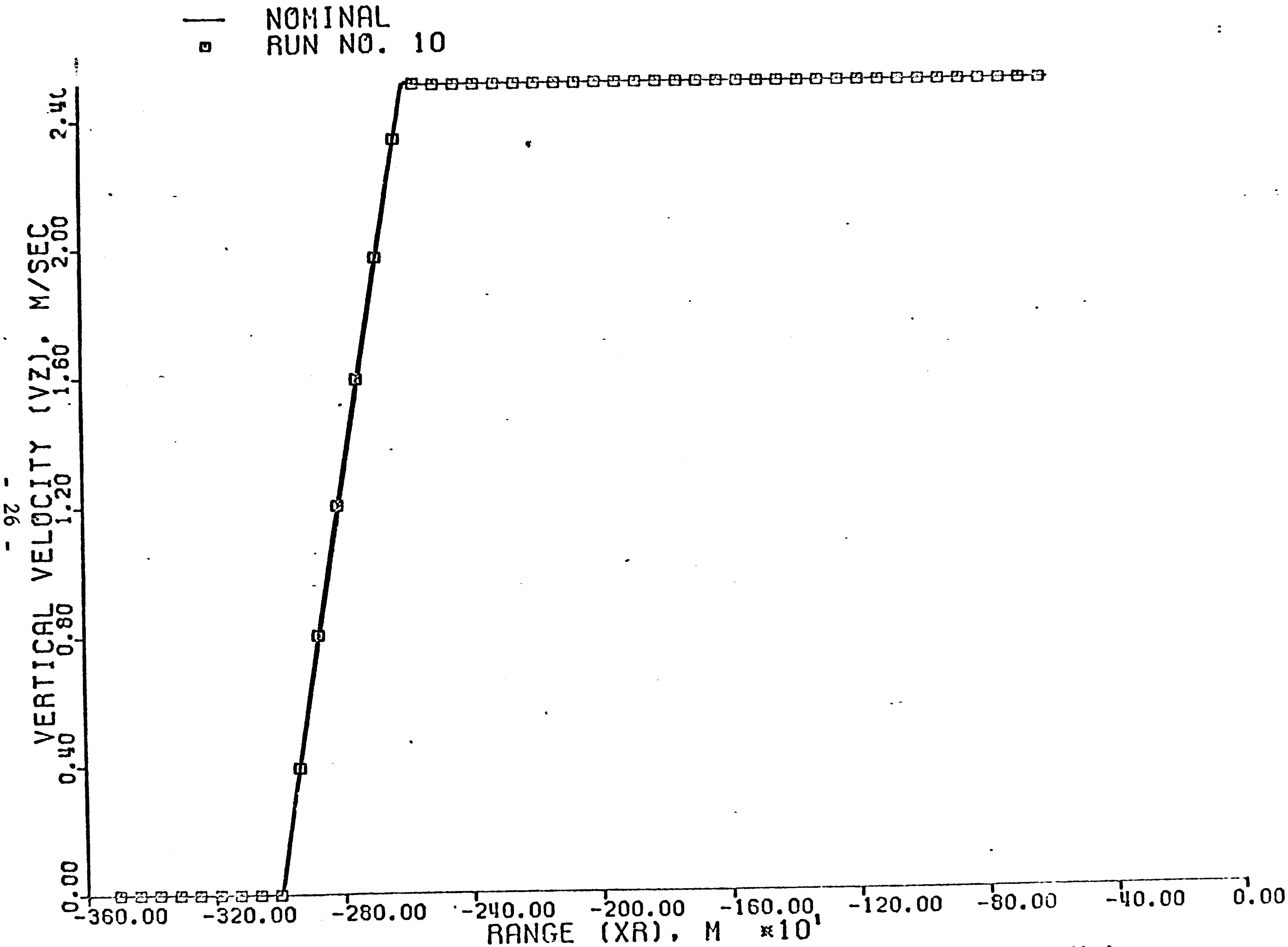

Figure 9c. Vertical Velocity vs Range with Nominal Initial Conditions

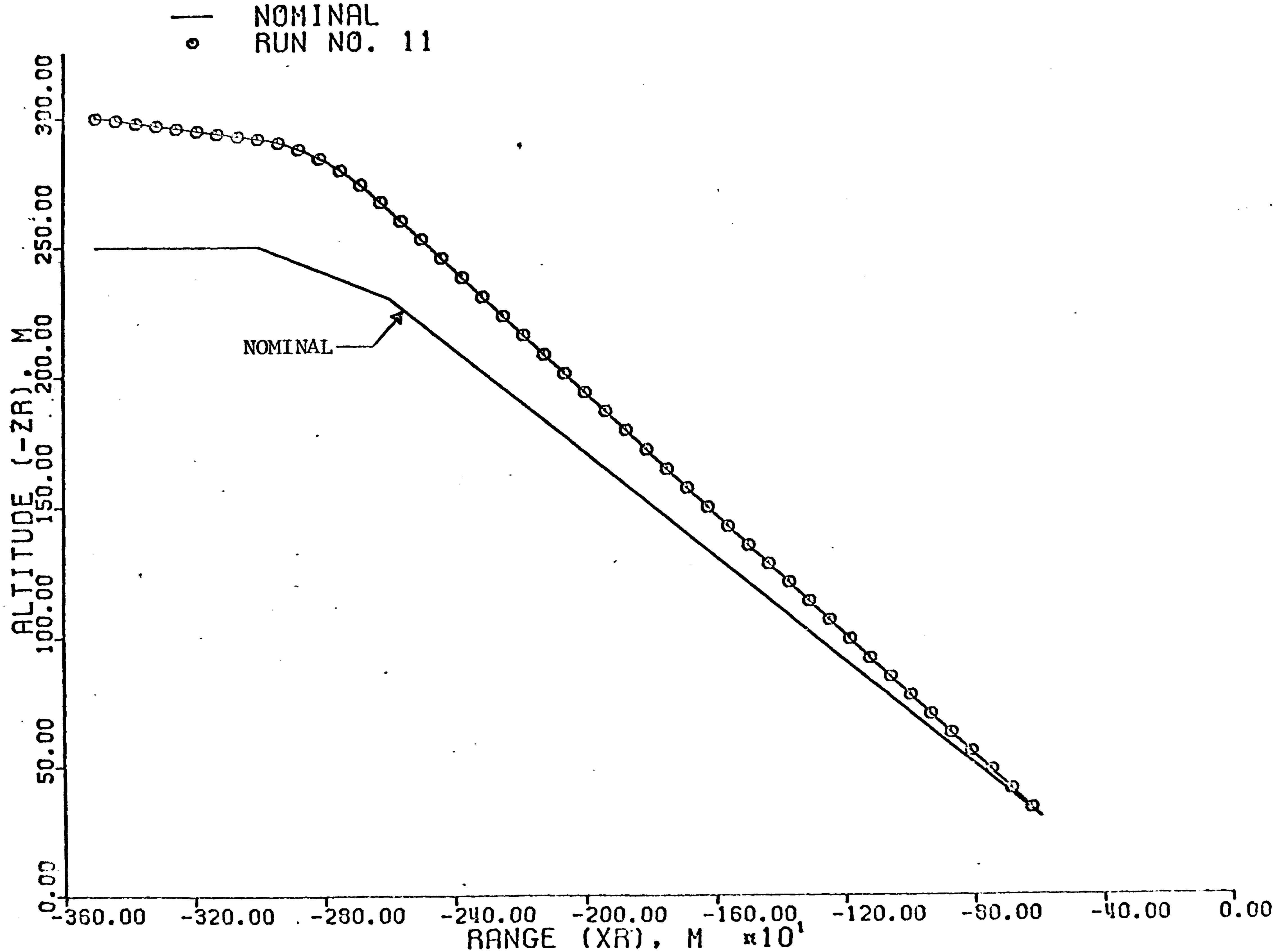

Figure 10a. Altitude vs Range with $\delta h_i = +50$ m

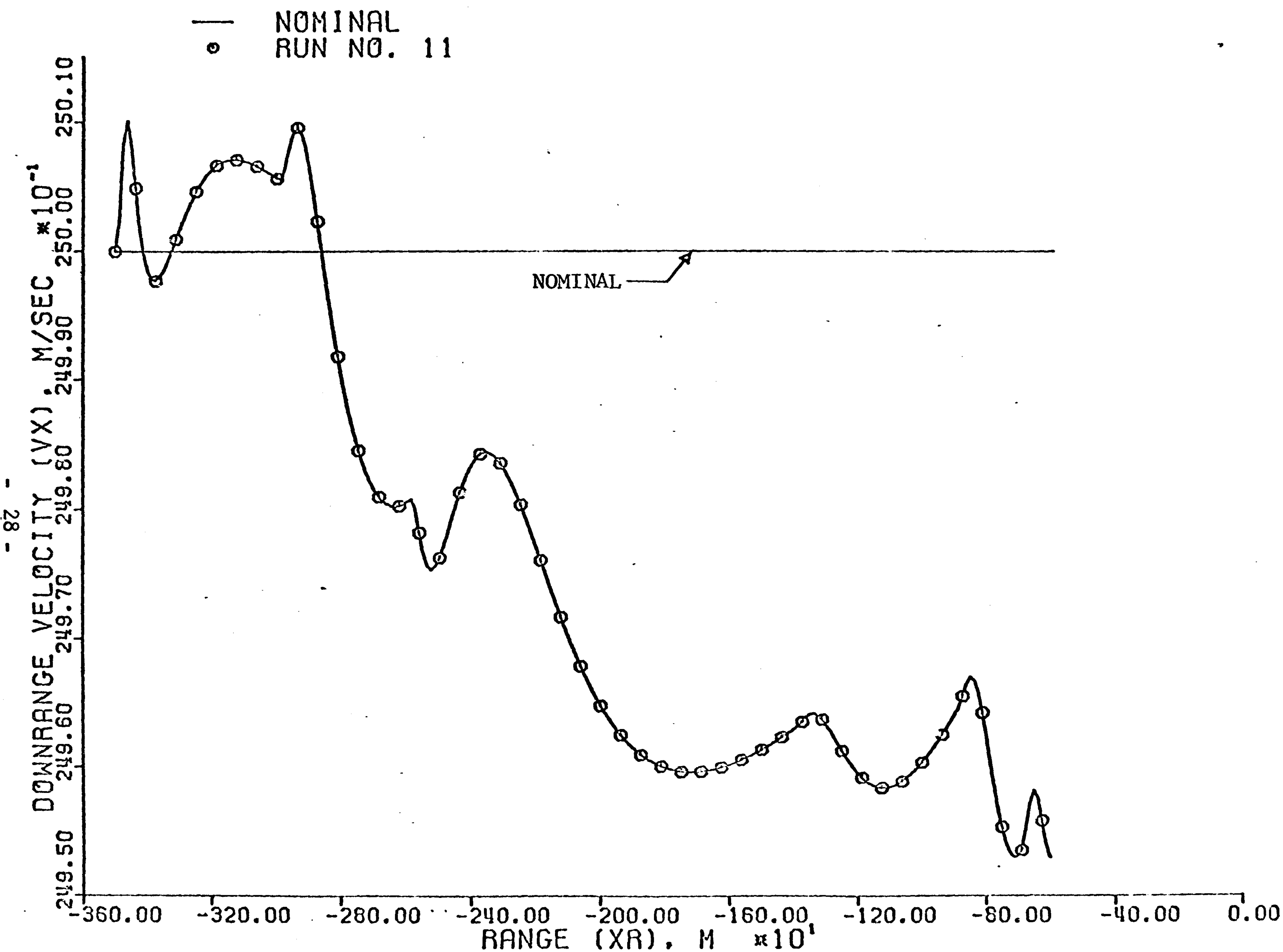

Figure 10b. Downrange Velocity vs Range with $\delta h_i = +50$ m

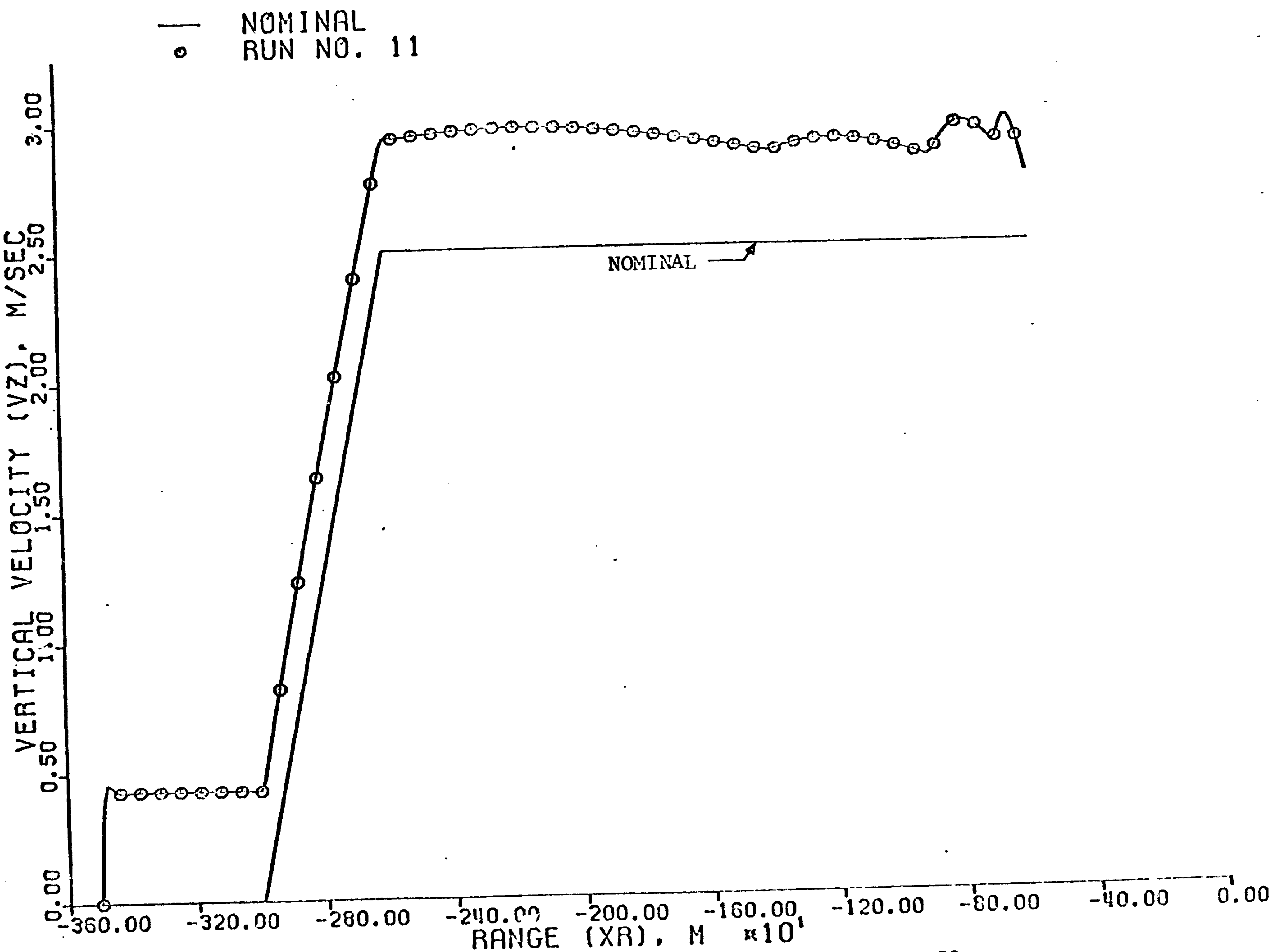

Figure 10c. Vertical Velocity vs Range with δh_i = +50 m

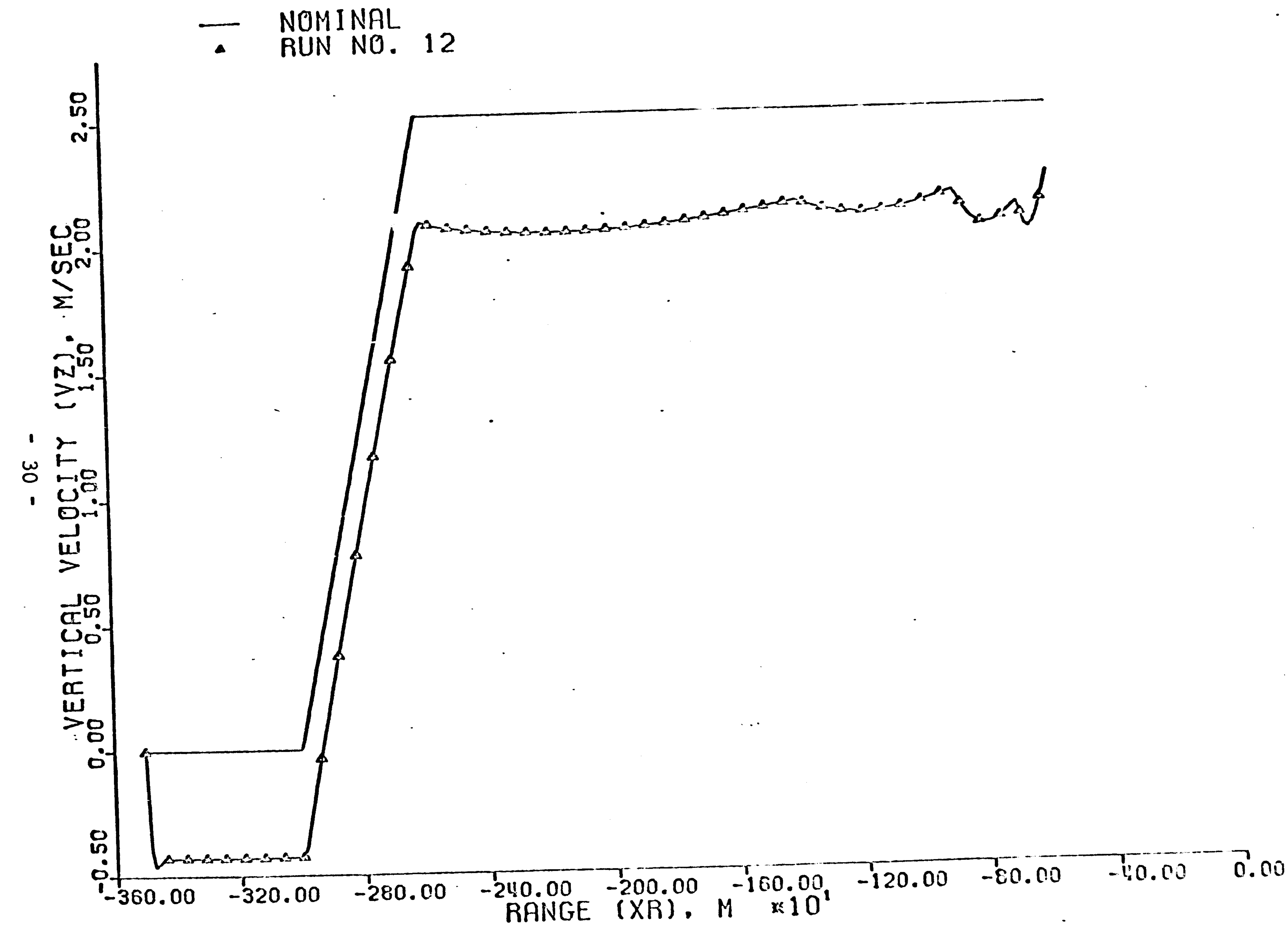

Figure 11a. Vertical Velocity vs Range with $\delta h_i = -50$ m

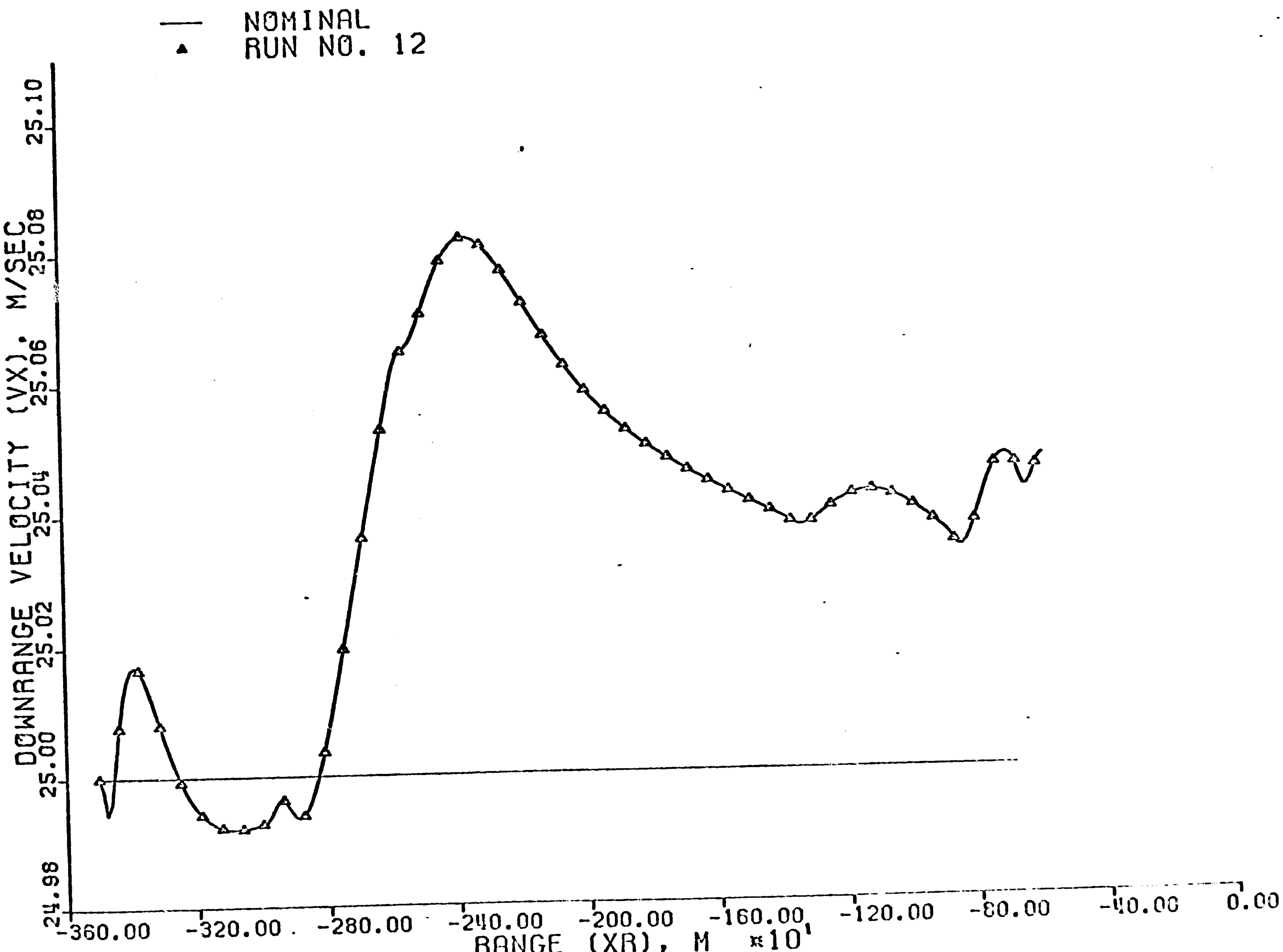

Figure 11b. Downrange Velocity vs Range with δh_i = -50 m

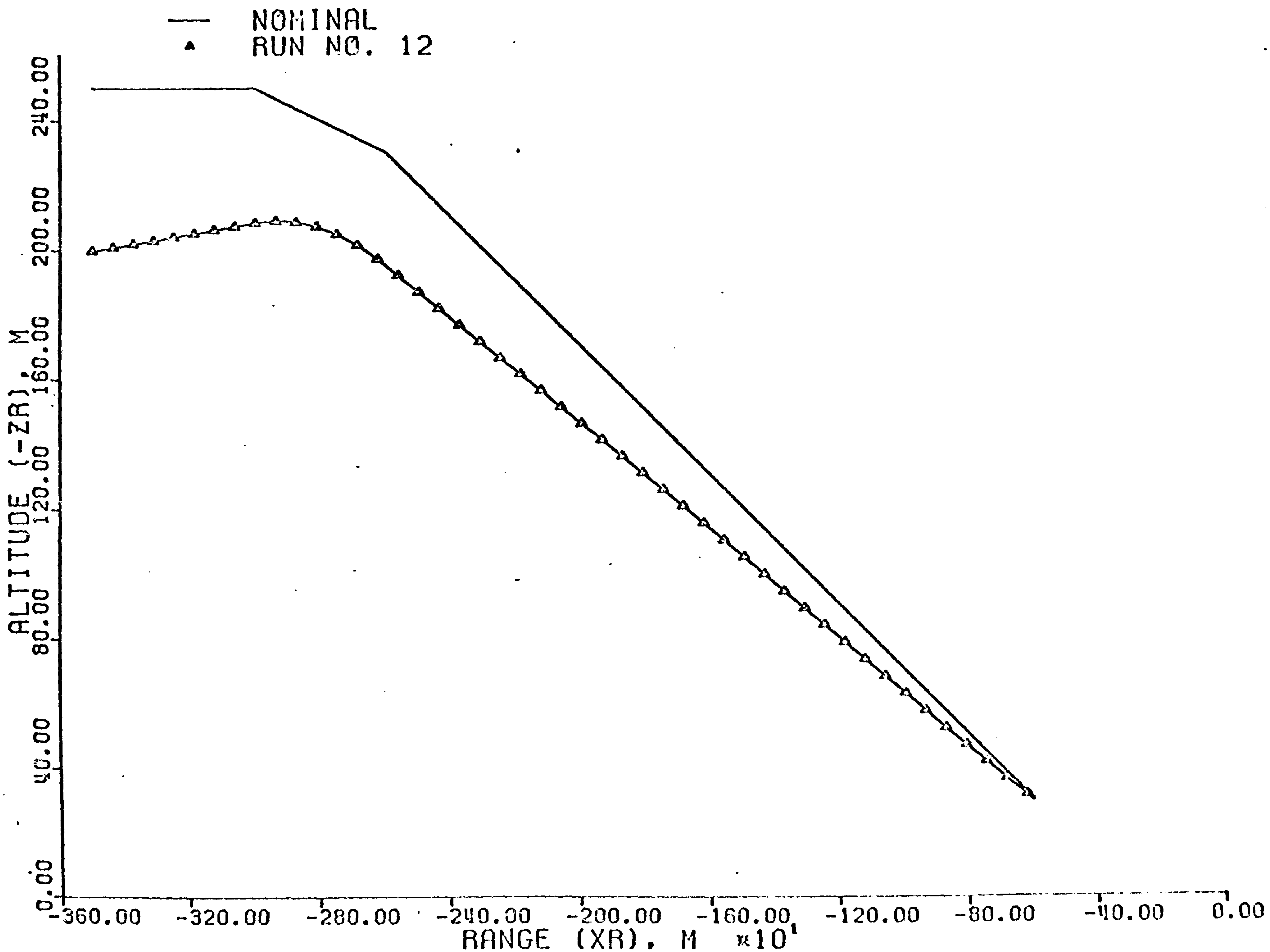

Figure 11c. Altitude vs Range with δh_i = -50 m

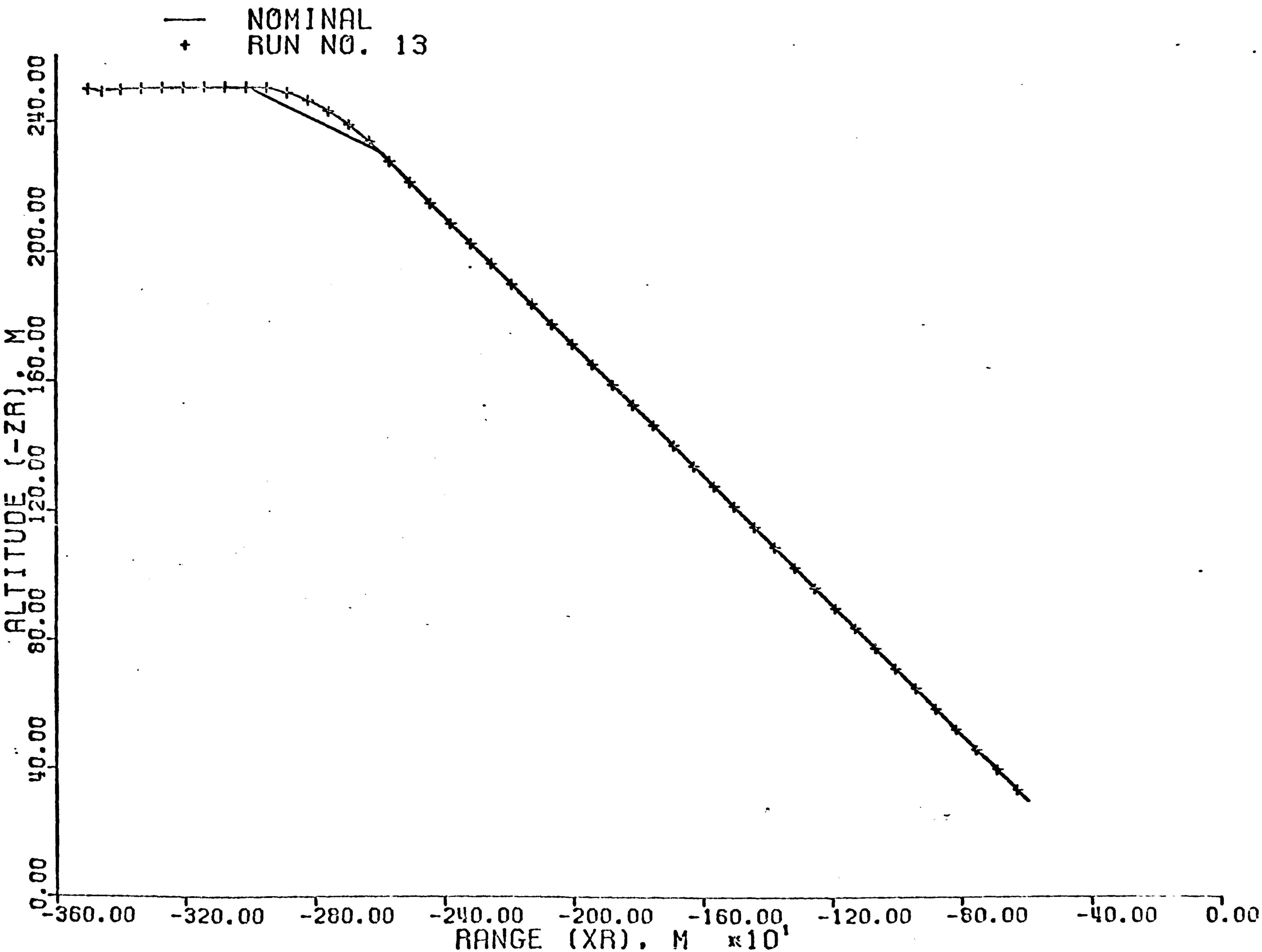

Figure 12a. Altitude vs Range with $\delta V_{x_i} = -10$ m/sec

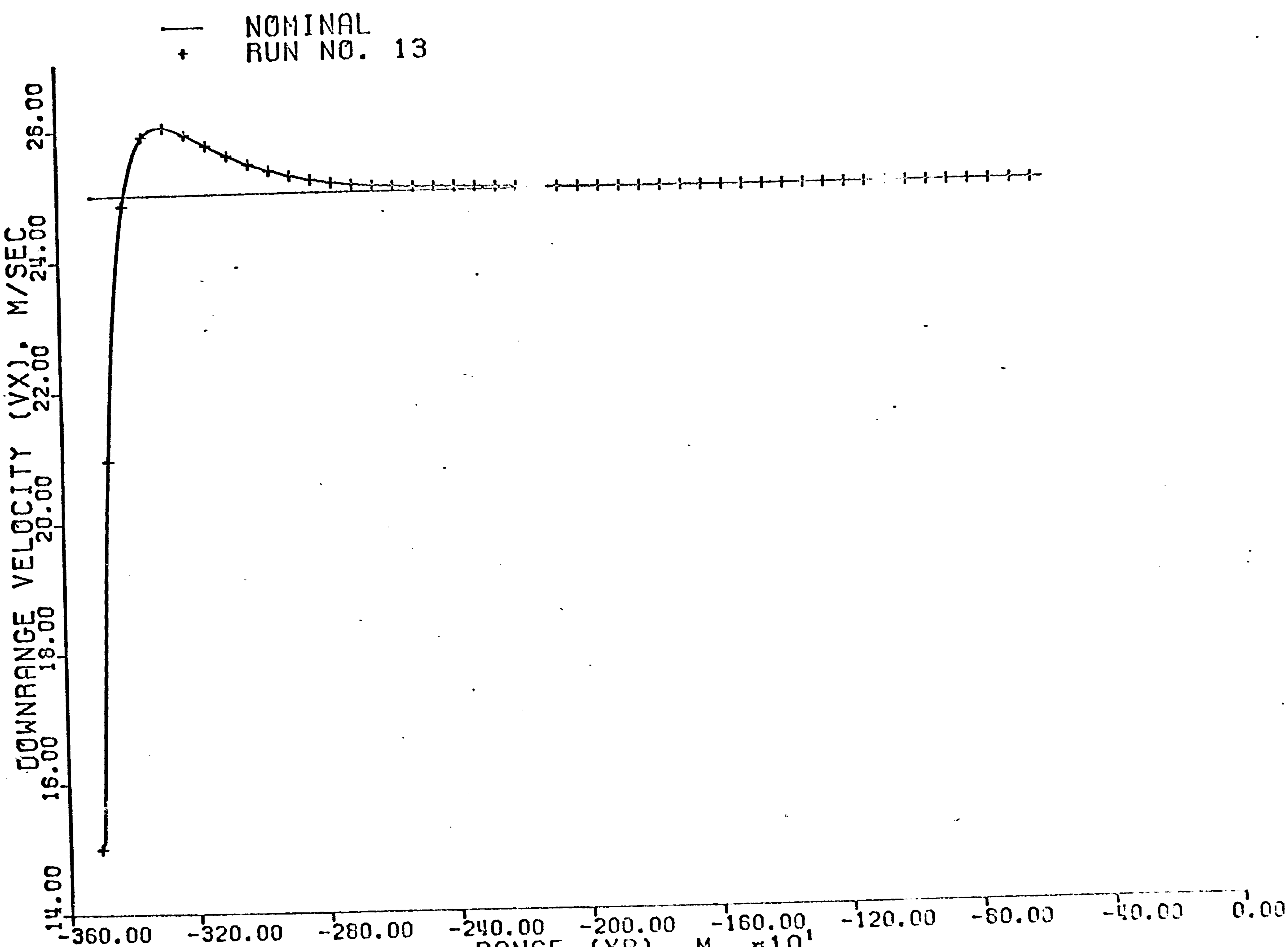

Figure 12b. Downrange Velocity vs Range with $\delta V_{x_i} = -10$ m/sec

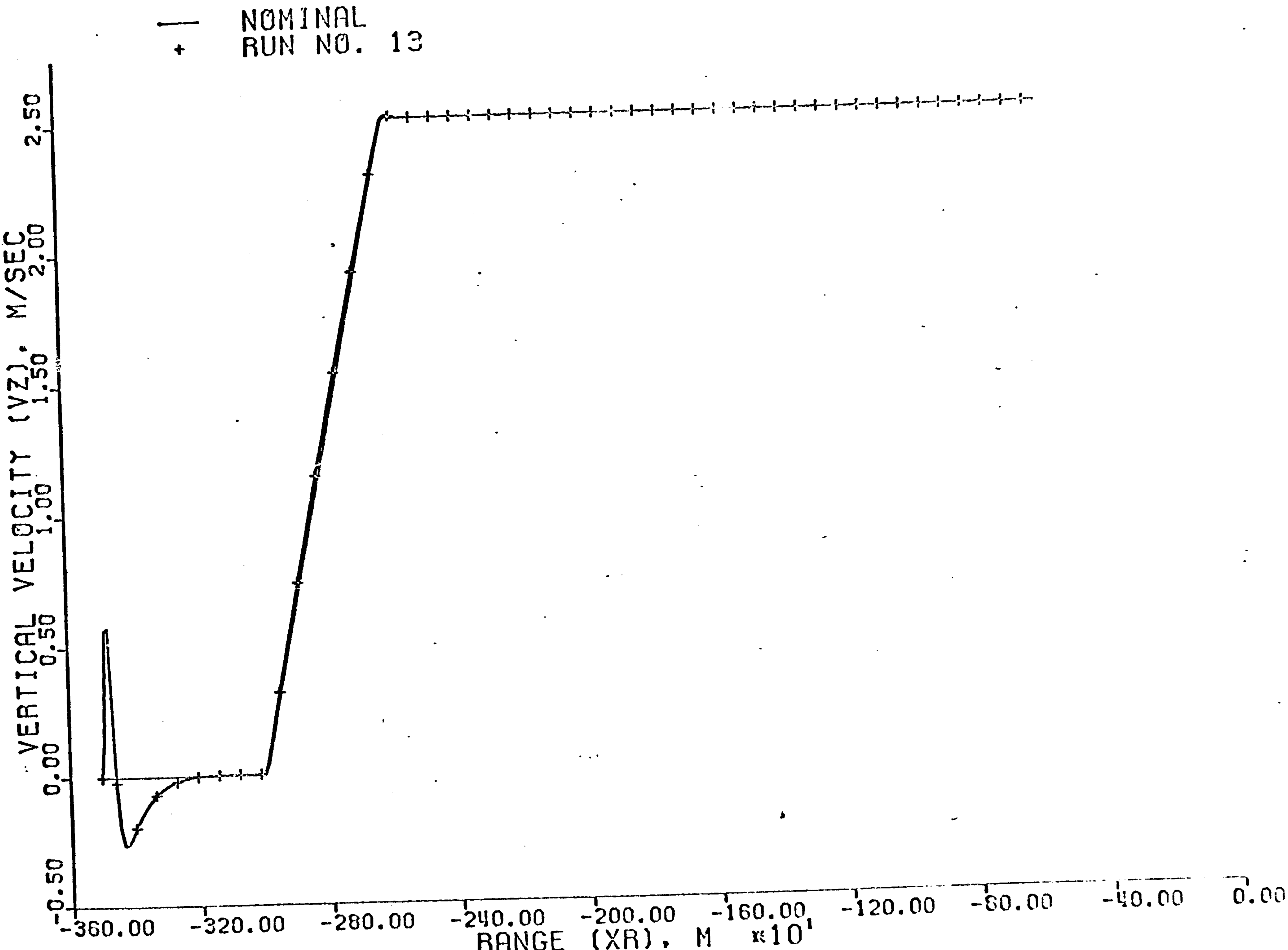

Figure 12c. Vertical Velocity vs Range with $\delta V_{x_i} = -10$ m/sec

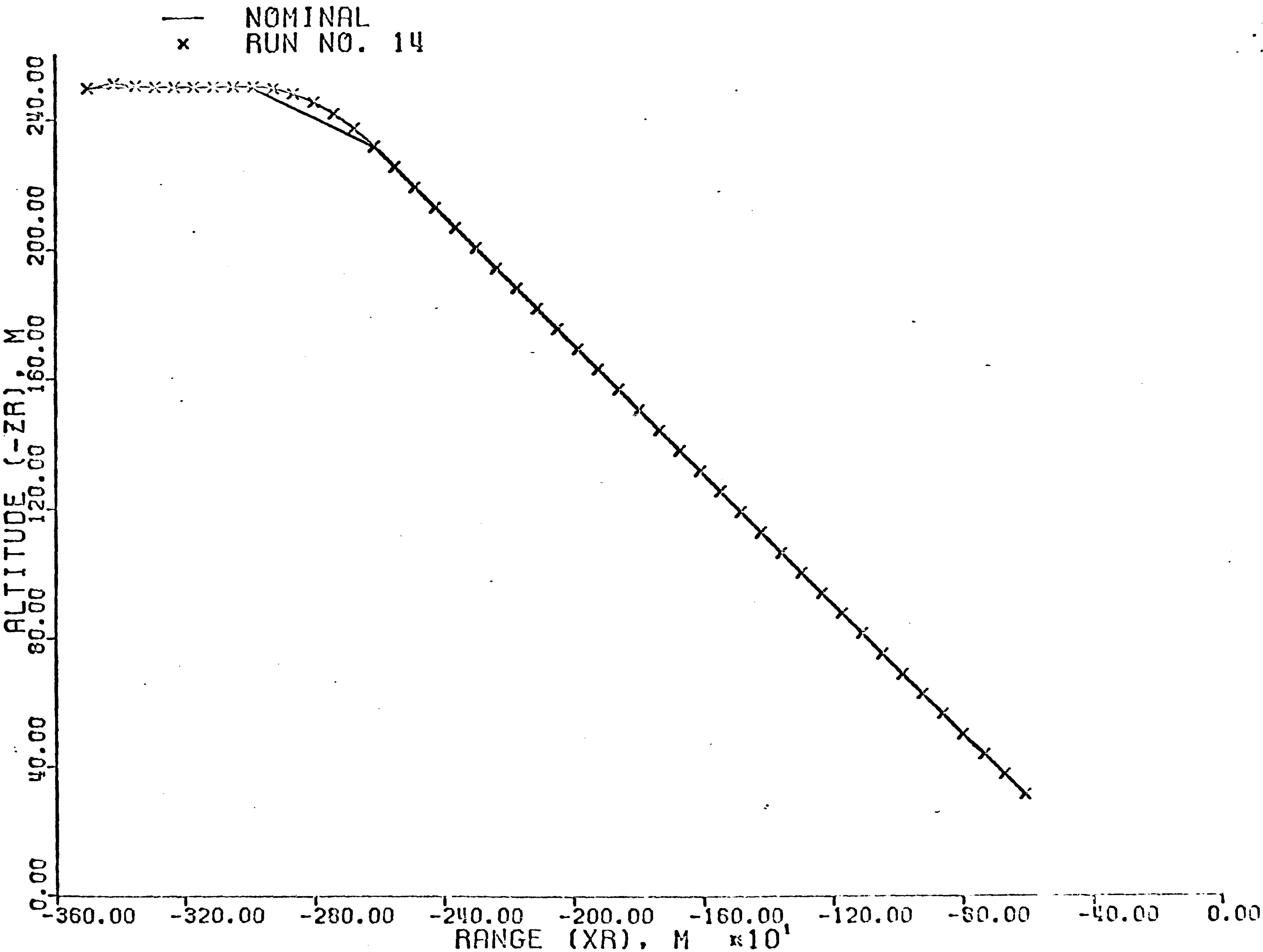

Figure 13a. Altitude vs Range with $\delta V_{x_i} = +10$ m/sec

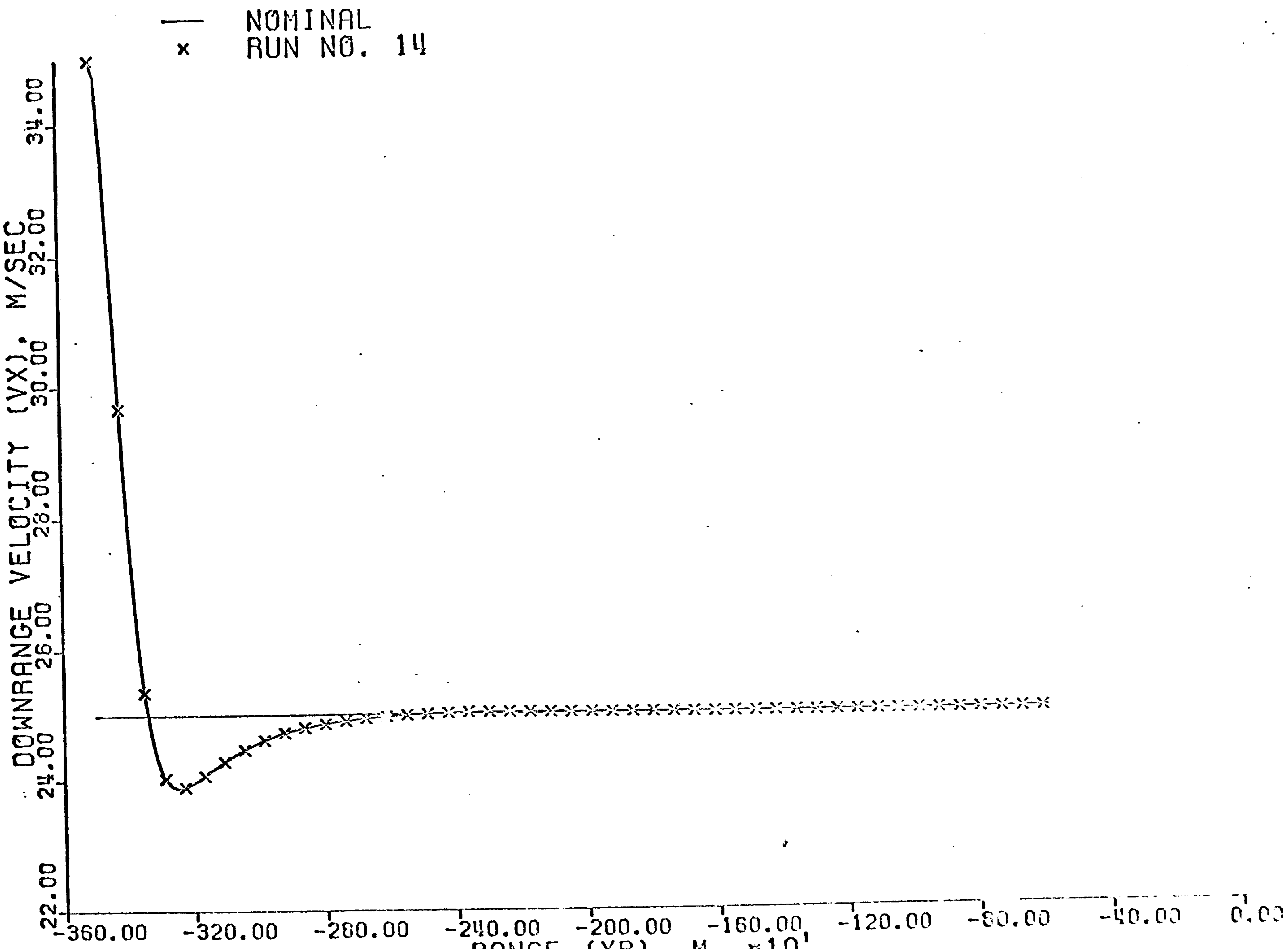

Figure 13b. Downrange Velocity vs Range with $\delta V_{x_i} = +10$ m/sec

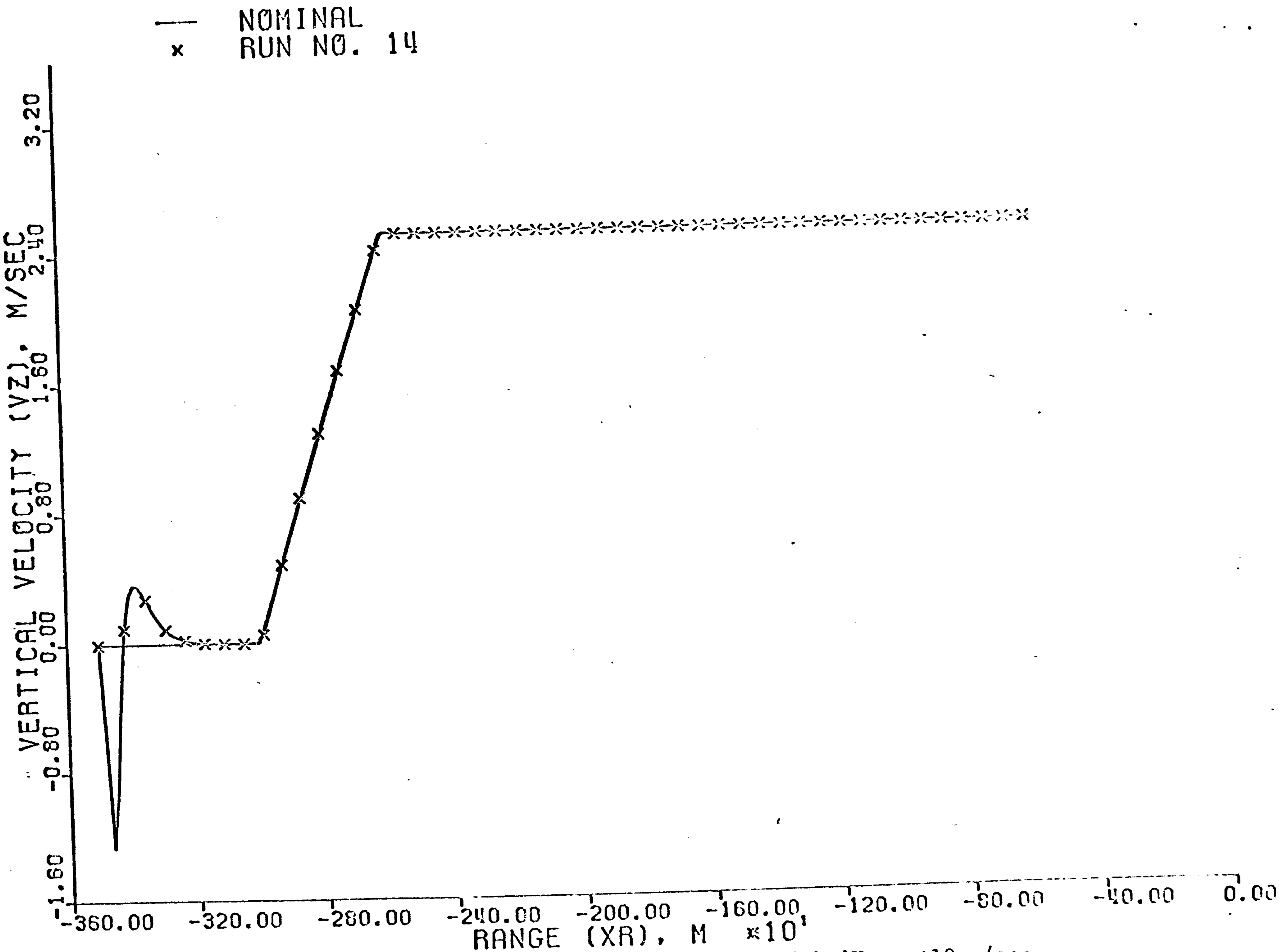

Figure 13c. Vertical Velocity vs Range with $\delta V_{x_i} = +10$ m/sec

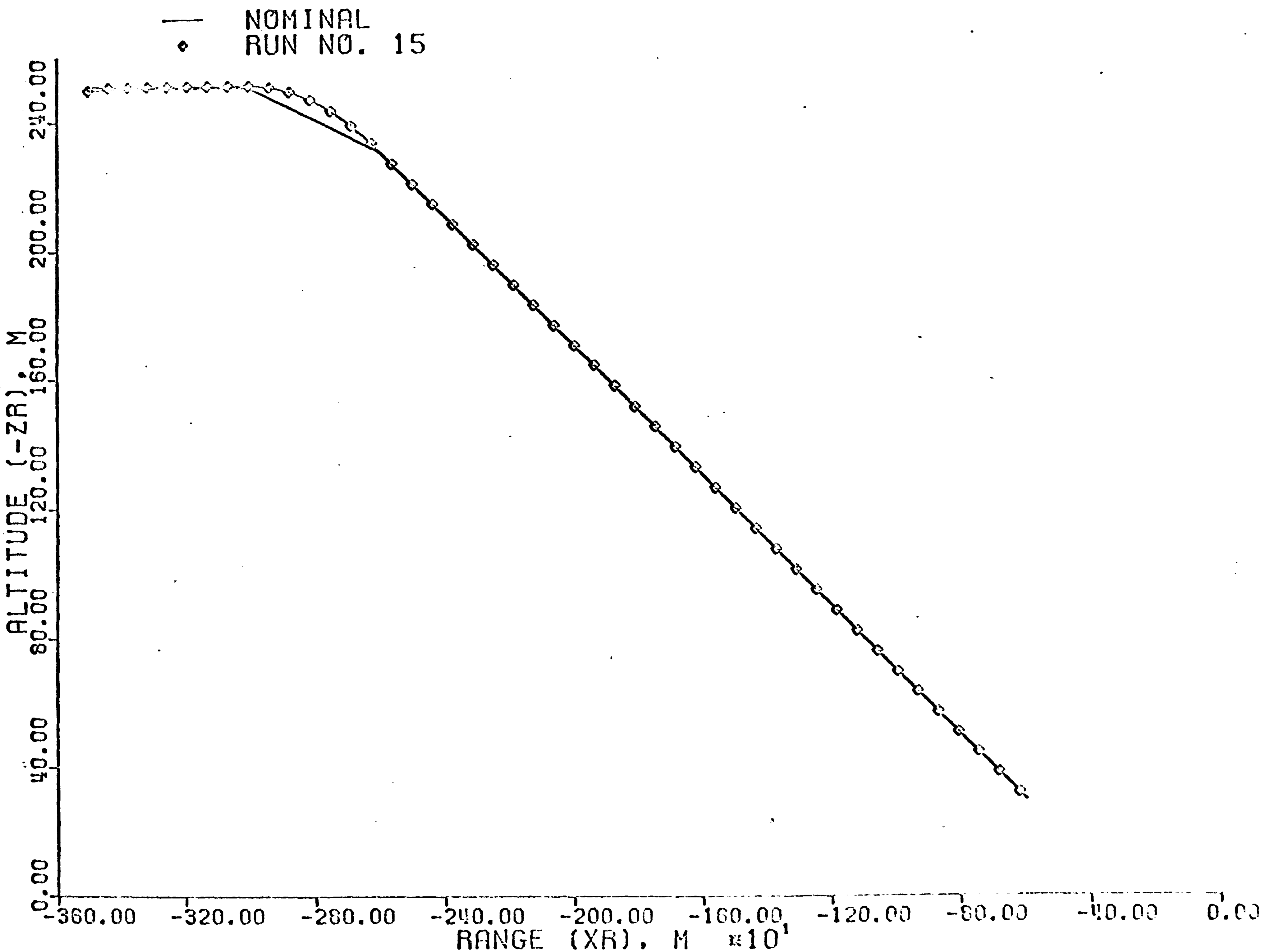

Figure 14a. Altitude vs Range with $\delta V_{z_i} = -5$ m/sec

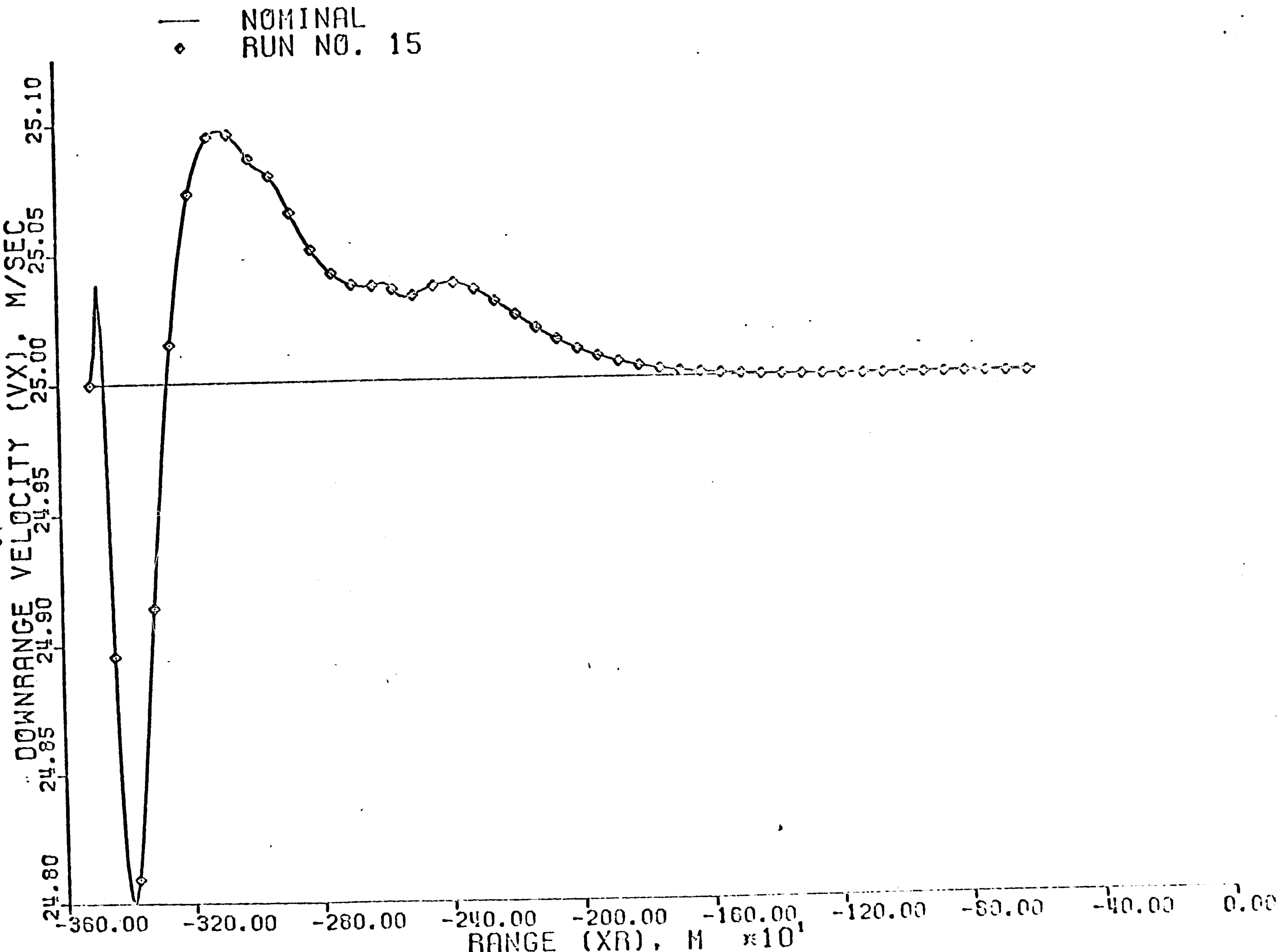

Figure 14b. Downrange Velocity v. Range with $\delta V_{z_i} = -5$ m/sec

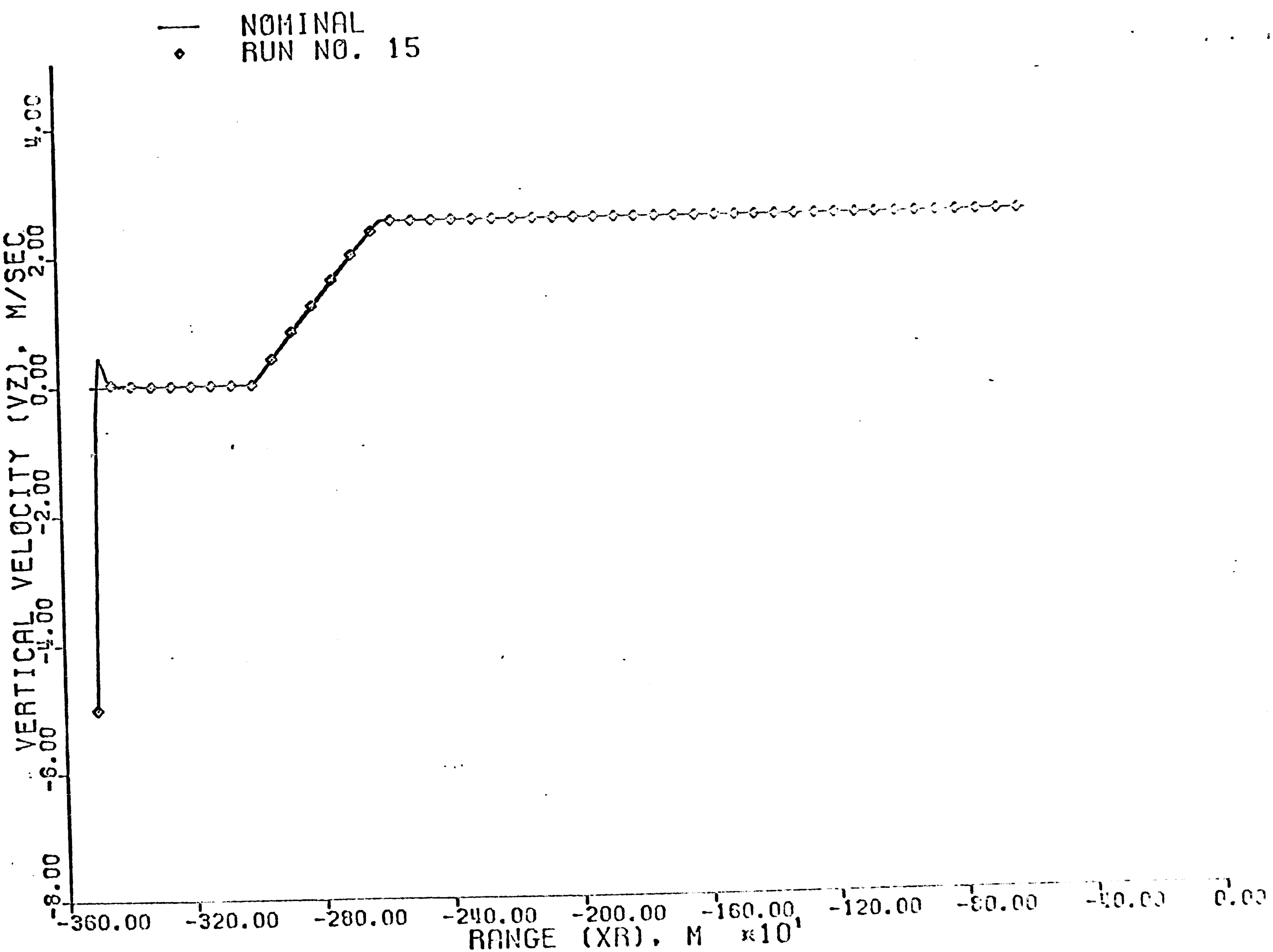

Figure 14c. Vertical Velocity vs Range with $\delta V_{z_i} = -5$ m/sec

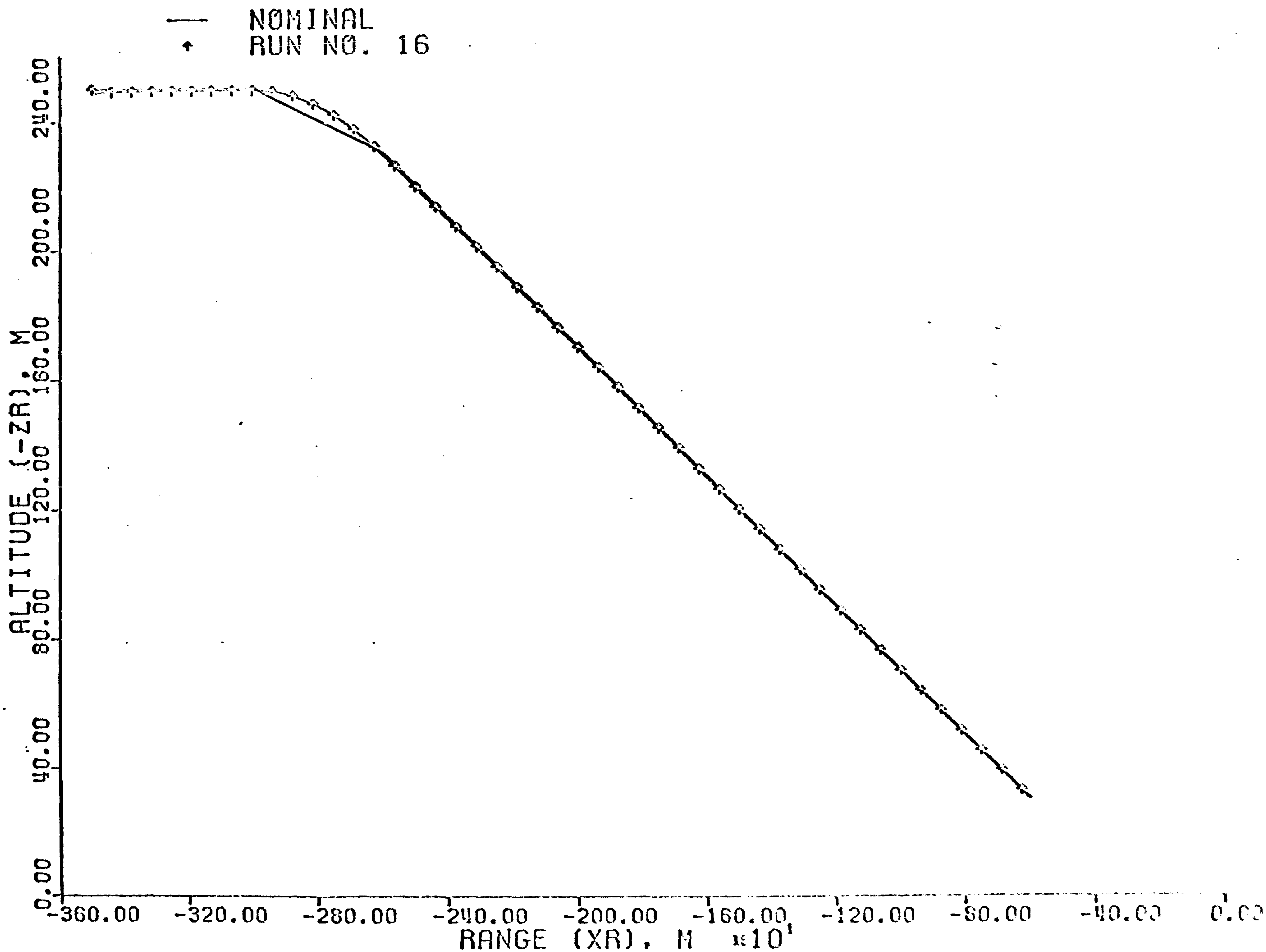

Figure 15a. Altitude vs Range with $\delta V_{z_i} = +5$ m/sec

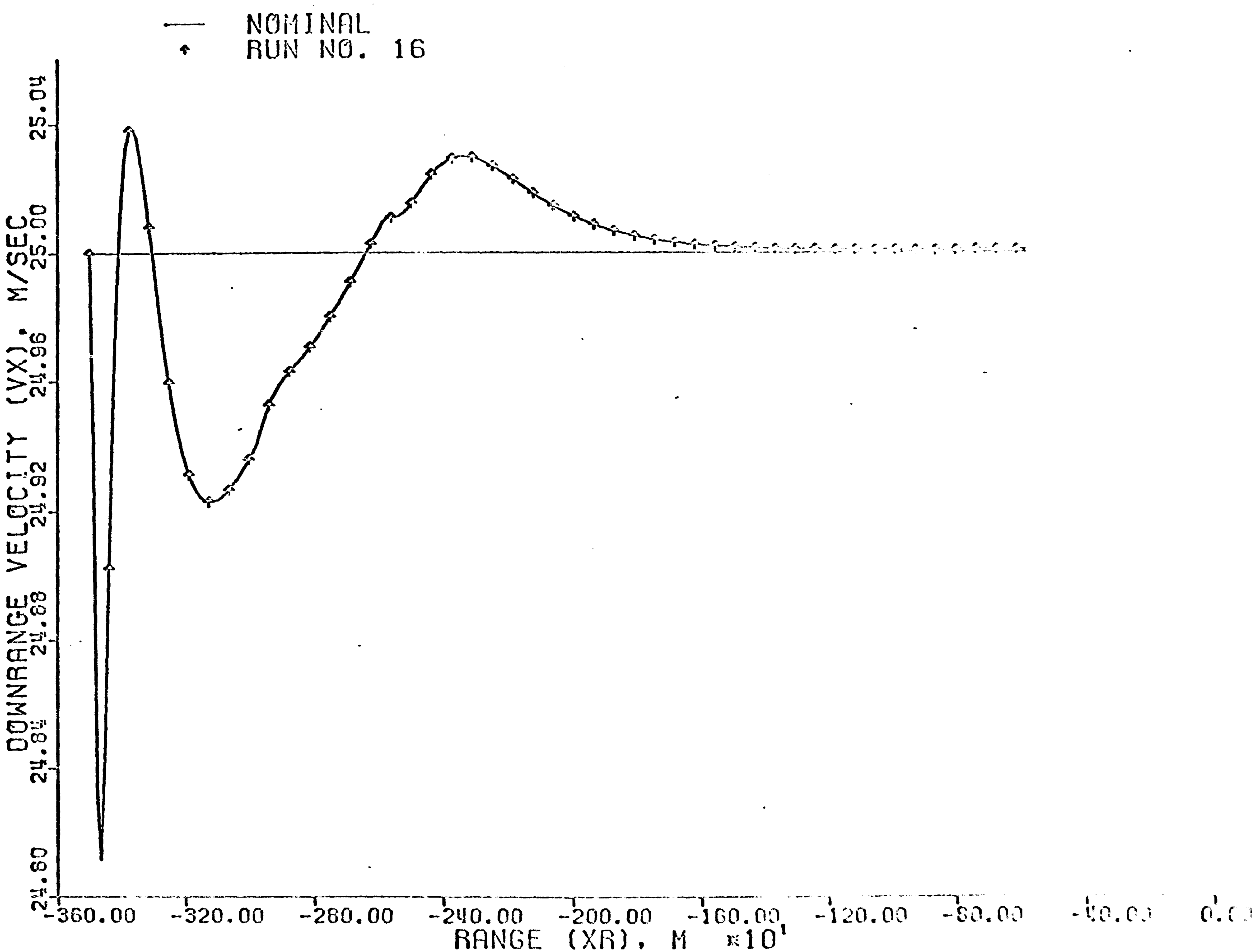

Figure 15b. Downrange Velocity vs Range with δV_{z_i} = +5 m/sec

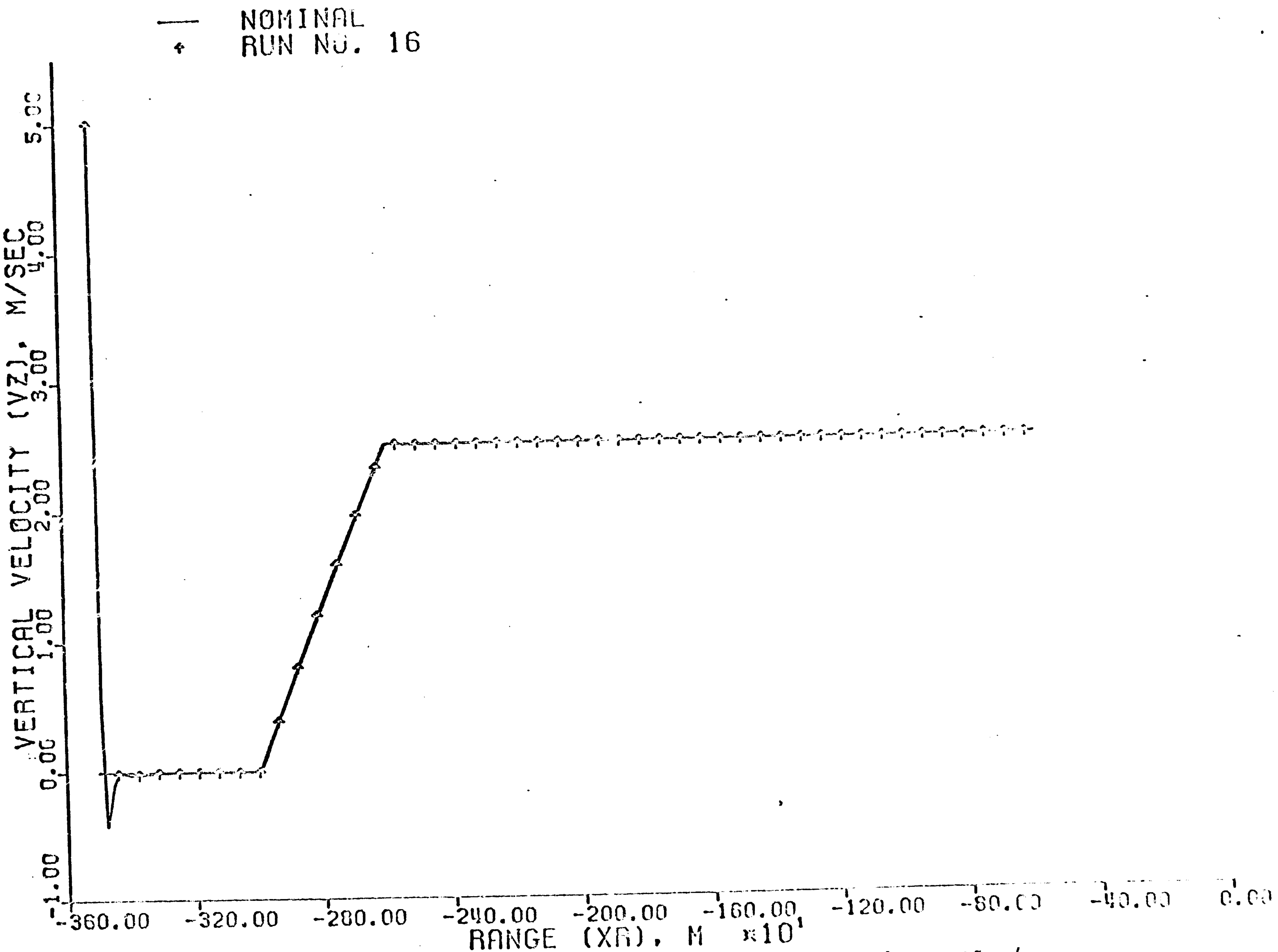

Figure 15c. Vertical Velocity vs Range with $\delta V_{z_i} = +5$ m/sec

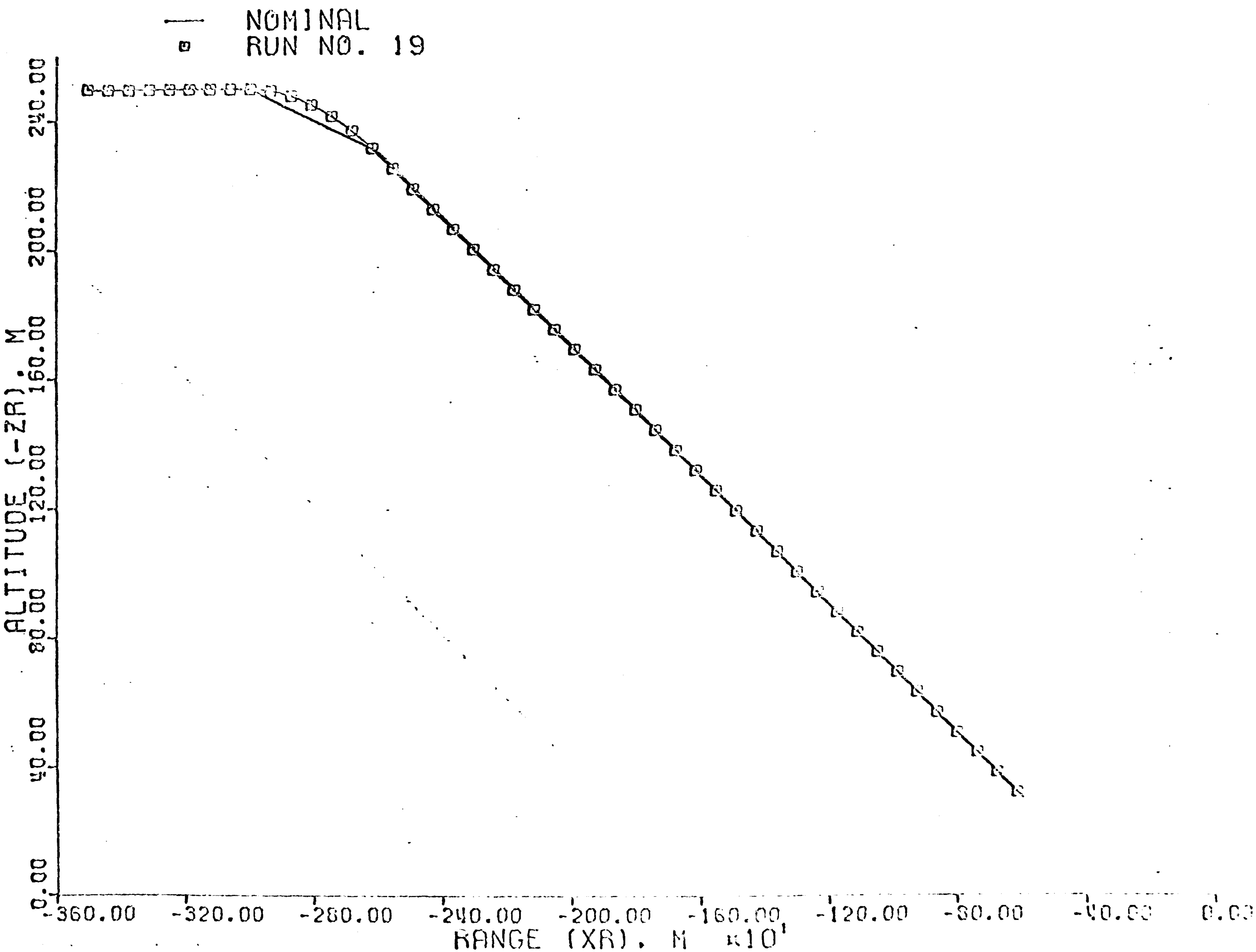

Figure 16a. Altitude vs Range with W_x = 10 m/sec

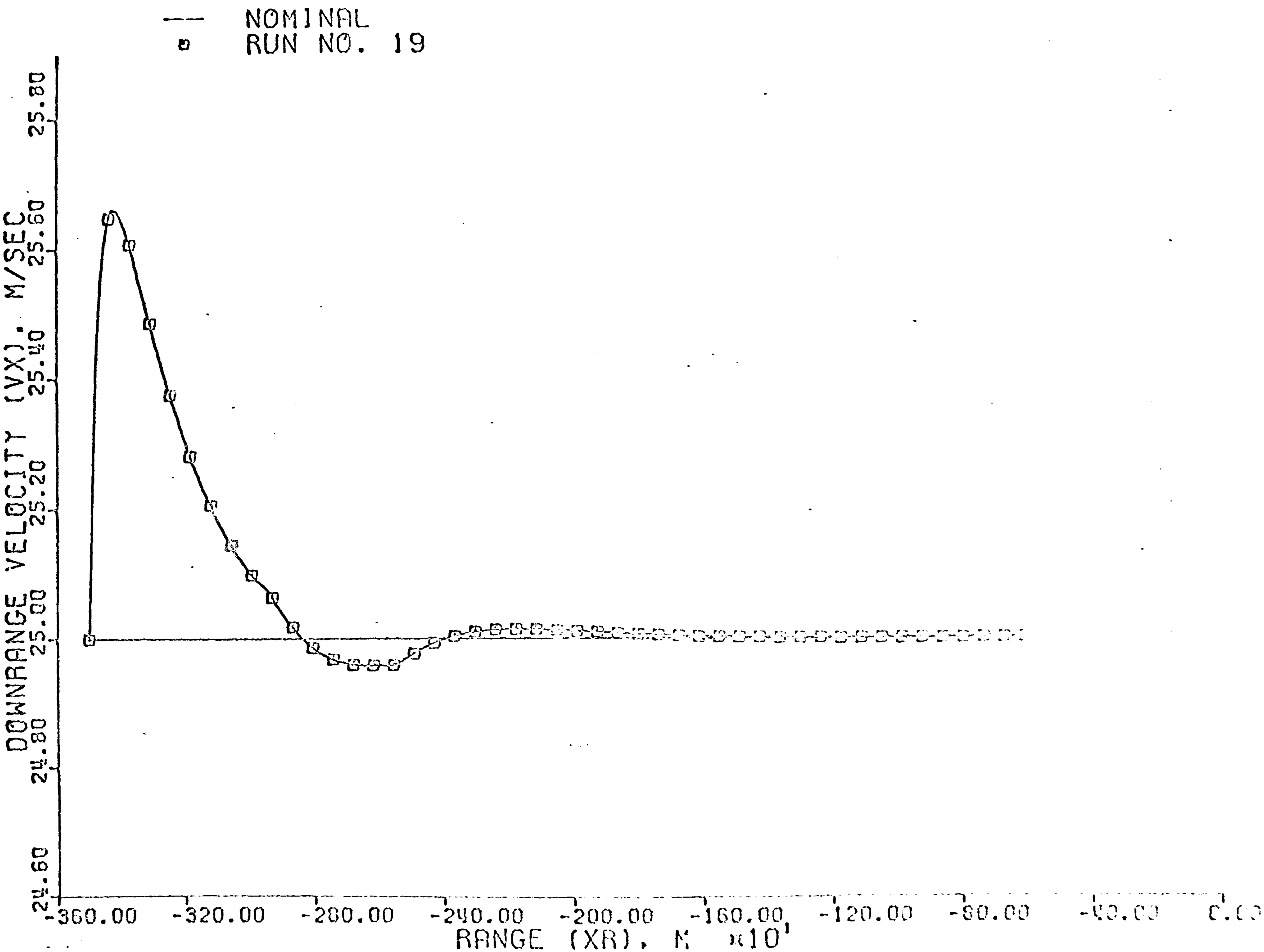

Figure 16b. Downrange Velocity vs Range with W_x = 10 m/sec

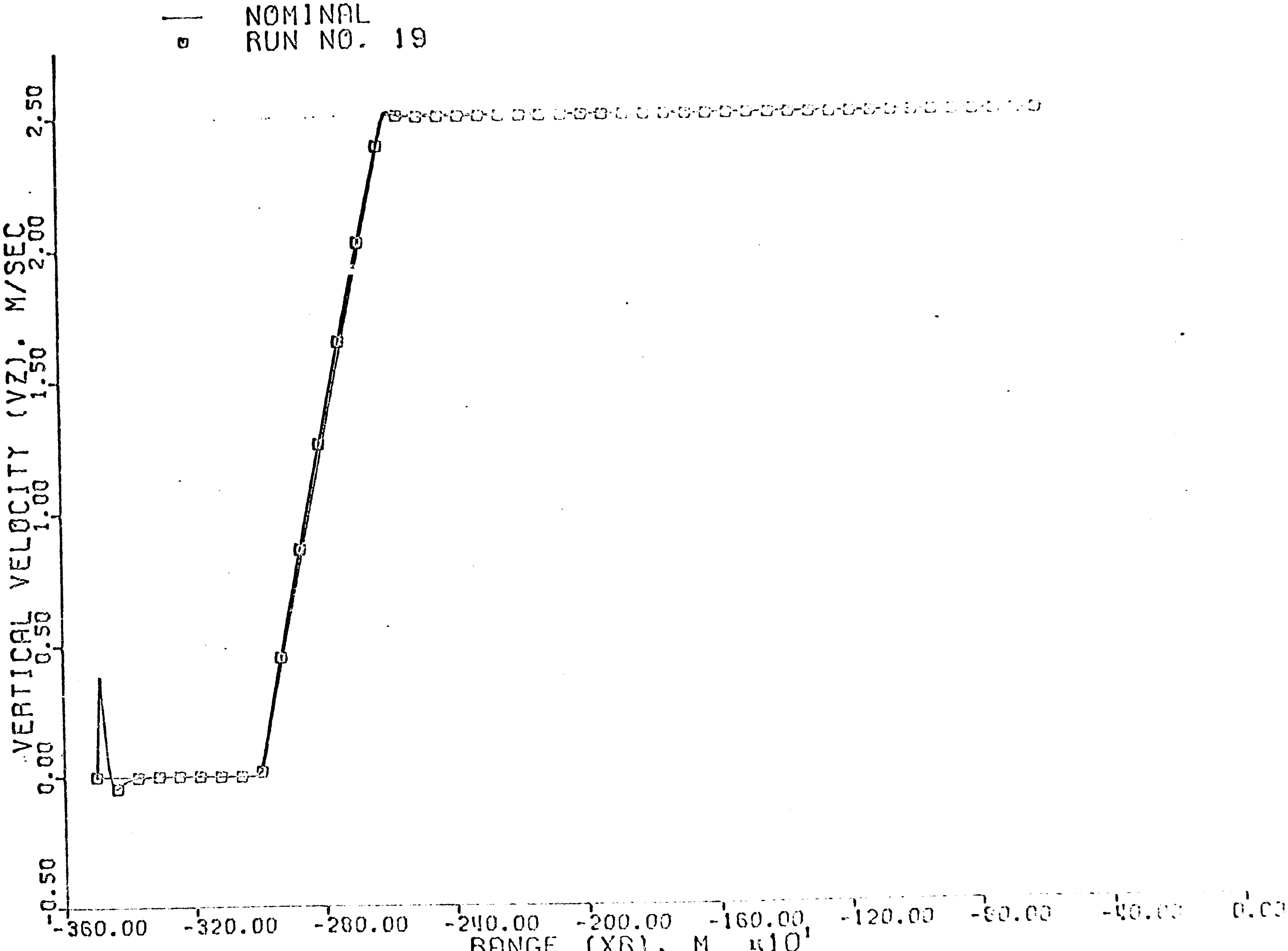

Figure 16c. Vertical Velocity vs Range with W_x = 10 m/sec

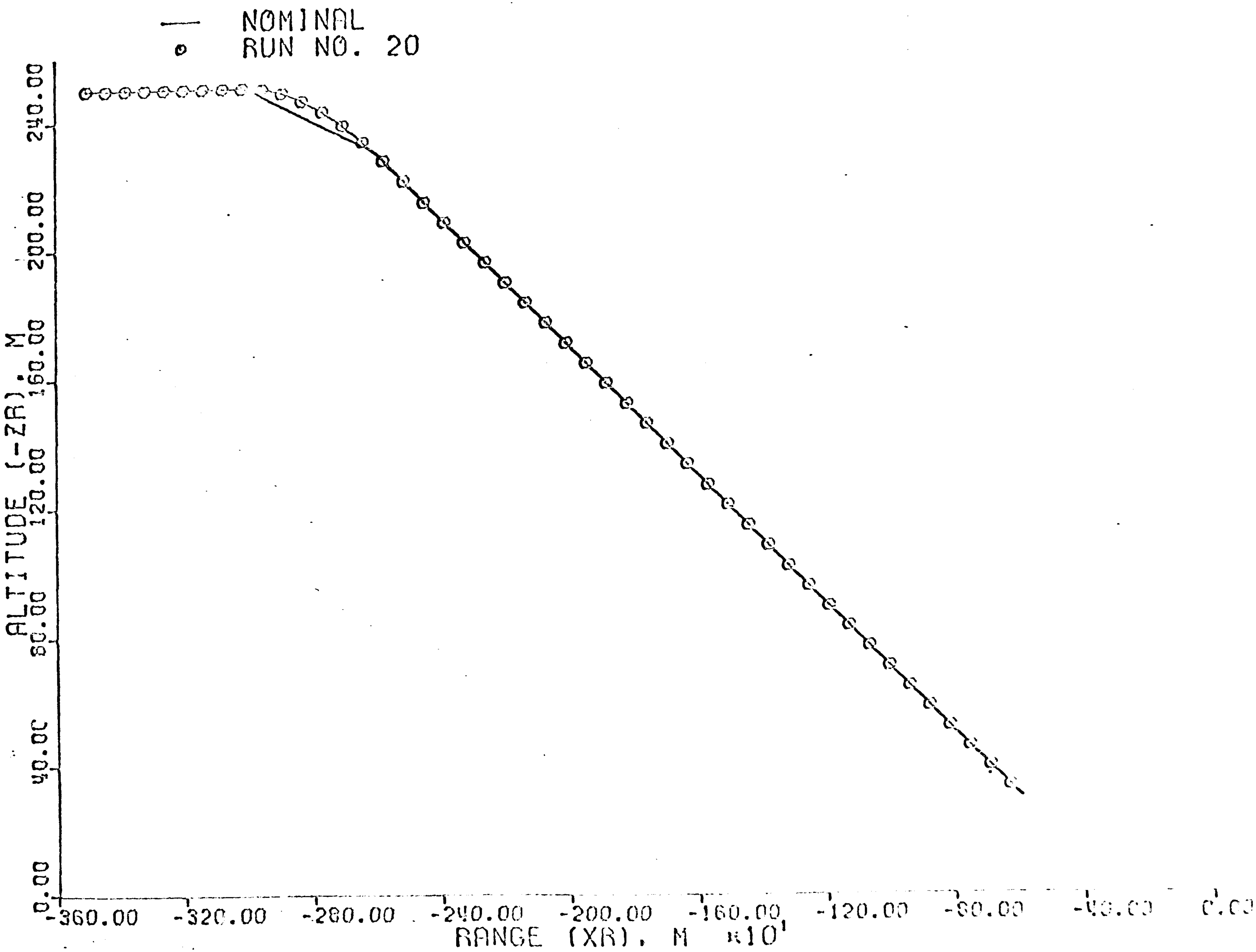

Figure 17a. Altitude vs Range with W_x = -10 m/sec

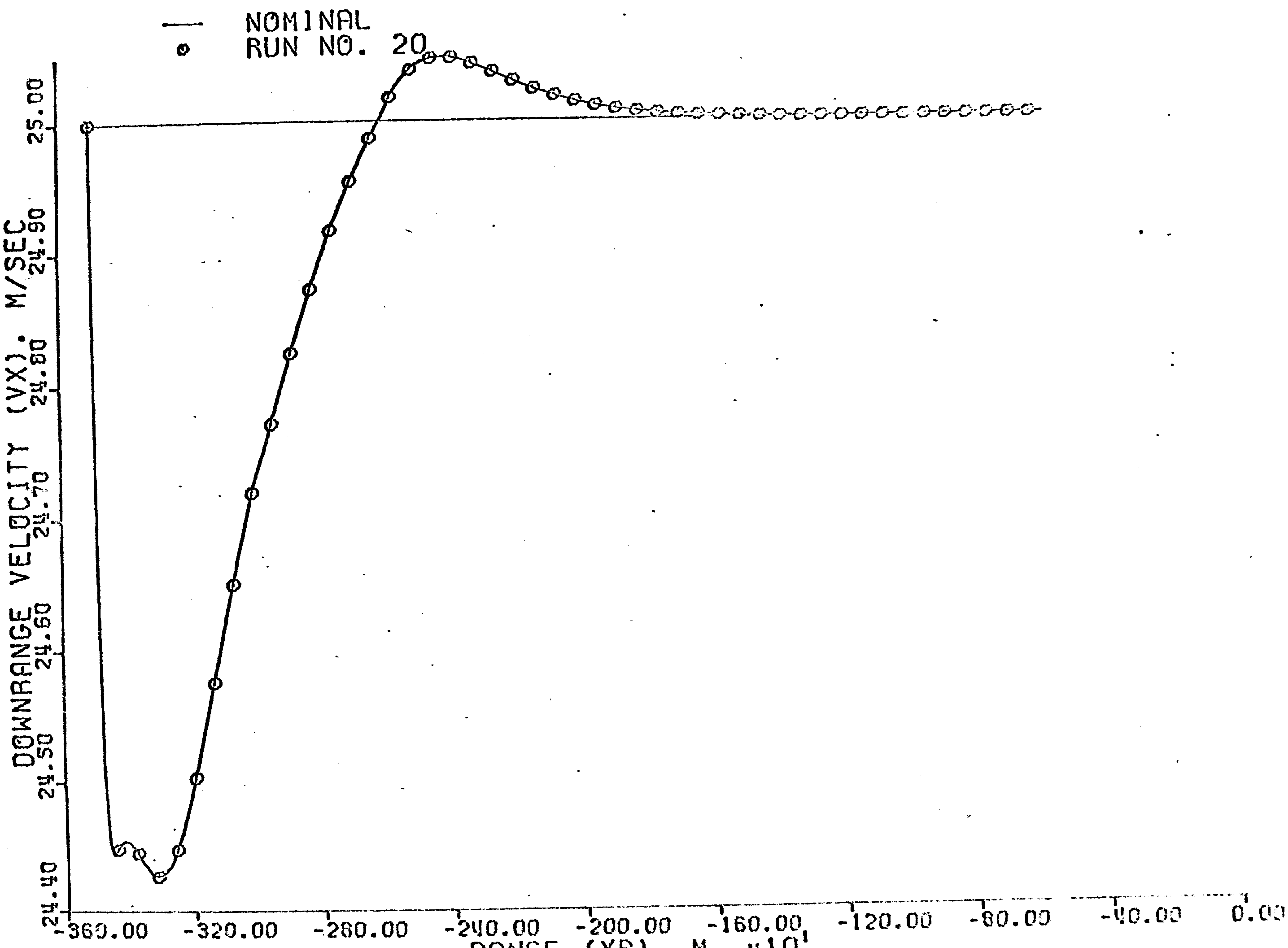

Figure 17b. Downrange Velocity vs Range with W_x = -10 m/sec

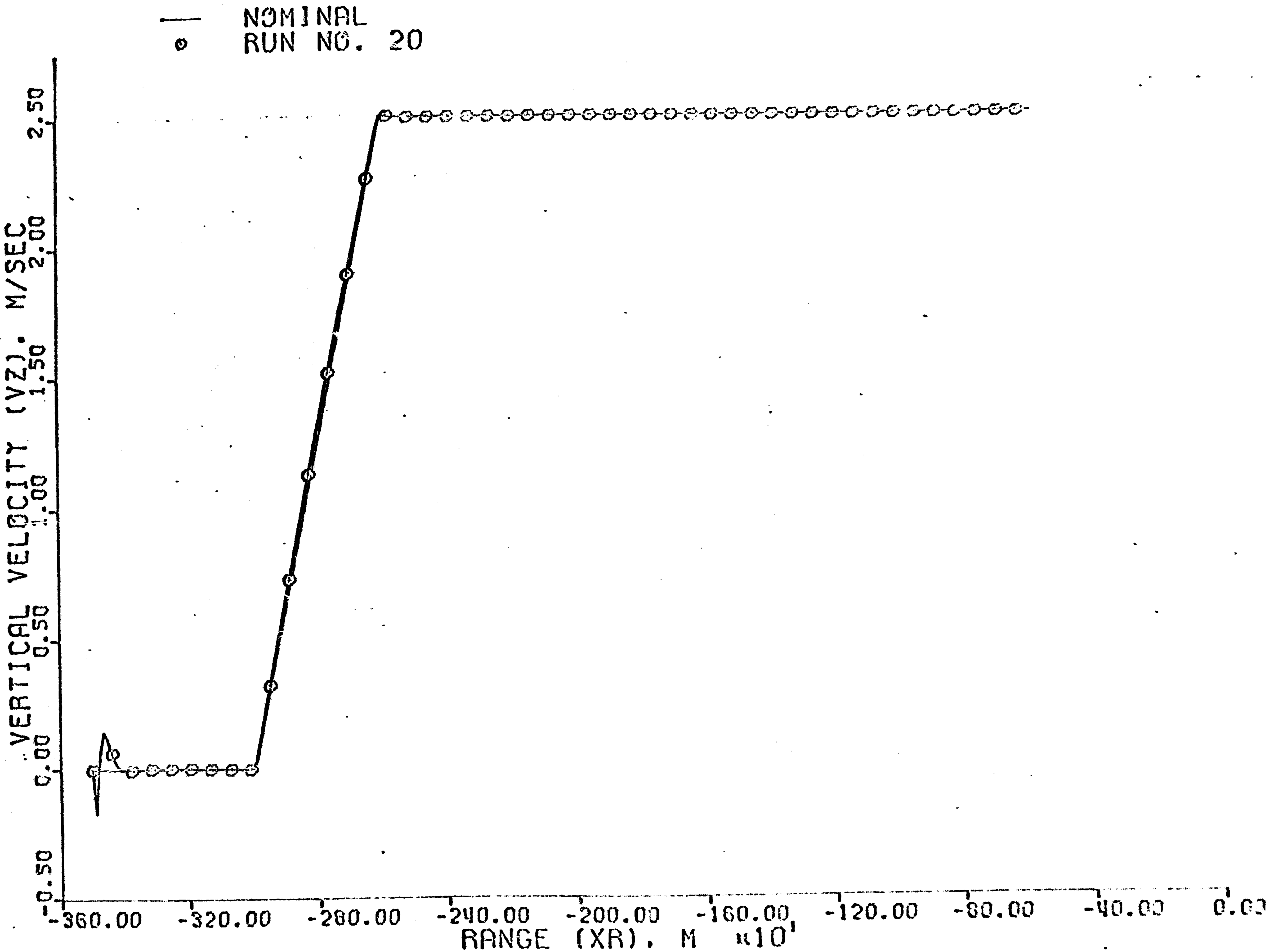

Figure 17c. Vertical Velocity vs Range with W_x = - 10 m/sec

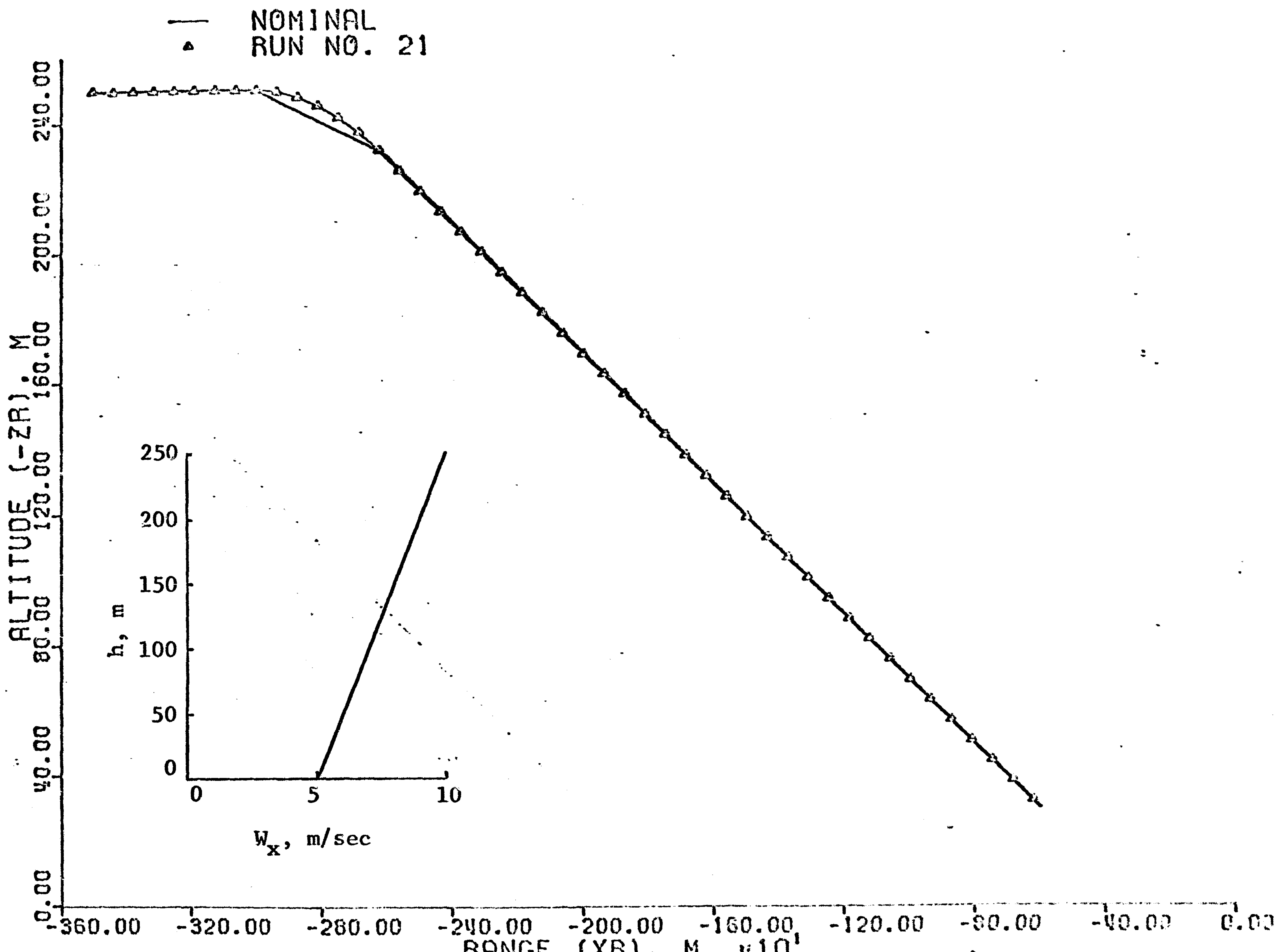

Figure 18a. Altitude vs Range with $W_x = (5.0 + 0.02h)$ m/sec

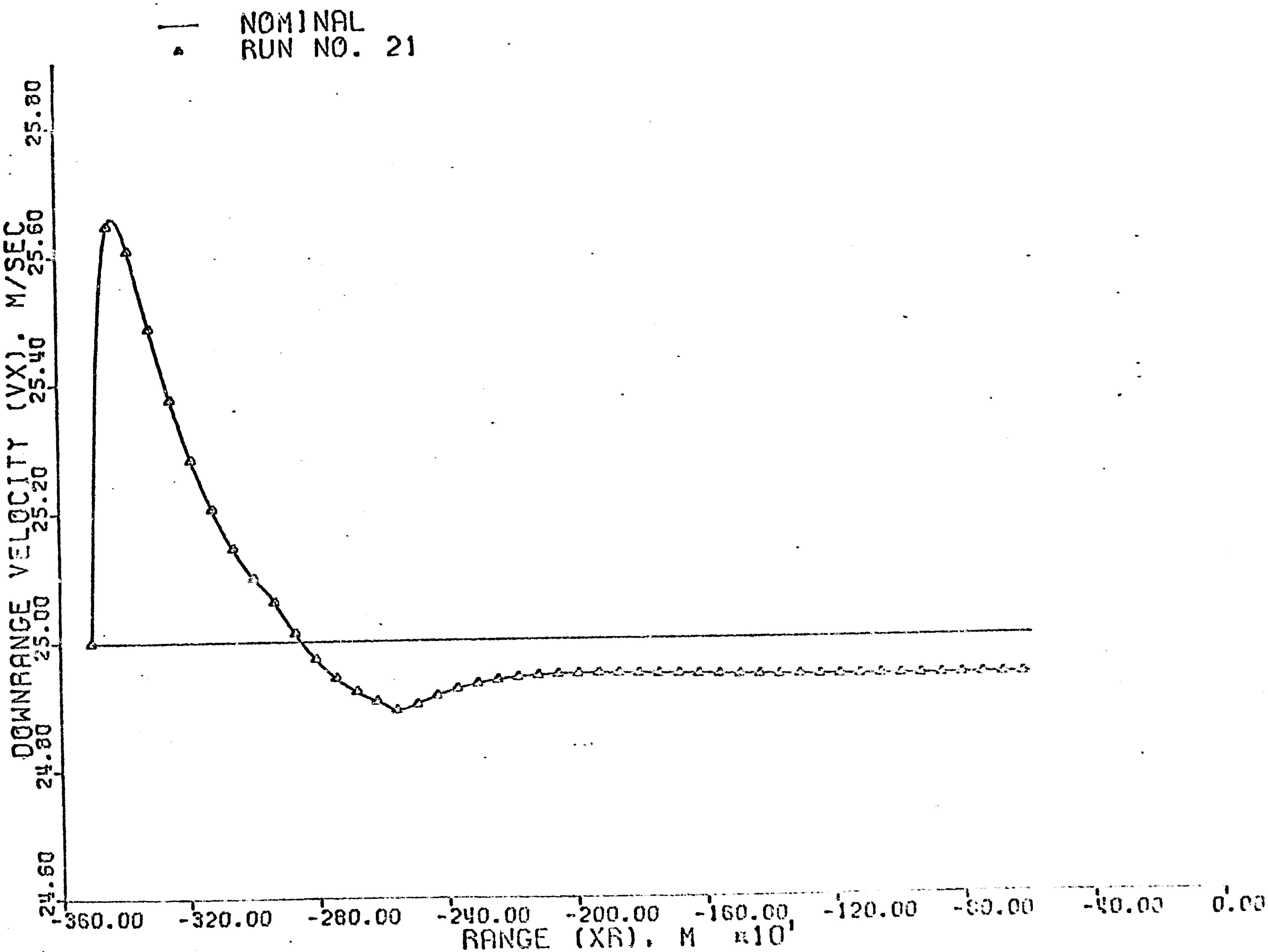

Figure 18b. Downrange Velocity vs Range with $W_x = (5.0 + 0.02h)$ m/sec

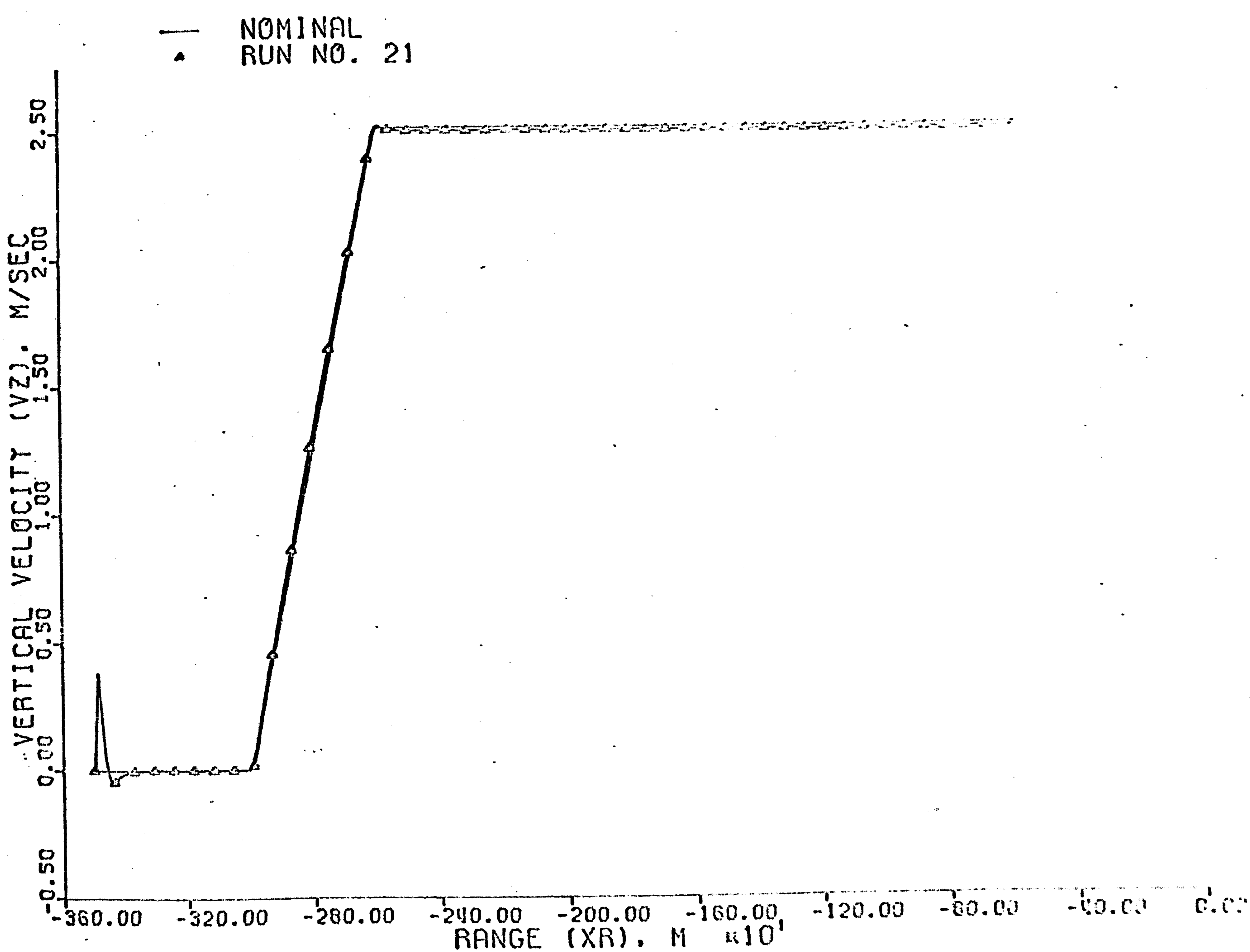

Figure 18c. Vertical Velocity vs Range with W_x = (5.0 + 0.02h) m/sec

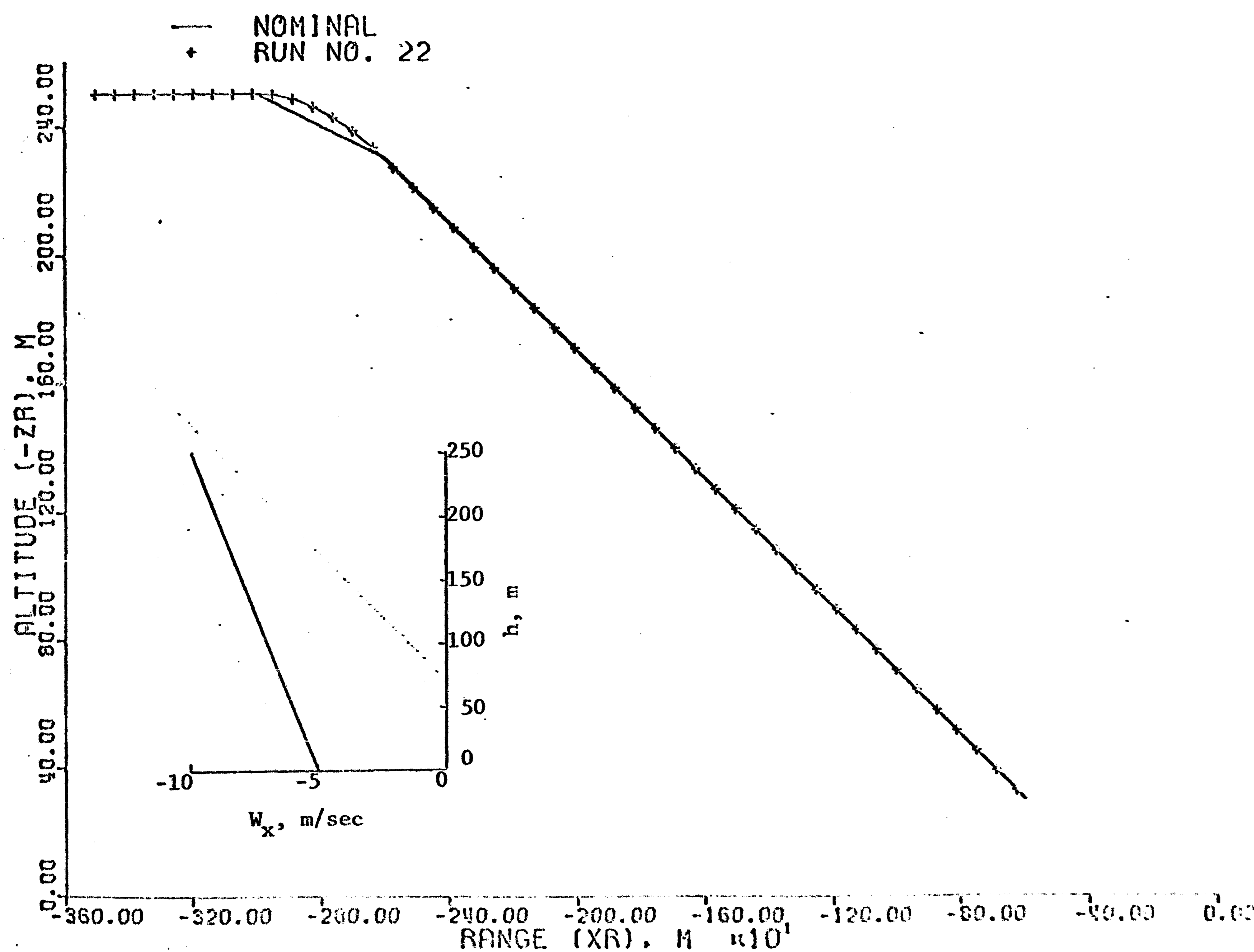

Figure 19a. Altitude vs Range with $W_x = -(5.0 + 0.02h)$ m/sec

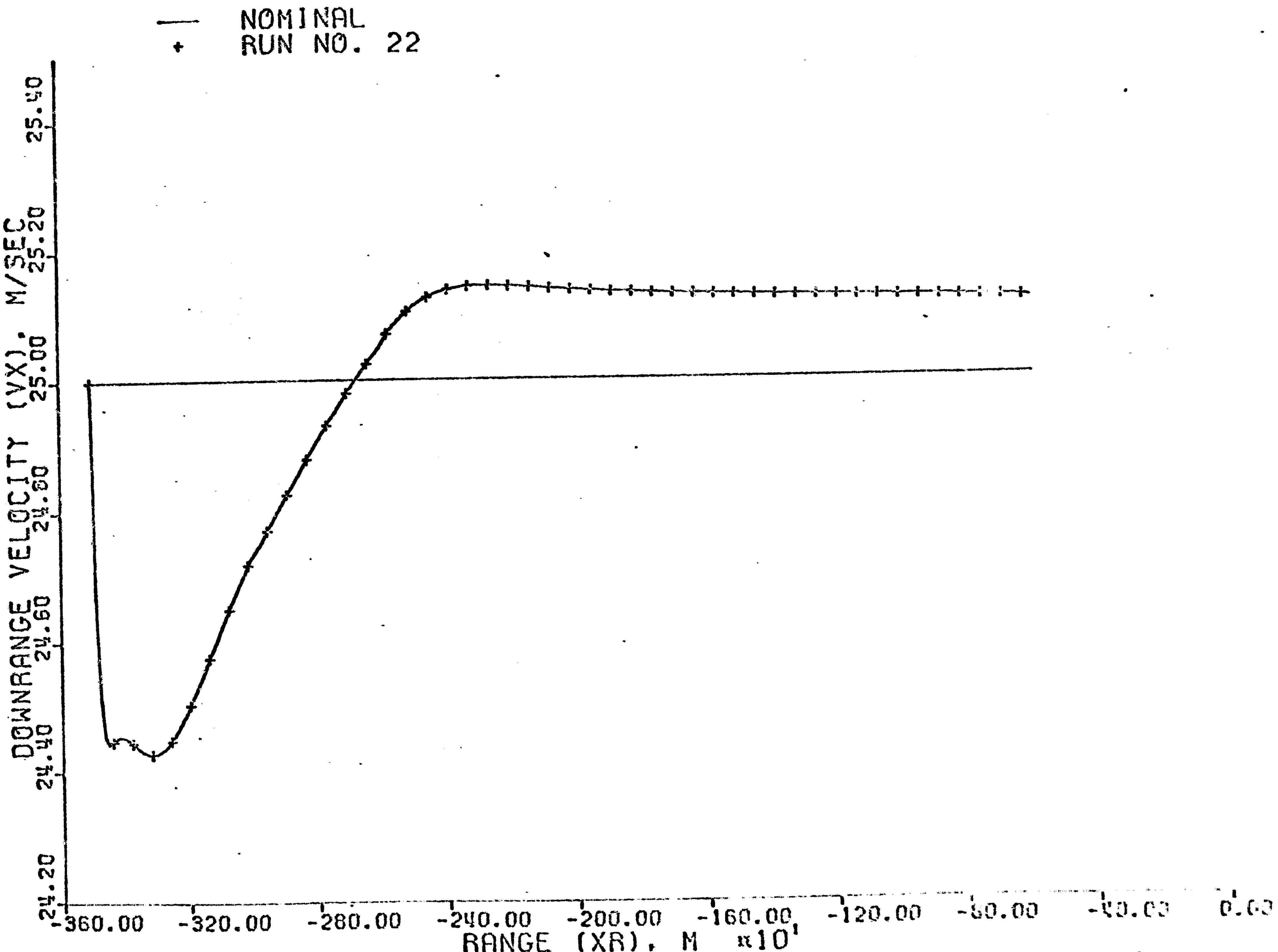

Figure 19b. Downrange Velocity vs Range with W_x = -(5.0 + 0.02 h) m/sec

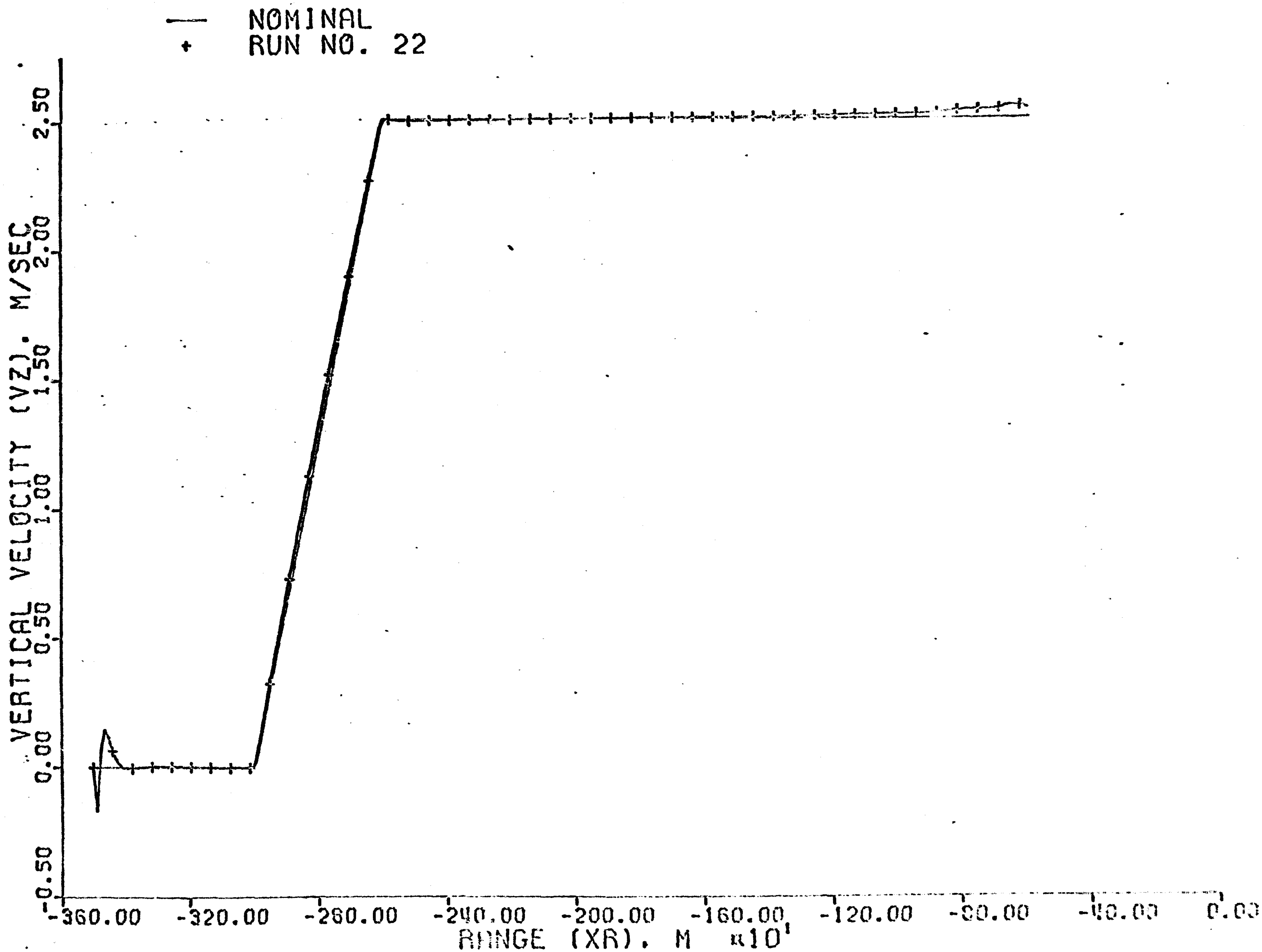

Figure 19c. Vertical velocity vs Range with $W_x = -(5.0 + 0.02h)$ m/sec

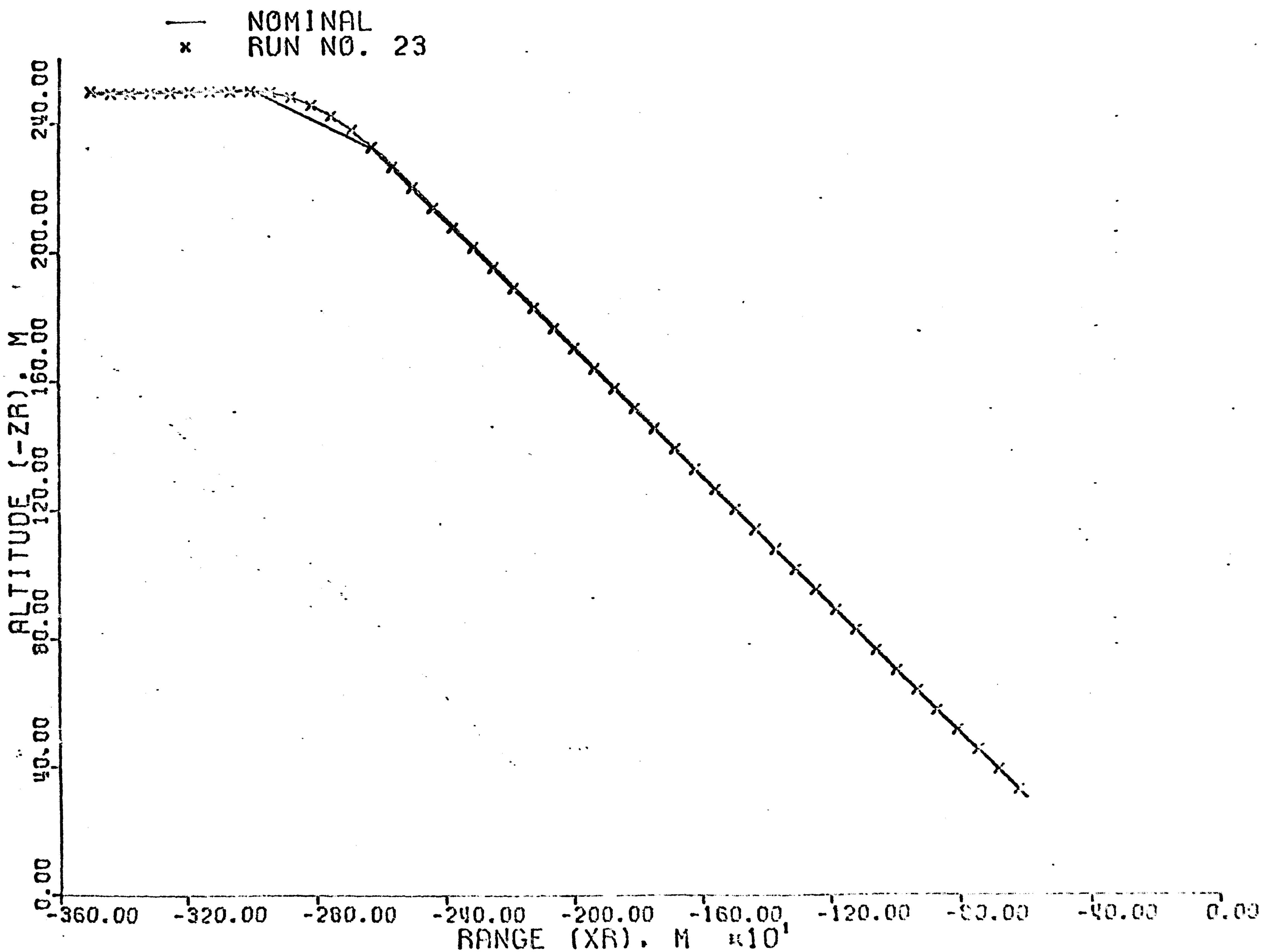

Figure 20a. Altitude vs Range with W_z = 5 m/sec

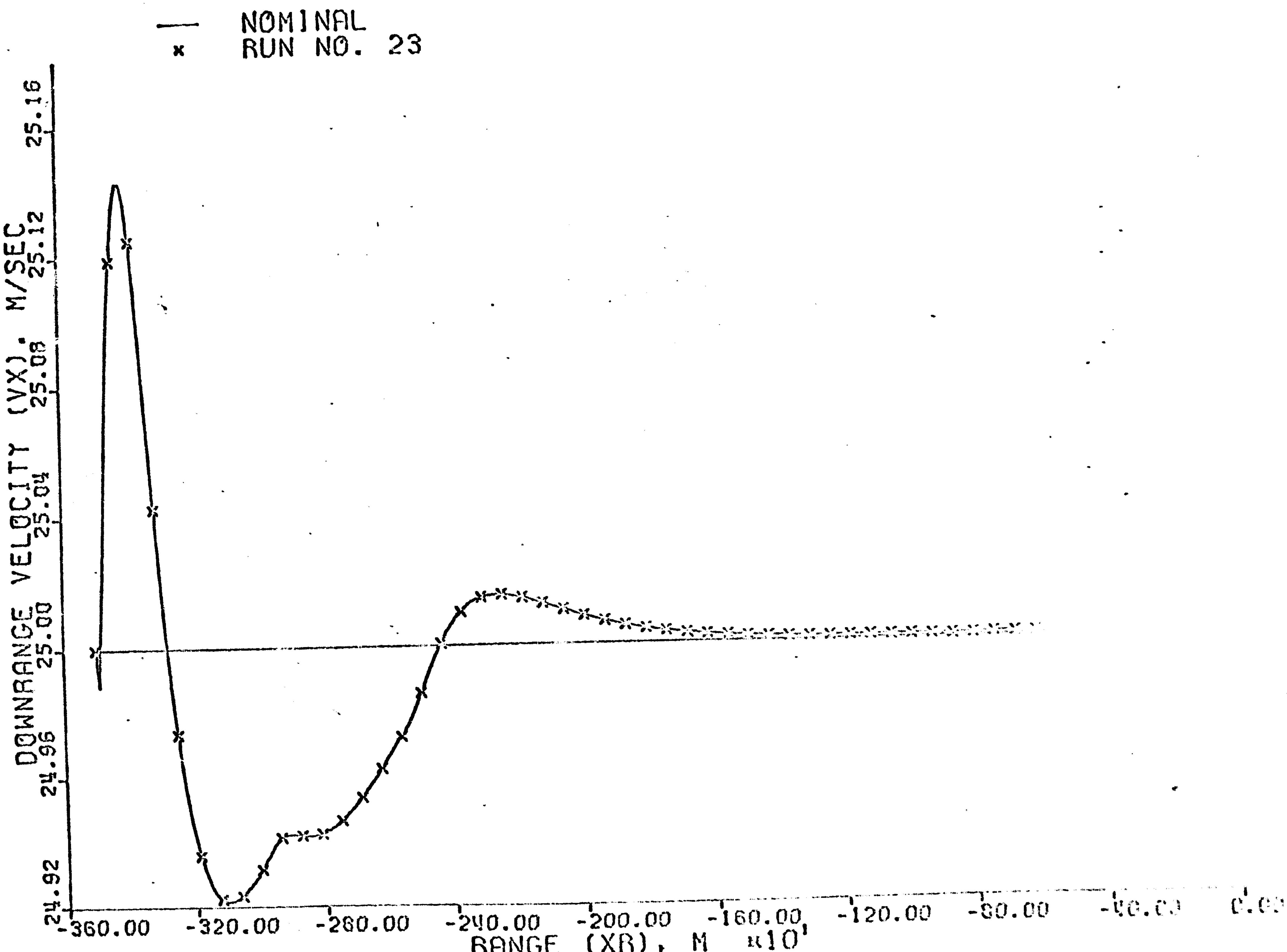

Figure 20b. Downrange Velocity vs Range with W_z = 5 m/sec

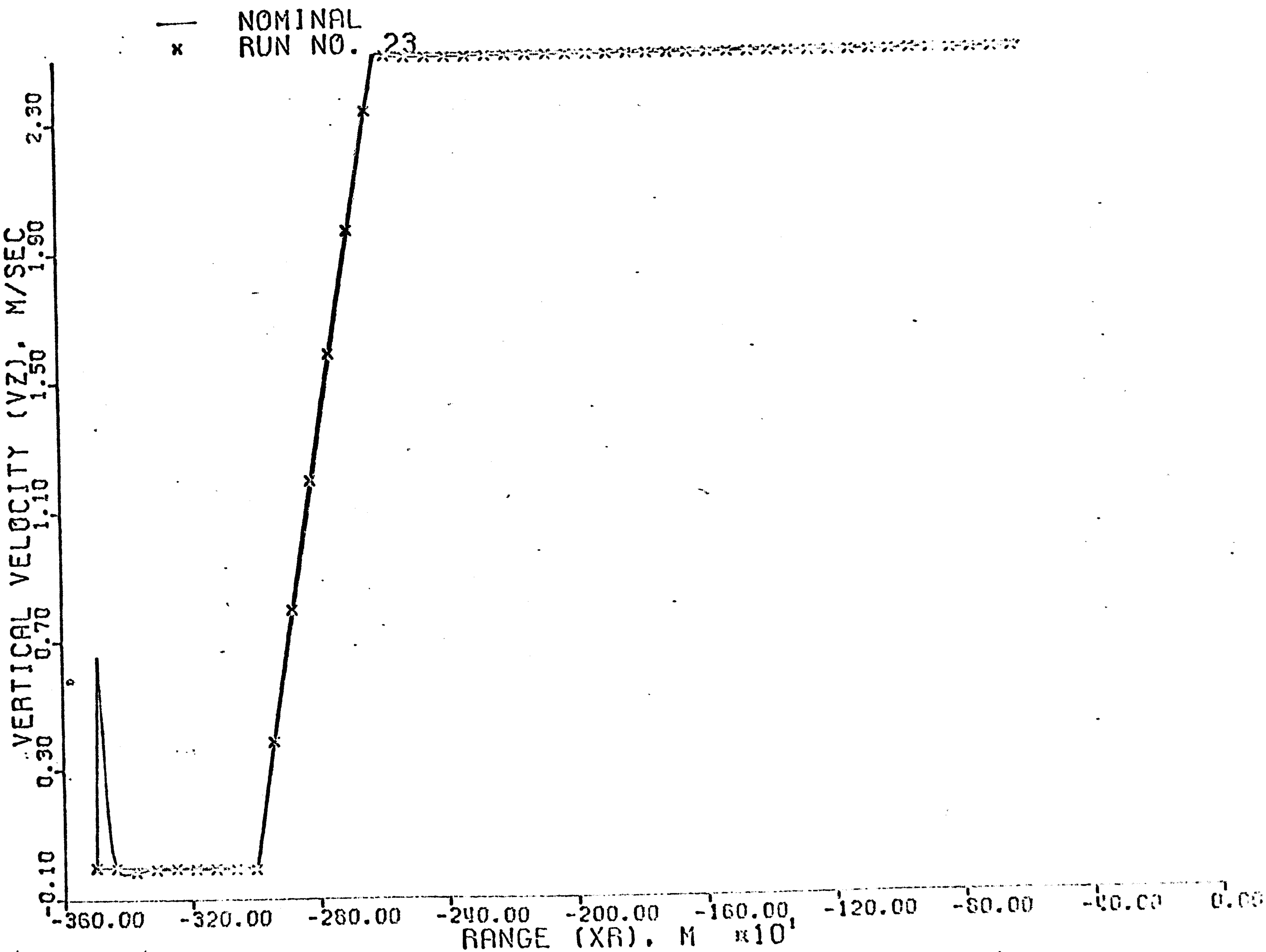

Figure 20c. Vertical Velocity vs Range with W_z = 5 m/sec

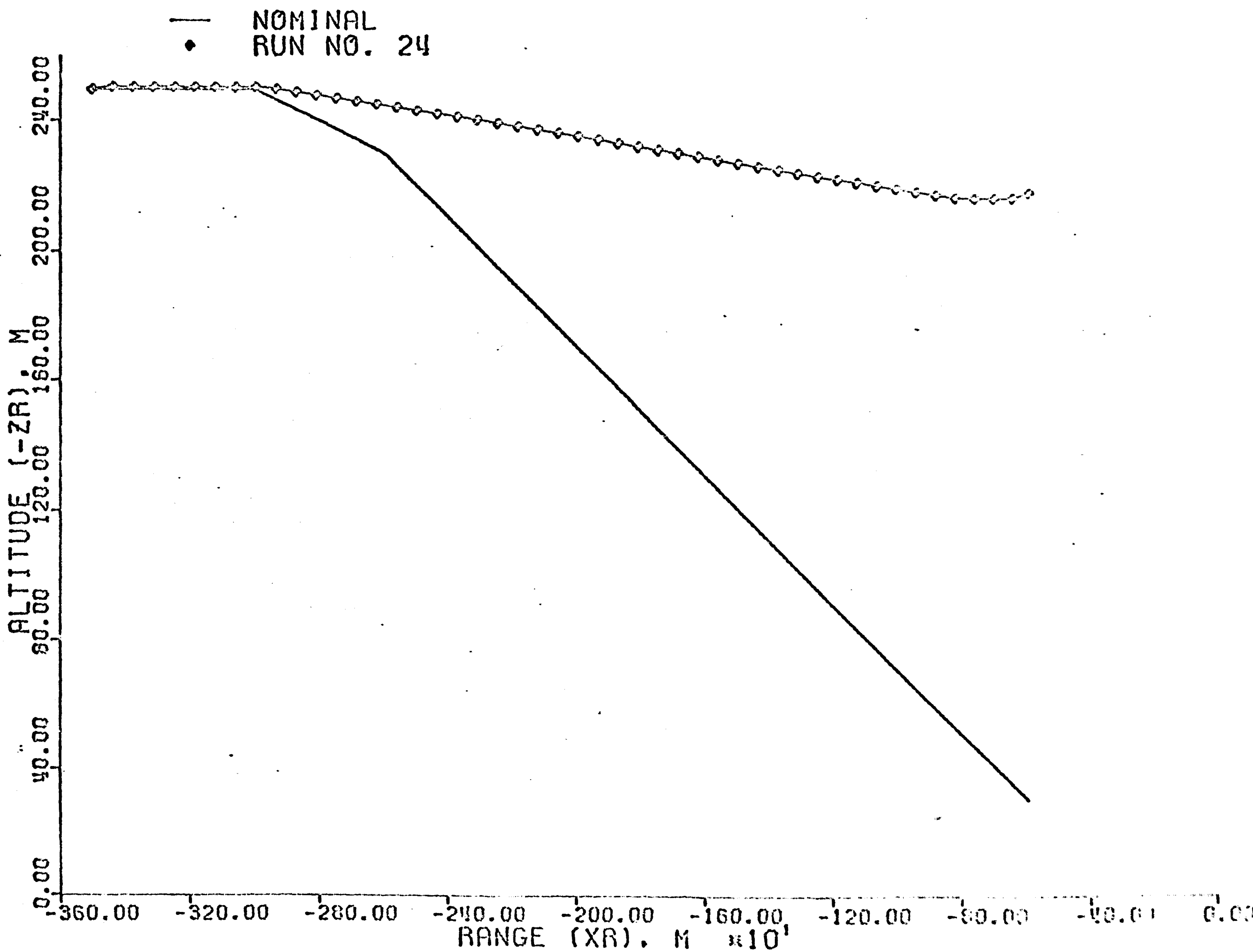

Figure 21a. Altitude vs Range with W_z = -5 m/sec

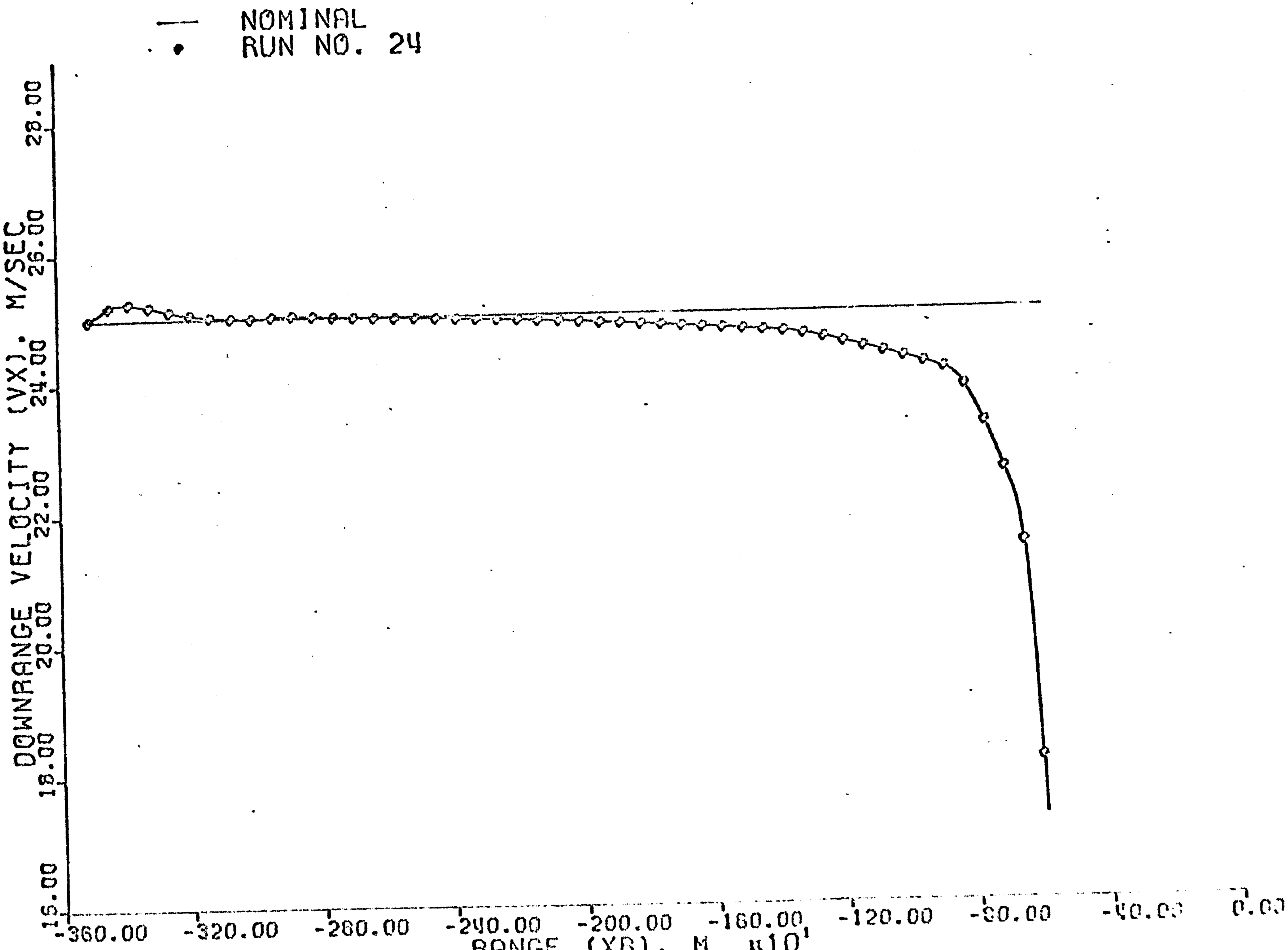

Figure 21b. Downrange Velocity vs Range with W_z = -5 m/sec

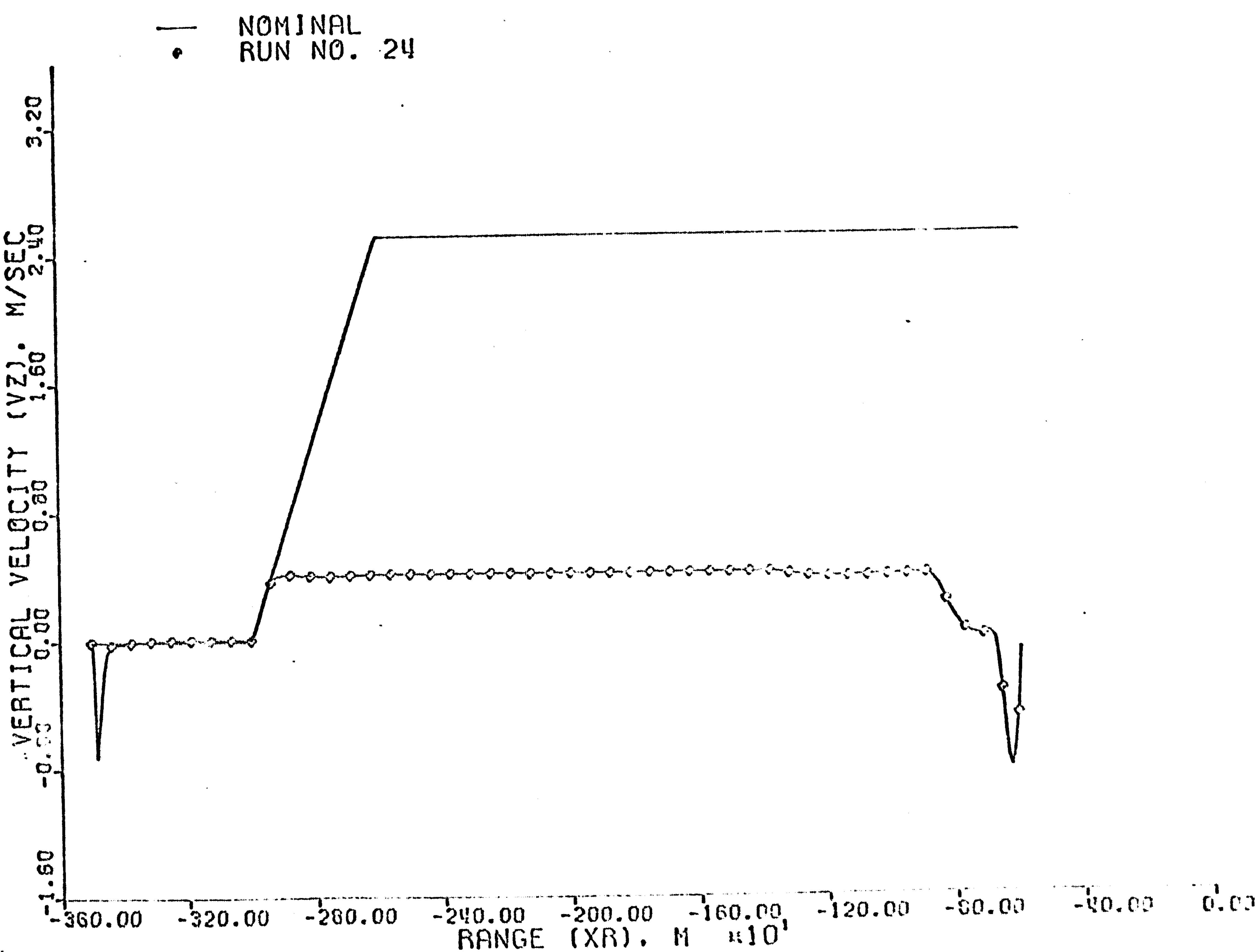

Figure 21c. Vertical Velocity vs Range with W_z = -5 m/sec

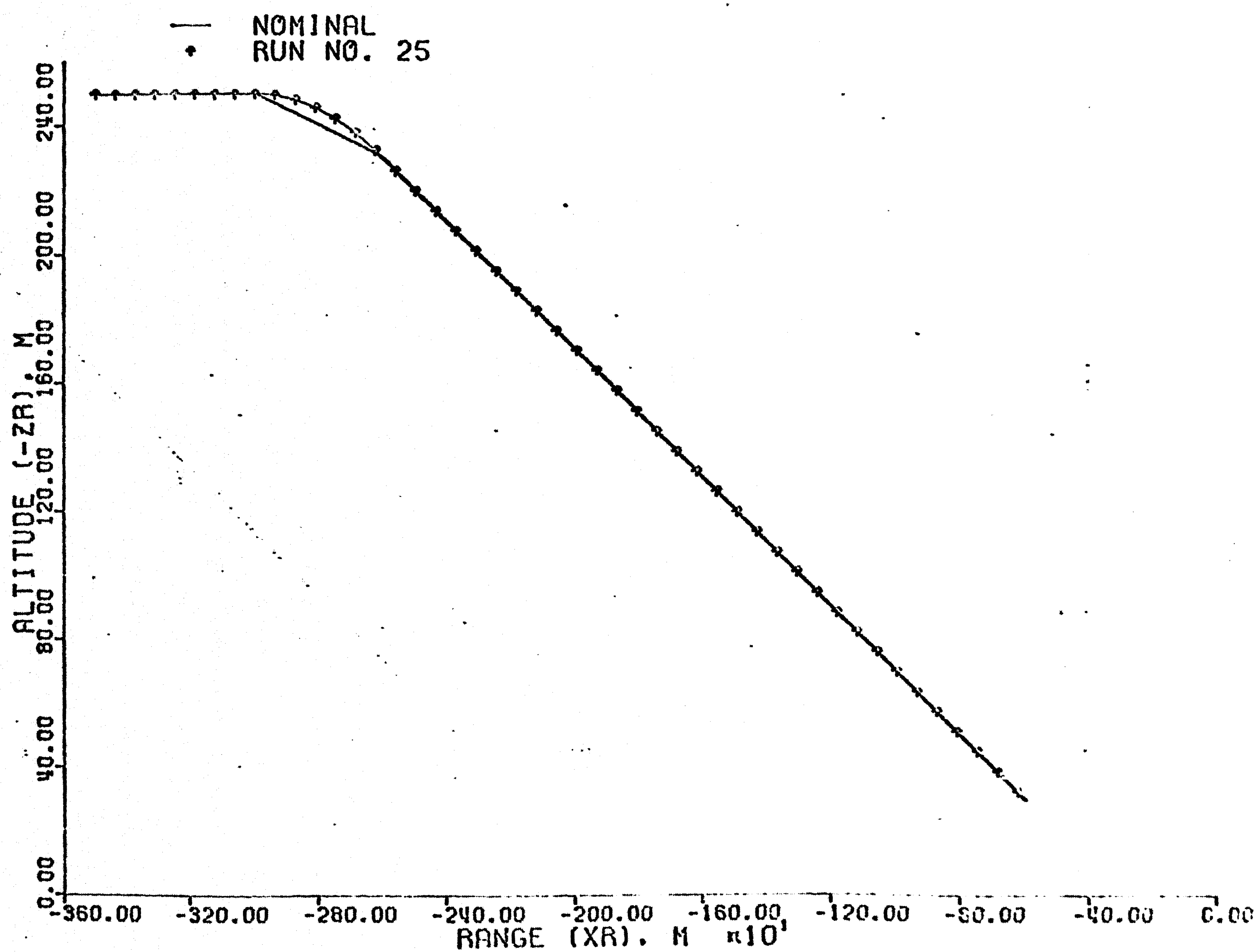

Figure 22a. Altitude vs Range with M_i = + 10%

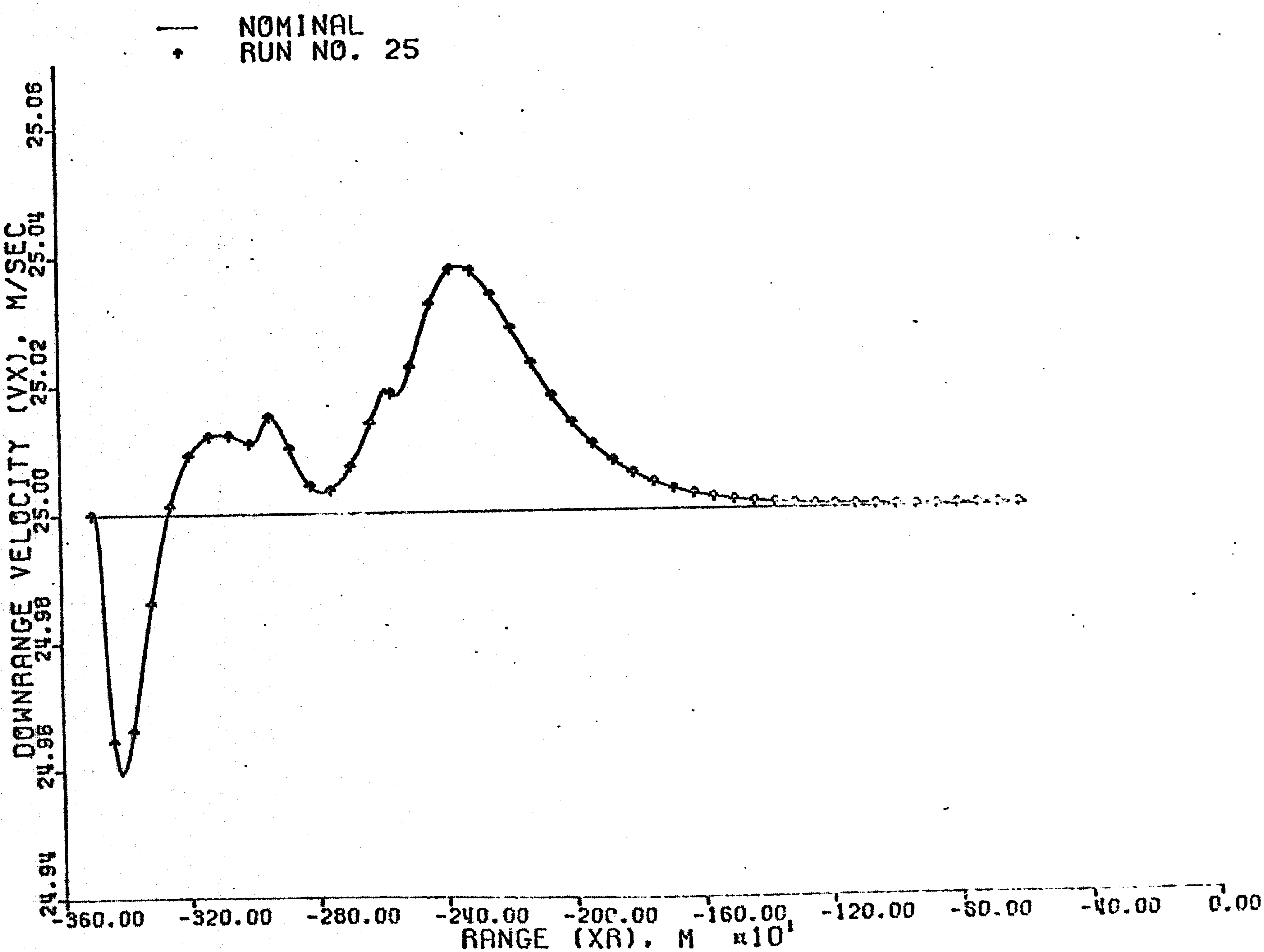

Figure 22b. Downrange Velocity vs Range with M_i = + 10%

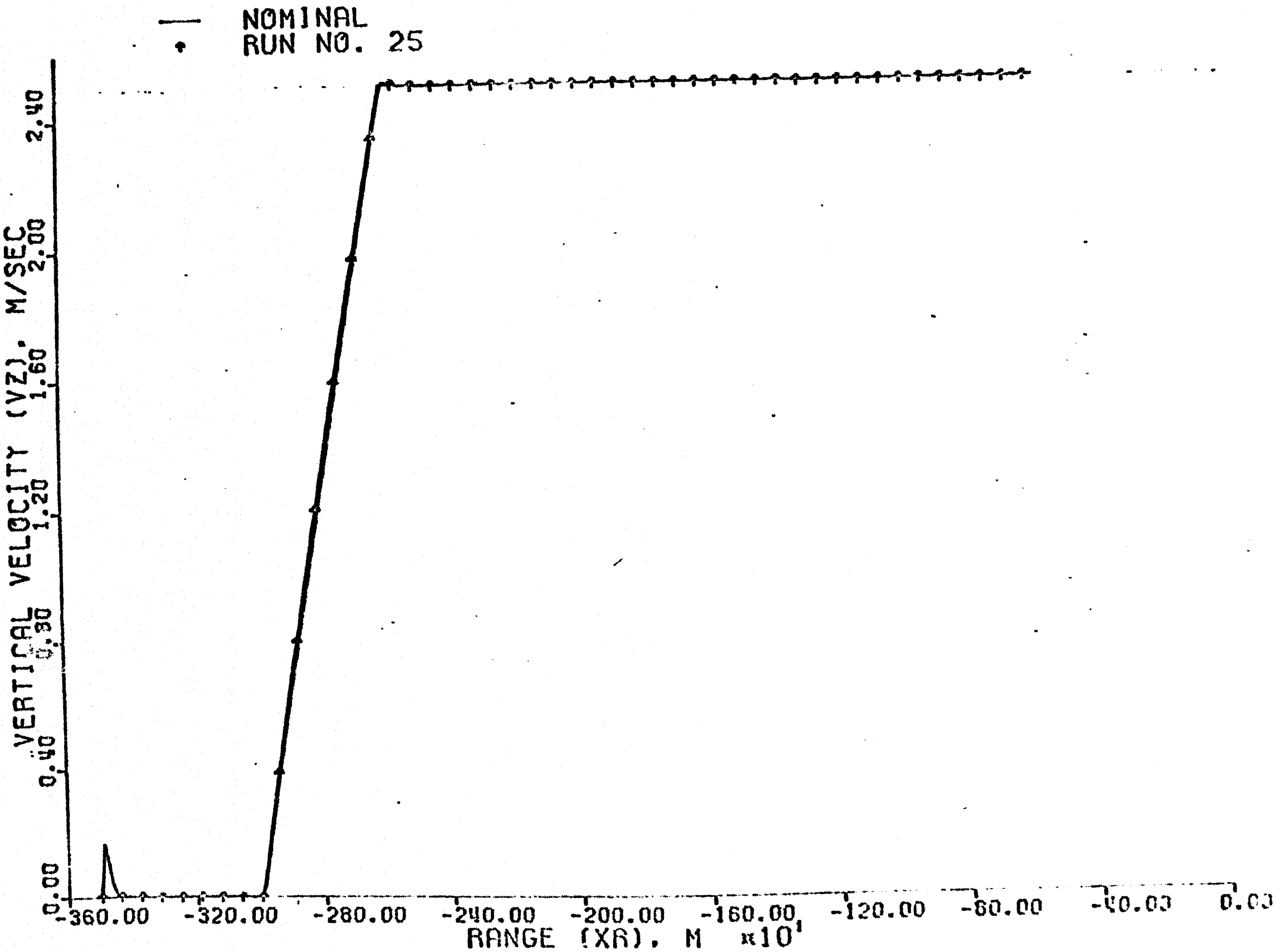

Figure 22c. Vertical Velocity vs Range with M_i = + 10%

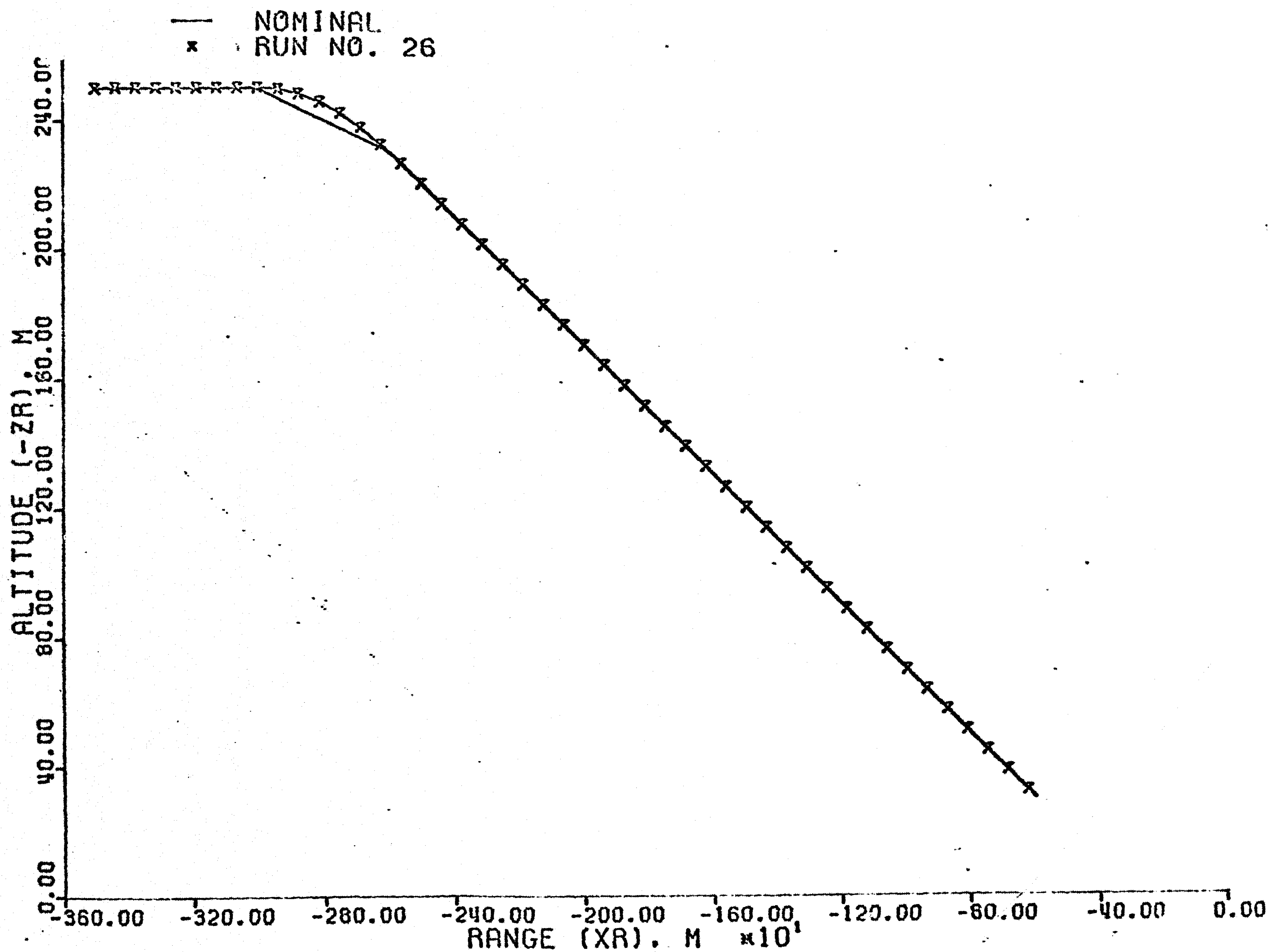

Figure 23a. Altitude vs Range with M_i = -10%

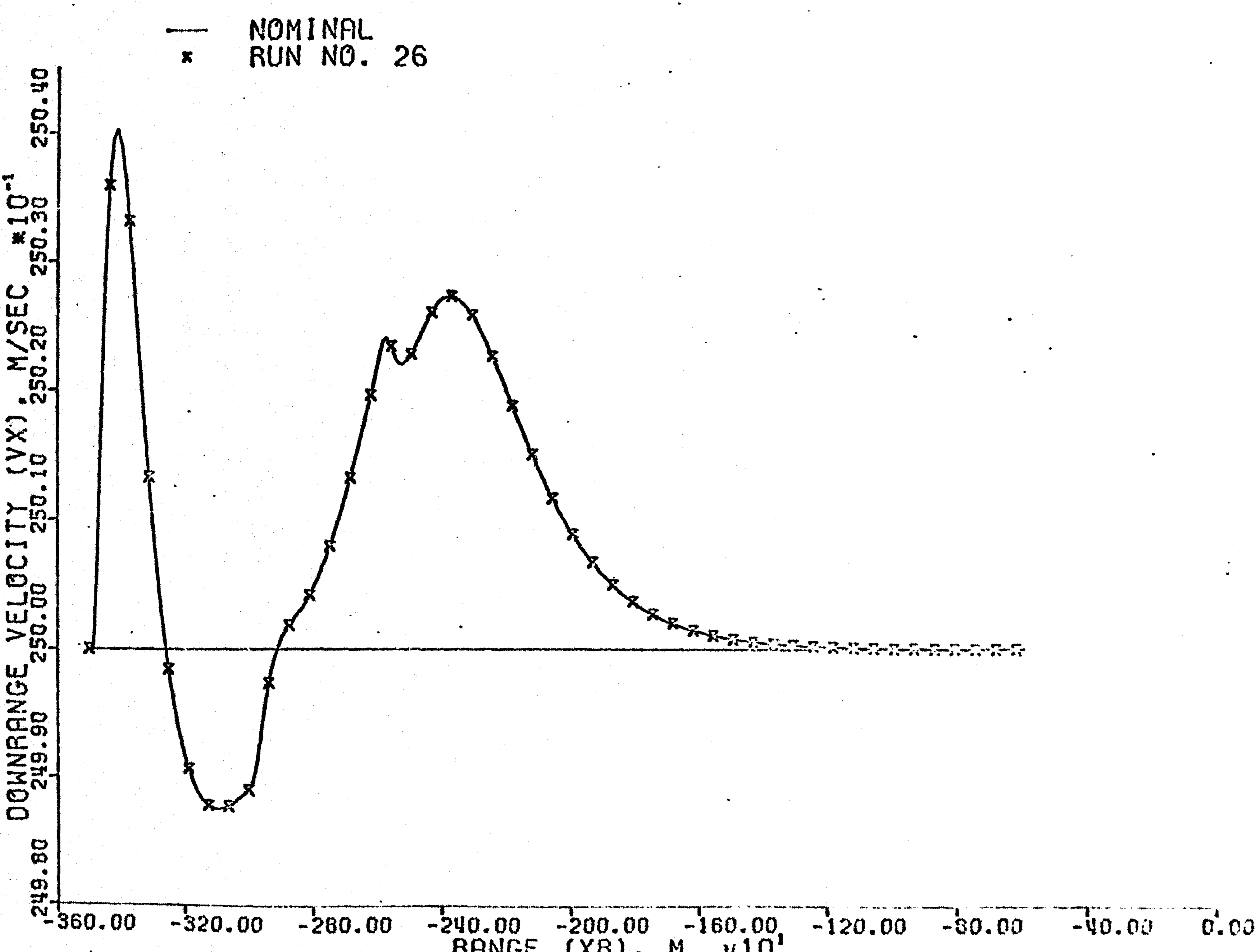

Figure 23b. Downrange Velocity vs Range with M_i = -10%

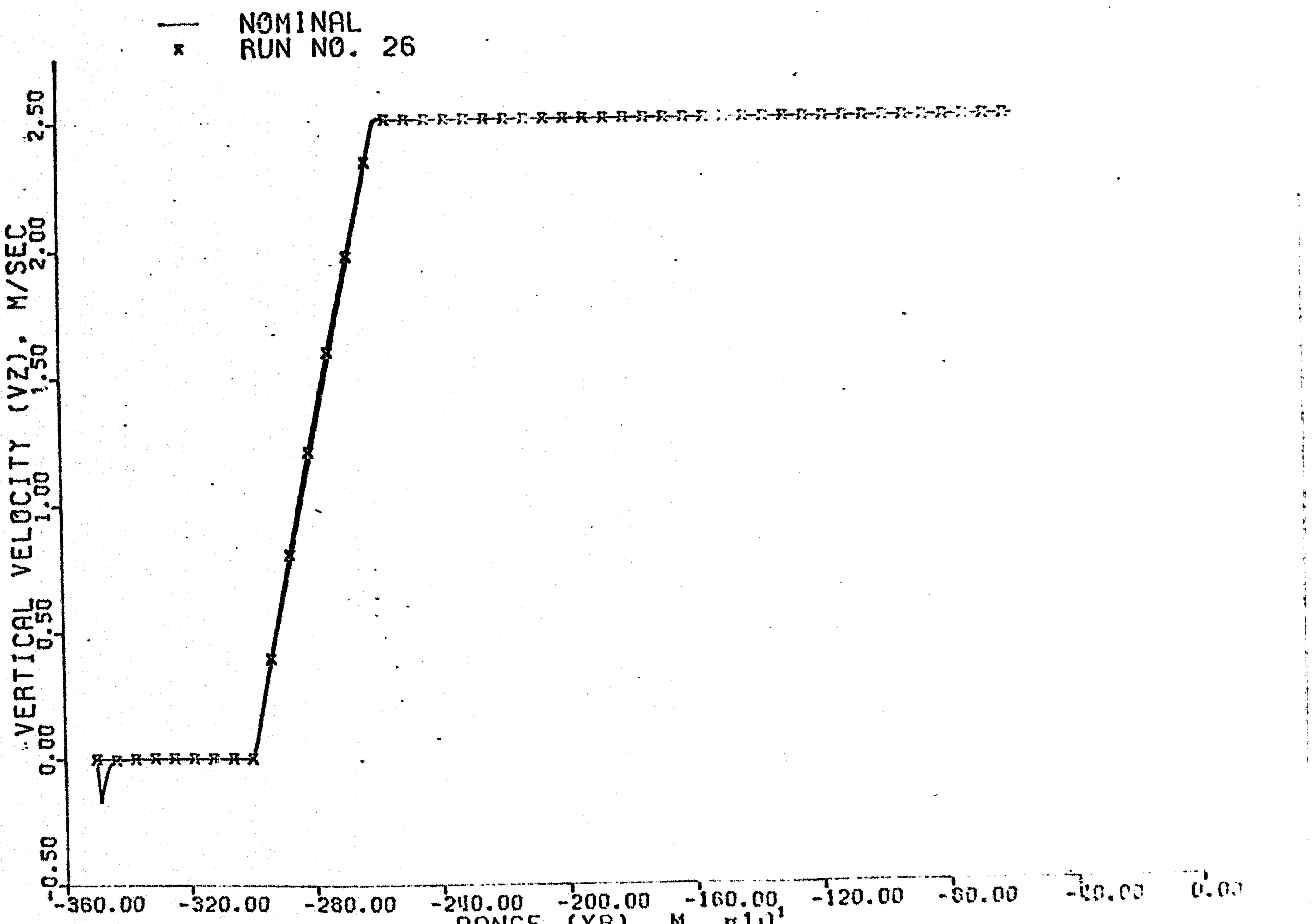

Figure 23c. Vertical Velocity vs Range with M_i = -10%

APPENDIX A

SIMPLIFIED HELICOPTER FORCE EQUATIONS

The simplest representation of a tandem rotor helicopter is in terms of an equivalent single rotor at an angle of attack equal to the mean angle of attack of the two rotors. The analysis below of helicopter lift and drag forces is based on this concept. The aerodynamic and gravitational forces acting on a helicopter in the vertical plane are shown in Figure A-1. Treating the helicopter as a point mass, the longitudinal equations of motion are:

$$m\dot{V} = -D_p - H\cos(\alpha-\alpha_o) - T\sin(\alpha-\alpha_o) - mg\sin\gamma \qquad \text{(A-1)}$$

$$mV\dot{\gamma} = T\cos(\alpha-\alpha_o) - H\sin(\alpha-\alpha_o) - mg\cos\gamma \qquad \text{(A-2)}$$

$$\dot{x} = V\cos\gamma \qquad \text{(A-3)}$$

$$\dot{z} = V\sin\gamma \qquad \text{(A-4)}$$

The state variables are the velocity V, the flight path angle γ, and the position coordinates x and z; the control variables are fuselage reference plane angle of attack α and collective pitch control deflection δ_c.

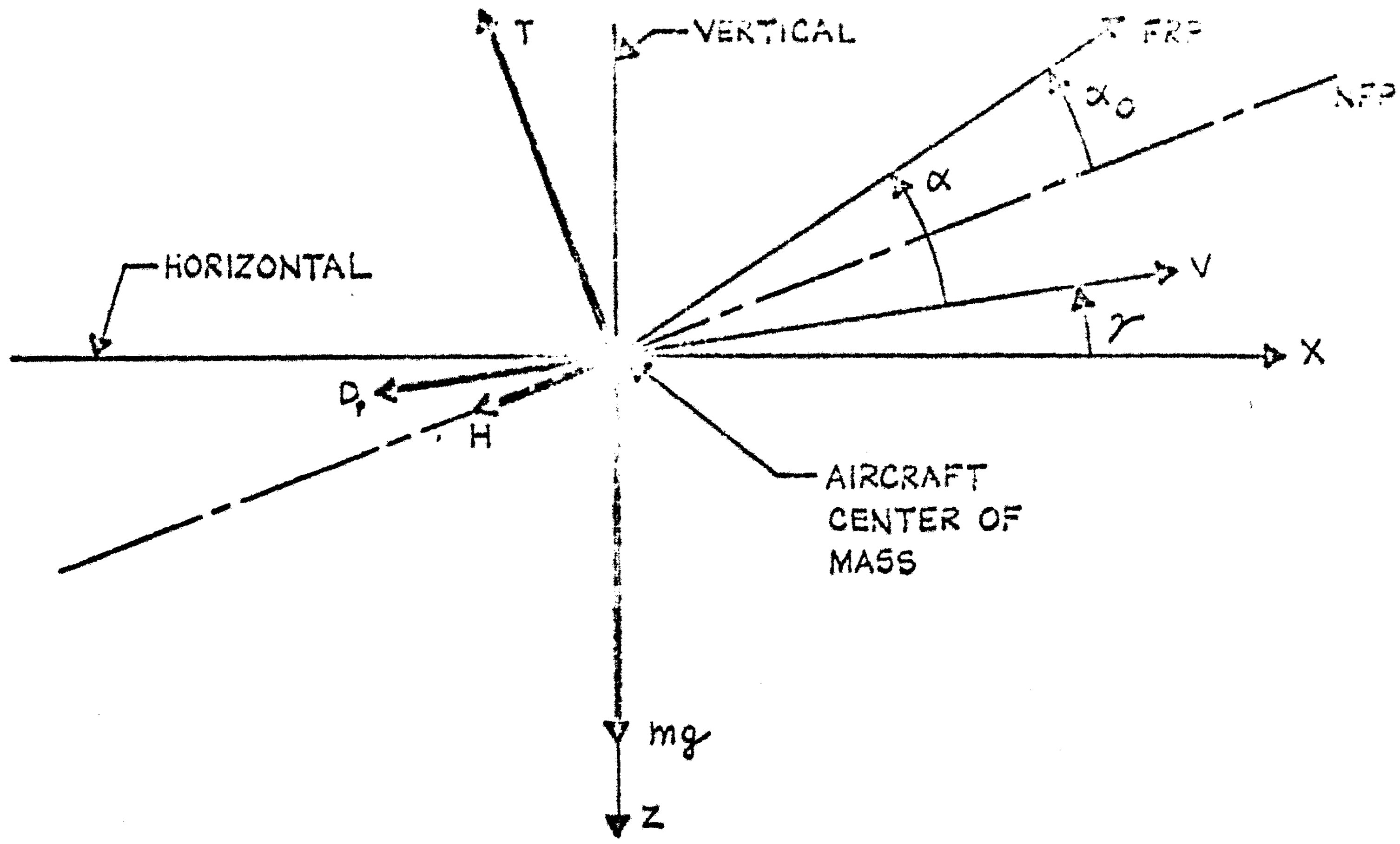

Figure A-1. Forces Acting on a Helicopter in the Vertical Plane

Where:

NFP	=	rotor no-feathering plane
FRP	=	fuselage reference plane
T	=	total thrust, both rotors
H_o	=	total profile "horizontal" force, both rotors
H_i	=	total induced "horizontal" force, both rotors
D_p	=	total non-rotor parasite drag
α_o	=	angle between NFP and FRP
α	=	FRP angle of attack, positive as shown
H	=	total "horizontal" force, both rotors

$$H = H_o + H_i \qquad \text{(A-5)}$$

For small angles and H << T, Eqs. (A-1) and (A-2) are approximately

$$m\dot{V} = -D_p - H - T(\alpha-\alpha_o) - mg \sin\gamma \qquad \text{(A-6)}$$

$$mV\dot{\gamma} = T - mg \cos(\alpha-\alpha_o) \qquad \text{(A-7)}$$

With respect to the NFP, for an equivalent single rotor, the thrust coefficient is (see Reference 6):

$$C_T = \frac{T}{\rho S(\Omega R)^2} = \frac{\sigma a}{2}\left[\frac{\theta_o}{3}\left(1 + \frac{3}{2}\mu^2\right) - \frac{\lambda}{2}\right] \qquad \text{(A-8)}$$

where:

S = total swept disk area, both rotors, ft^2

σ = rotor solidity

ΩR = rotor tip speed, ft/sec

a = blade section lift curve slope, per rad.

θ_o = blade collective pitch angle @ 3/4 radius, rad.

μ = rotor advance ratio = $\dfrac{V\cos(\alpha-\alpha_o)}{\Omega R} \approx \dfrac{V}{\Omega R}$ (A-9)

λ = rotor inflow ratio with respect to NFP:

$$\lambda = -\mu\tan(\alpha-\alpha_o) + \frac{C_T}{2\sqrt{\mu^2+\lambda^2}} \qquad \text{(A-10)}$$

$$\lambda \approx -\mu(\alpha-\alpha_o) + \frac{C_T}{2\mu} \quad (\mu \geq 0.1) \qquad \text{(A-11)}$$

Substituting (A-11) into (A-8) leads to

$$C_T \approx \frac{\frac{\sigma a}{2}}{1 + \frac{\sigma a}{8\mu}} \left[\frac{\theta_o}{3}\left(1 + \frac{3}{2}\mu^2\right) + \frac{\mu}{2}\left(\alpha - \alpha_o\right)\right] \tag{A-12}$$

With respect to the NFP, the profile horizontal force coefficient is

$$C_{H_o} = \frac{H_o}{\rho S(\Omega R)^2} = 0.45\, \sigma C_{D_o} \mu \tag{A-13}$$

where C_{D_o} = blade section profile drag coefficient.

Again with respect to the NFP, the total induced horizontal force coefficient is (see Reference 6):

$$C_{H_i} = \frac{H_i}{\rho S(\Omega R)^2} = \frac{\sigma a}{2}\left[\frac{\theta_o}{3} a_1 + \frac{1}{2}\mu\lambda\theta_o - \frac{3}{4}\lambda a_1 + \frac{1}{4}\mu a_1^2 - \frac{1}{6} a_o b_1 + \frac{1}{4}\mu a_o^2\right] \tag{A-14}$$

where

$$a_o = \frac{\gamma}{2}\left[\frac{\theta_o}{4}(1 + \mu^2) - \frac{\lambda}{3}\right]$$

$$a_1 = \frac{\frac{8}{3}\mu\left[\theta_o - \frac{3}{4}\lambda\right]}{1 - \frac{1}{2}\mu^2}$$

$$b_1 = \frac{\frac{4}{3}\mu a_o}{1 + \frac{1}{2}\mu^2}$$

γ = blade mass constant

The total non-rotor parasite drag coefficient is defined with respect to the flight velocity vector:

$$C_{D_p} = \frac{D_p}{qS} = \frac{f}{S} \qquad (A\text{-}15)$$

where

f = parasite equivalent flat plate area, ft^2.

The above analysis was applied to the calculation of equilibrium flight values of δ_c and α for the LaRC YHC-1A helicopter, where (see References 4 and 5):

$$\alpha_o = \begin{cases} 9.0^\circ & V \leq 80 \text{ kts} \\ 11.25^\circ & V > 80 \text{ kts} \end{cases}$$

$\theta_o = (1.25\ \delta_c + 1)^\circ$

$\sigma = .0593$

$a = 5.7$

$C_{D_o} = .012$

$\gamma = 10$

$\Omega R = 678$ ft/sec

$f = 36.7$ ft^2

$S = 367$ ft^2

Results are compared with trim values calculated by the Vertol Division, Boeing Co., in Table A-1. It is apparent from the table that, for the cases compared, the present method agrees quite well with the more accurate calculations obtained by Vertol. The results indicate that the simple force model would be adequate for performing preliminary guidance analyses.

Table A-I. Comparison of Trim Calculations for δ_c and α
(G.W. 13400 lb ., C.G. Normal, Sea Level)

$V_{Horiz.}$ kts	V_{Climb} fpm	$\delta_c^{(1)}$ in	$\delta_c^{(2)}$ in	$\alpha^{(1)}$ deg	$\alpha^{(2)}$ deg
40	1500	5.94	6.12	-13.8	-14.5
40	0	3.73	3.47	6.55	6.35
40	-1500	1.25	0.92	27.2	27.1
80	1500	6.39	7.36	-8.8	-10.5
80	0	3.85	4.24	2.3	1.6
80	-1500	1.16	1.48	13.7	13.2
100	0	4.68	4.80	1.4	1.0

Note: (1) Calculated by Vertol Division, Boeing Co.

(2) Calculated by present method.

APPENDIX B

PHYSICAL AND AERODYNAMIC CHARACTERISTICS OF NASA/LaRC YHC-1A HELICOPTER

This appendix summarizes the data which has been used in Program LIFT to simulate the longitudinal dynamics of the LaRC YHC-1A helicopter. All of the data presented here were obtained from References 3 and 4.

Table B-I summarizes the pertinent physical characteristics of the vehicle, including control displacement limits. Tables B-II through B-IV give the trim conditions, fuel flow and stability derivatives as functions of forward speed for three rates of descent. The data in Tables B-II through B-IV were calculated for a gross weight of 13,400 lbs, normal c.g. position and sea level flight. In Tables B-III and B-IV (non-zero rate of descent), the data for forward speeds greater than 80 knots were extrapolated from 80 knot values by assuming constant offset from corresponding zero rate of descent (Table B-II) data. For the reader's convenience, the data in Tables B-II through B-IV are plotted in Figures B-1 to B-4.

Because of the different units in which the data was provided and used in Program LIFT, Table B-V contains a number of convenient conversion factors.

Table B-I. Physical Characteristics of LaRC YHC-1A Helicopter

Operating mass	6078	kg	(13,400 lbs)
Pitching moment of inertia, I_{yy}	102,898	$kg\text{-}m^2$	(75,914 $slug\text{-}ft^2$)
Reference area, S	341	m^2	(3670 ft^2)
Reference chord, c	0.4572	m	(1.5 ft)
Control travel limits			
Collective stick, δ_c	0 – 32.512	cm	(0 – 12.8 in)
Longitudinal stick, δ_e	±13.97	cm	(±5.5 in)

Table B-II. YHC-1A Longitudinal Stability Derivatives (Rate of Descent = 0 ft/min)

FORWARD VELOCITY	KTS	0	20	40	60	80	100	120	140
θ_o	deg	9.30627	8.19834	6.62235	4.75227	2.32294	1.43387	-2.28871	-6.63310
δ_{e_o}	in	.66523	-.06503	-.23518	.28888	.77817	-.06119	.16392	.34293
δ_{c_o}	in	5.01959	4.47346	3.73135	3.51111	3.84917	4.67777	6.04983	8.02025
f	lb/hr	921.685	854.123	763.341	732.363	755.190	827.894	869.854	1230.747
X_u/m	$\frac{ft/sec^2}{ft/sec}$	-.02540	-.00181	-.02156	-.03604	-.04642	-.05579	-.06456	-.07206
X_w/m	$\frac{ft/sec^2}{ft/sec}$	.05449	.06818	.08255	.08944	.08548	.10343	.08523	.05666
X_q/m	$\frac{ft/sec^2}{rad/sec}$	.60185	.74915	.87508	.84957	.73079	1.24872	.77601	.25183
X_{δ_e}/m	$\frac{ft/sec^2}{in}$	.17696	.13988	.12312	.14237	.16406	-.05165	-.03776	-.01954
X_{δ_c}/m	$\frac{ft/sec^2}{in}$	1.20482	.97467	.87948	.80253	.68335	.88200	.72040	.48341
Z_u/m	$\frac{ft/sec^2}{ft/sec}$	.06009	-.12594	-.08296	-.02192	.01396	.06077	.06546	.04980
Z_w/m	$\frac{ft/sec^2}{ft/sec}$	-.36933	-.48399	-.63639	-.80152	-.92055	-1.00063	-1.04552	-1.10516
Z_q/m	$\frac{ft/sec^2}{rad/sec}$	-.71511	-1.16872	-1.77844	-1.81400	-1.81986	-2.22039	-2.25955	-2.47935
Z_{δ_e}/m	$\frac{ft/sec^2}{in}$	-.00407	.21188	.51943	.56820	.52527	.46341	.41480	.36743
Z_{δ_c}/m	$\frac{ft/sec^2}{in}$	-7.43006	-7.23138	-7.65410	-8.52446	-9.49008	-10.26600	-11.08740	-11.71110
M_u/I_{yy}	$\frac{rad/sec^2}{ft/sec}$	.00656	.00645	-.00587	-.00670	-.00582	-.00185	-.00120	-.00089
M_w/I_{yy}	$\frac{rad/sec^2}{ft/sec}$	-.00285	.00978	.01630	.01363	.01154	.00956	.00774	.00691
M_q/I_{yy}	$\frac{rad/sec^2}{rad/sec}$	-.73173	-.96002	-1.31158	-1.45996	-1.52219	-1.62003	-1.59067	-1.51570
M_{δ_e}/I_{yy}	$\frac{rad/sec^2}{in}$	.35447	.35364	.40144	.45022	.48135	.51572	.53335	.54565
M_{δ_c}/I_{yy}	$\frac{rad/sec^2}{in}$	-.04765	-.04252	.04556	.06776	.06725	.04707	.03948	.03505

Table B-III. YHC-1A Longitudinal Stability Derivatives (Rate of Descent = 1500 ft/min)

FORWARD VELOCITY	KTS	0	20	40	60	80	100*	120*	140*
θ_o	deg	8.9881	8.13867	6.99471	5.34340	3.21352	2.32445	-1.37813	-5.74252
δ_{e_o}	in	.03060	-1.69234	-.56815	.11550	.60565	-.23371	-.00860	.17046
δ_{c_o}	in	3.89872	3.25038	1.25071	.90347	1.15881	1.98741	3.35947	5.32989
f	lb/hr	791.849	711.302	500.687	470.262	495.961	568.665	610.625	971.518
X_u/m	$\frac{ft/sec^2}{ft/sec}$	.01143	.02237	-.01281	-.03179	-.04306	-.05243	-.06120	-.06870
X_w/m	$\frac{ft/sec^2}{ft/sec}$	.04368	.05111	.10637	.10919	.10653	.12448	.10628	.07771
X_q/m	$\frac{ft/sec^2}{rad/sec}$	1.02536	.93903	1.55534	1.45965	1.37043	1.88836	1.41565	.89147
X_{δ_e}/m	$\frac{ft/sec^2}{in}$	.16625	.12347	.08223	.12593	.14599	-.06972	-.05583	-.03761
X_{δ_c}/m	$\frac{ft/sec^2}{in}$	1.13928	.94352	.82126	.88028	.82702	1.02567	.86407	.62708
Z_u/m	$\frac{ft/sec^2}{ft/sec}$	-.13435	-.23640	-.12619	-.02151	.01777	.06458	.06927	.05361
Z_w/m	$\frac{ft/sec^2}{ft/sec}$	-.28748	-.26321	-.82254	-.90575	-.98052	-1.06060	-1 10549	-1.16513
Z_q/m	$\frac{ft/sec^2}{rad/sec}$	-.79039	.30060	-2.45731	-2.40596	-2.42975	-2.83028	-2.86944	-3.08924
Z_{δ_e}/m	$\frac{ft/sec^2}{in}$	.00615	.19996	.94841	.77315	.71536	.65350	.60489	.55752
Z_{δ_c}/m	$\frac{ft/sec^2}{in}$	-7.45257	-7.38250	-6.35173	-8.00904	-9.05358	-9.82953	-10.65093	-11.27463
M_u/I_{yy}	$\frac{rad/sec^2}{ft/sec}$	.01308	.01863	-.00906	-.00696	-.00635	-.00238	-.00173	-.00142
M_w/I_{yy}	$\frac{rad/sec^2}{ft/sec}$	.00368	.03420	.00228	.00469	.00683	.00485	.00303	.00220
M_q/I_{yy}	$\frac{rad/sec^2}{rad/sec}$	-.58241	-.81810	-1.48310	-1.56553	-1.62309	-1.72093	-1.69157	-1.61660
M_{δ_e}/I_{yy}	$\frac{rad/sec^2}{in}$	.34363	.30612	.43861	.47166	.50338	.53775	.55538	.56768
M_{δ_c}/I_{yy}	$\frac{rad/sec^2}{in}$	-.05591	-.16472	.15368	.11620	.10884	.09602	.08843	.08400

* Data extrapolated from values at 80 knots.

Table B-IV. YHC-1A Longitudinal Stability Derivatives (Rate of Descent = -1500 ft/min)

FORWARD VELOCITY	KTS	0	20	40	60	80	100*	120*	140*
θ_o	deg	9.09615	8.24561	6.51804	4.34680	1.74707	.85800	-2.84458	-7.20897
δ_{e_o}	in	.56611	.45244	.38166	.63183	1.02115	.18179	.40690	.58596
δ_{c_o}	in	6.51301	6.30131	5.94168	5.94845	6.38886	7.21746	8.58952	10.55994
f	lb/hr	1102.055	1076.035	1023.741	1012.939	1055.591	1128.295	1170.255	1531.148
X_u/m	$\frac{ft/sec^2}{ft/sec}$	-.02649	-.01935	-.03260	-.04491	-.05277	-.06214	-.07091	-.07841
X_w/m	$\frac{ft/sec^2}{ft/sec}$	.07505	.08122	.08209	.07521	.06568	.08363	.06543	.03686
X_q/m	$\frac{ft/sec^2}{rad/sec}$	.15633	.20875	.26690	.17058	.09717	.61510	.14239	-.38179
X_{δ_e}/m	$\frac{ft/sec^2}{in}$	.17842	.16228	.14484	.16227	.18105	-.03466	-.02077	-.00255
X_{δ_c}/m	$\frac{ft/sec^2}{in}$	1.16992	1.04008	.90570	.78861	.62563	.82428	.66268	.42569
Z_u/m	$\frac{ft/sec^2}{ft/sec}$	.04316	-.02454	-.00971	.00737	.02520	.07201	.07620	.06104
Z_w/m	$\frac{ft/sec^2}{ft/sec}$	-.52217	-.60121	-.72925	-.85332	-.94171	-1.02179	-1.06668	-1.12632
Z_q/m	$\frac{ft/sec^2}{rad/sec}$	-1.07268	-1.20010	-1.25010	-1.38662	-1.47426	-1.87479	-1.91395	-2.13375
Z_{δ_e}/m	$\frac{ft/sec^2}{in}$	.05444	.16010	.36218	.41296	.41472	.35286	.30425	.25688
Z_{δ_c}/m	$\frac{ft/sec^2}{in}$	-7.5865	-7.64041	-8.2477	-8.9541	-9.7090	-10.48495	-11.30635	-11.93005
M_u/I_{yy}	$\frac{rad/sec^2}{ft/sec}$	.00251	.00163	.00321	-.00458	-.00467	-.00070	-.00005	.00025
M_w/I_{yy}	$\frac{rad/sec^2}{ft/sec}$	-.00148	.00327	.00726	.00765	.00730	.00532	.00350	.00267
M_q/I_{yy}	$\frac{rad/sec^2}{rad/sec}$	-.93433	-1.03020	-1.24040	-1.37428	-1.4243	-1.52214	-1.4[illegible]78	-1.41781
M_{δ_e}/I_{yy}	$\frac{rad/sec^2}{in}$	.37472	.37930	.40095	.43815	.46558	.49995	.51758	.52988
M_{δ_c}/I_{yy}	$\frac{rad/sec^2}{in}$	-.04570	-.03118	.01909	.03637	.04212	.02194	.01435	.00992

* Data extrapolated from values at 80 knots.

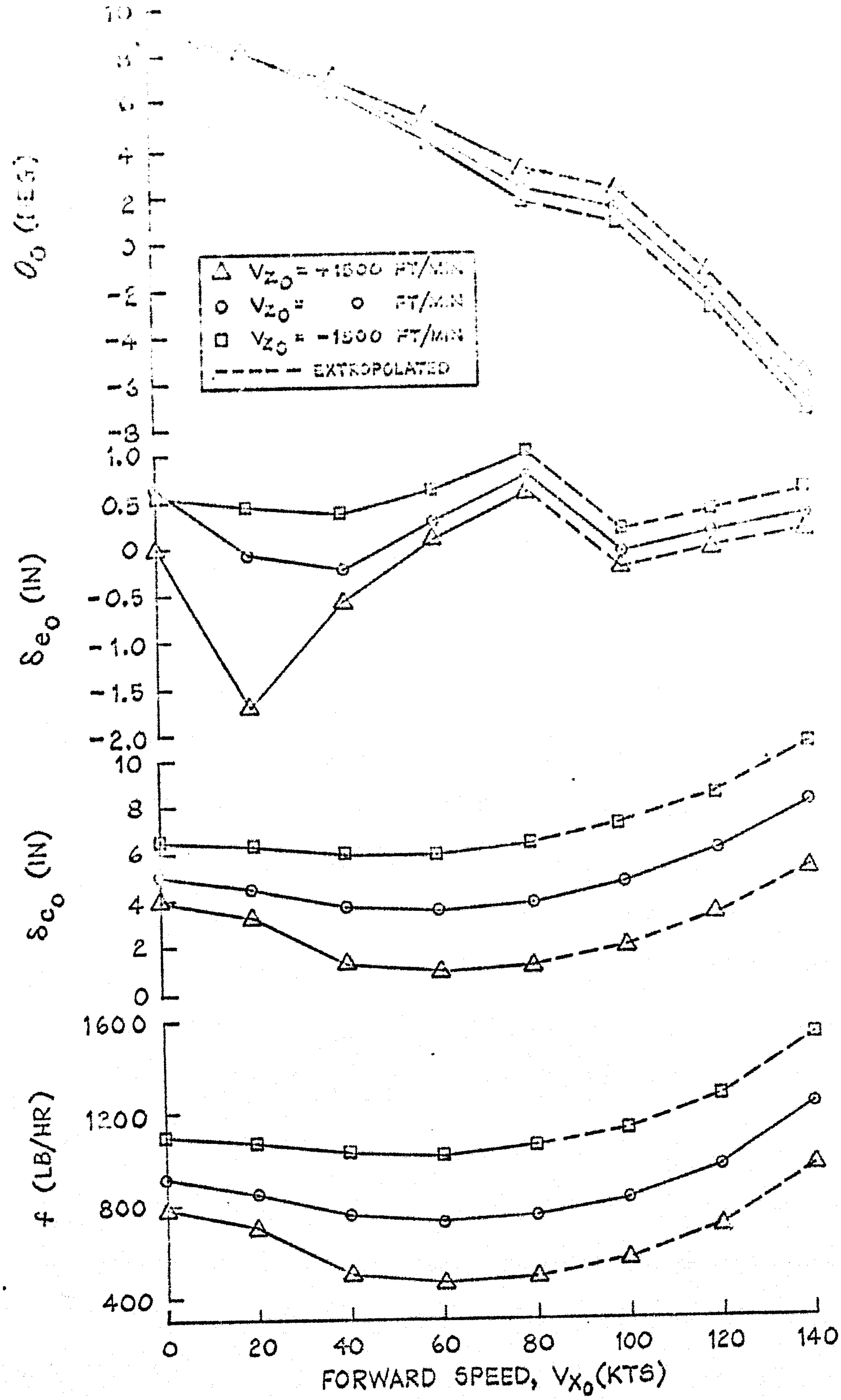

Figure B-1. YHC-1A Trim Pitch Attitude, Control Deflections and Fuel Flow (13,400 lbs, sea level, normal c.g.)

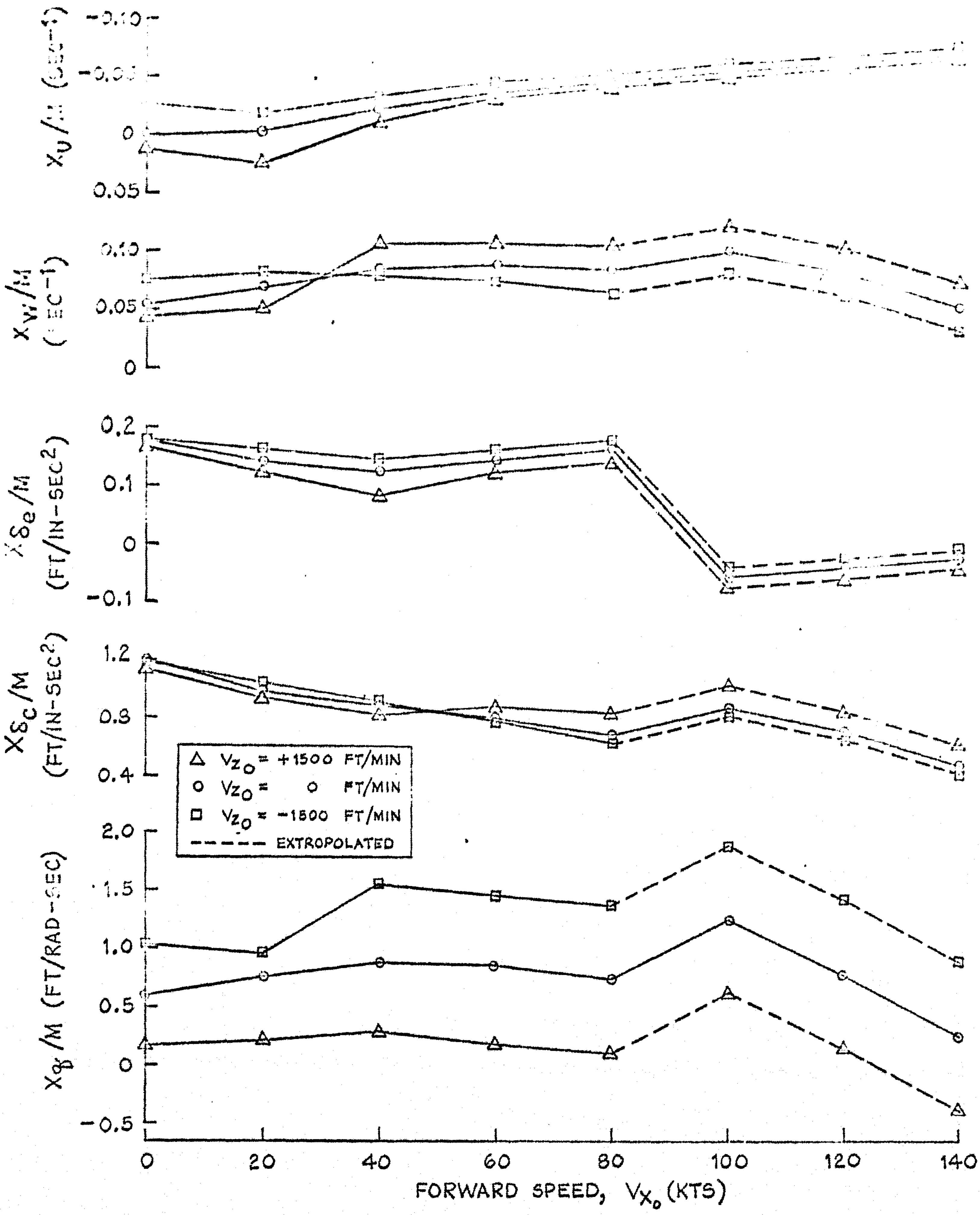

Figure B-2. YHC-1A Trim Axial Force Derivatives
(13,400 lbs, sea level, normal c.g.)

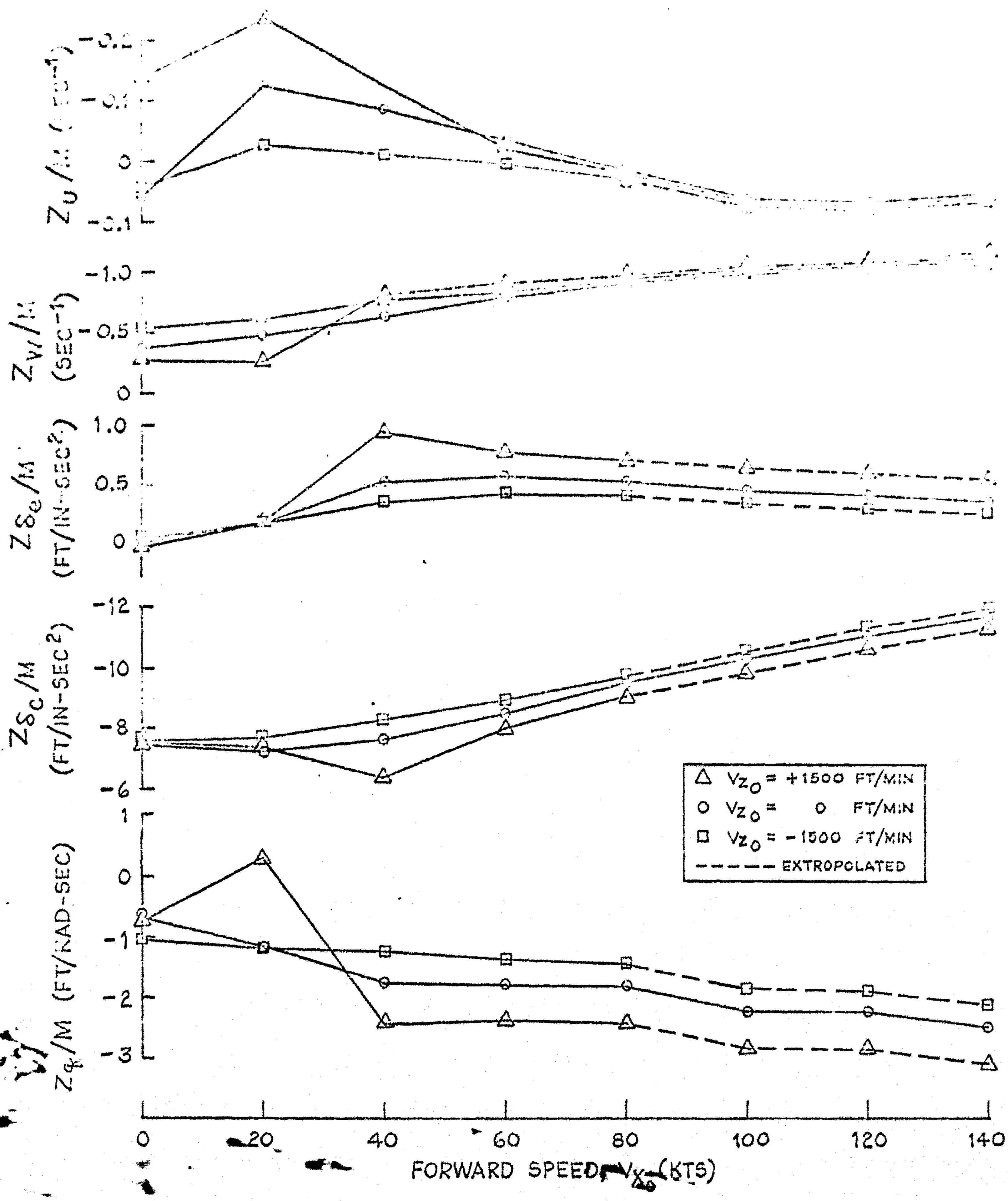

Figure B-3. YHC-1A Trim Normal Force Derivatives (13,400 lbs, sea level, normal c.g.)

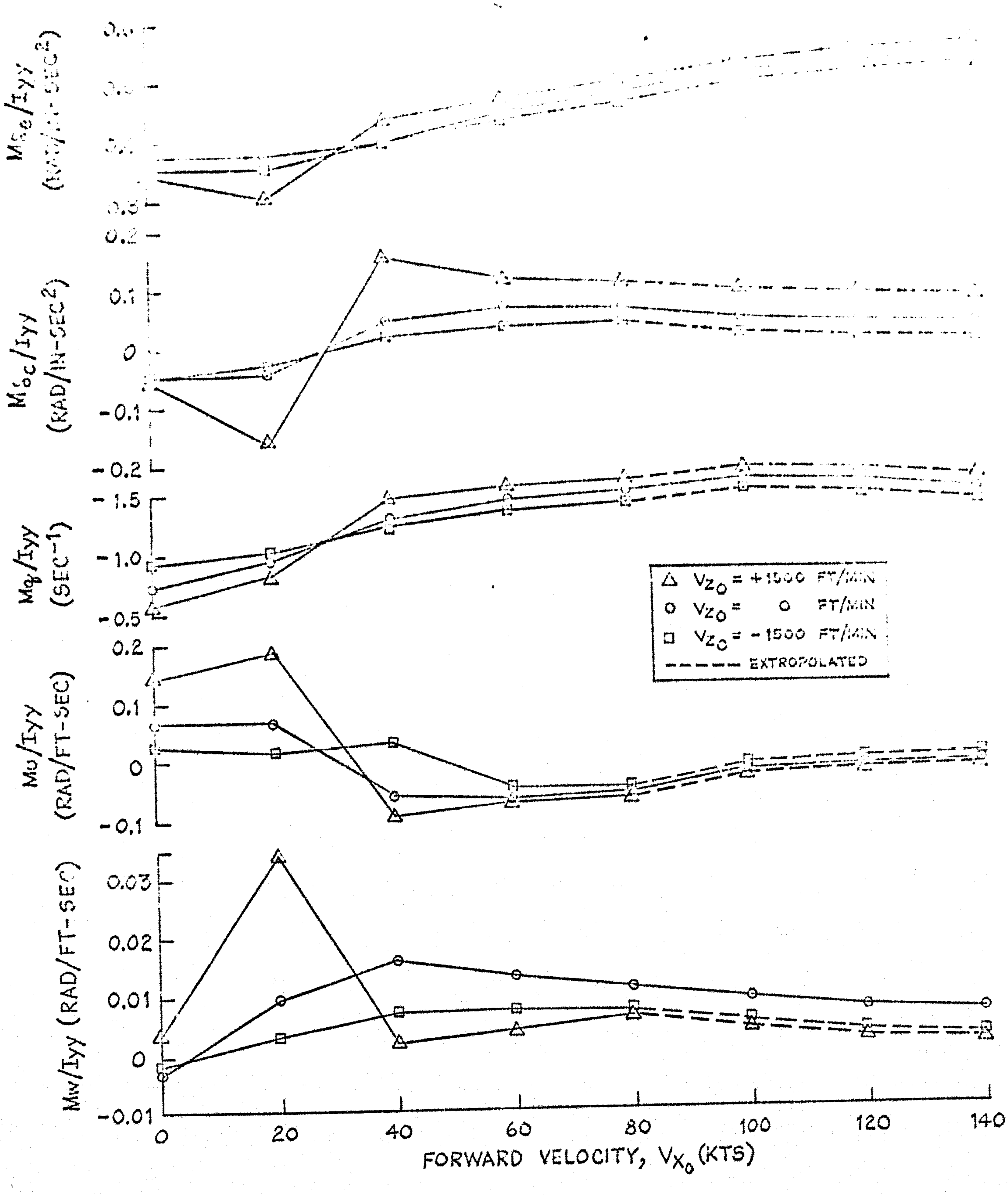

Figure B-4. YHC-1A Trim Pitching Moment Derivatives
(13,400 lbs, sea level, normal c.g.)

Table B-V. Conversion Factors

MULTIPLY	BY	TO OBTAIN
centimeters	0.39370	inches
meters	3.2808	feet
kilometers	0.53996	nautical miles
meters/second	3.2808	feet/second
meters/second	196.85	feet/minute
meters/second	1.9438	knots
kilograms	2.2046	pounds
kilograms/second	7936.6	pounds/hour
kilograms-meters^2	0.73756	slugs-feet^2
inches	2.540	centimeters
feet	0.30480	meters
nautical miles	1.8520	kilometers
feet/second	0.30480	meters/second
feet/minute	0.005080	meters/second
knots	0.51444	meters/second
pounds	0.45359	kilograms
pounds/hour	0.0001260	kilograms/second
slugs-feet^2	1.3558	kilograms-meters^2

REFERENCES

1. Hoffman, W. C., Bryson, A. E., Jr. and Zvara, J., A Terminal Guidance Scheme for Lifting Body Entry Vehicles, NASA CR-86126, Kaman AviDyne TR-55, Kaman AviDyne, Burlington, Massachusetts, October 1968.

2. McKeon, K. A., Mikami, K., Thompson, J. H. and Zvara, J., Six Degree-of-Freedom Analysis of Lifting Entry Vehicle Terminal Landing, Volume II, Computer Program LIFT User's Manual, Kaman AviDyne TR-45, Kaman AviDyne, Burlington, Massachusetts, June 1967.

3. Anon., Data Package - Digital Flight Control and Landing System in the LaRC CH-46C Helicopter, NASA Electronics Research Center, September 19, 1968.

4. Anon., Output from Trim and Stability Analysis Program, Job No. 6377 et al., Vertol Division, The Boeing Company, Morton, Pennsylvania.

5. Benson, R. et al, Substantiation Report for the CH-46D — Flight Manual Performance, Report No. A02-AD-007, Vertol Division, The Boeing Company, Morton, Pennsylvania, July 21, 1967.

6. Gessow and Myers, Aerodynamics of the Helicopter, Unger, 1967.